THESIS

REAL-TIME VISUALIZATION OF ADVECTIVE GROUNDWATER FLOW

Submitted by

Zach Ferrie

Department of Civil and Environmental Engineering

In partial fulfillment of the requirements

For the Degree of Master of Science

Colorado State University

Fort Collins, Colorado

Spring 2020

Master's Committee:

Advisor: Thomas Sale
Co-advisor: Jens Blotevogel

Jay Ham

ABSTRACT

As the portfolio of sites with subsurface contamination matures, long-term monitoring is becoming the primary factor governing costs for managing historical releases of contaminants to soil and groundwater. Hydraulic gradients are the primary factor driving the velocity and direction in which subsurface contaminants move, making them an important parameter to resolve. Current best practices for tracking groundwater flow include either collecting head data by hand or deploying pressure transducers and periodically returning to manually download the data. Unfortunately, cost restraints and infrequent data collection and processing are not conducive to timely responses to adverse conditions.

In this study, two low-cost cellular connected data acquisition systems are developed which allow for collection and analysis of head data in real-time. Using planar regressions of three head values, automated algorithms are used to estimate the direction and rate of groundwater flow on an hourly basis. Another novel addition is the integration of real-time alerts. By automating various alerts, site managers can be notified when conditions reach a pre-determined threshold. Automated alerts allow for swift action to be taken to adverse conditions and can lead to greater safety for the public while saving sites from costly mistakes.

Following Devlin and McElwee (2007), uncertainty in groundwater flow direction is a function of measurement error, spacing between wells, and local hydraulic gradients. By using these sources of uncertainty to create synthetic datasets, algorithms are used to estimate the likely range of a groundwater flow path. The effects of pressure transducer drift (i.e. increasing measurement error over time) and their effect on uncertainty are also explored. Results from this

study show that as long as the drift is similar in magnitude and direction for all pressure transducers, the effect on the uncertainty in the model is negligible.

Additionally, the effects of uncertainty in anisotropy on deviation from the estimated flow path are considered by way of synthetic datasets, which is novel to this research. The results of this research reveal that the effects of anisotropy uncertainty on groundwater flow direction and seepage velocity are also tied to well spacing. Comparisons of the effects of measurement error vs anisotropy uncertainty are compared for four field sites. Results show that the magnitudes of each source of error are site specific and that the effects of measurement error are not always greater than the effects of anisotropy uncertainty and vice versa. Lastly, the seepage velocities are expressed by way of a color scheme common across sites. This novel addition allows for easy visualization of seepage velocities across time and space.

Overall, the vision from this research is that real-time, continuous collection and analysis of head data can proceed as outlined in this Thesis. In the future manually collected and interpreted head data need to be compared to the automated analyses described in this Thesis to further support the validity of the methods proposed herein. Another future test is to investigate alternative technologies to pressure transducers for gaining head measurements that are more accurate and reliable.

ACKNOWLEDGEMENTS

Thank you to all my committee members and those who supported me throughout this process. I would like to thank Dr. Tom Sale for providing me with the opportunity to study and conduct groundwater research as his graduate student at Colorado State University. His knowledge and help was critical to the development of the work presented in this Thesis as well as my development as a scientist.

I would like to thank Dr. Jens Blotevogel who was particularly helpful with my early work as a graduate student. From scientific input to aid in navigating field sites and field installations his input helped me grow during my early period as a graduate student.

I would like Dr. Jay Ham for all his help, particularly with the development of the hardware developed in this Thesis. Without his input my knowledge of electronics and sensors would not be what it is today.

I would like to thank all members of the Center for Contaminant Hydrology and everyone who has helped with field installations and given various input for the work in this Thesis. The work presented in this Thesis was not possible without your help and I am very grateful to all of you. I would like to thank Jacobs Engineering Group Inc., Chemours Co., SUNCOR Energy Inc., and the other sponsors who made this work possible through their sponsorship.

Last but not least, I would like to thank my friends and family who supported me through this journey. Without your patience, support, and motivation I would have considerably more grey hairs at the end of this journey.

TABLE OF CONTENTS

CHAPTER 1 - INTRODUCTION

1.1 Motivation

As the portfolio of contaminated sites matures, long-term monitoring of subsurface contaminants is becoming the primary factor governing costs for managing historical releases of contaminants to soil and groundwater. Groundwater flow directions and seepage velocities are key elements for assessing risks posed by subsurface contaminants. Current best practices for resolving groundwater flow include manually collecting head data on a quarterly to annual basis. Infrequent collection of head data can miss important events in the studied aquifer (Gao, 2017). Alternatively, pressure transducers can be installed in monitoring wells to continuously collect head data. Unfortunately, infrequent manual downloads of head data can miss important events that require timely response.

In addition to a need for larger, more timely datasets, appropriate methods are needed to interpret acquired data. One common approach is to use head data to track the transport of contaminants in the subsurface. Advection (mass transport solely due to the flow of water) represents the primary process conveying groundwater contaminants from one point to the other in the subsurface (Schwartz and Zhang, 2002). A common method for determining advective transport rates is by particle tracking. The idea of particle tracking is to follow the movement of infinitely small fluid particles placed in a flow field using either analytical or numerical methods (Lu, 1994). For numerical models the modeling codes MODFLOW and MODPATH are commonly used for groundwater flow and particle tracking. Gao (2017) used an analytical model and continuous head data as an alternative approach for particle tracking.

Often overlooked in analytical and numerical models is the effect that uncertainty has on the reliability of model results. Bright et al. (2002) found that increasing the amount of gathered hydraulic conductivity values significantly decreased model uncertainty when predicting contaminant concentrations. Burger and Belitz (1997) studied the variability of anisotropy, finding that horizontal to vertical anisotropy ratios varied widely from site to site and measurement to measurement. Measurement error in collected head data used to parametrize models also has an effect. Silliman and Mantz (2000) found field sites where measurement error caused the vertical hydraulic gradient estimate to be both oriented vertically upward and vertically downward at the same site. Devlin and McElwee (2007) found measurement error to have a significant effect on horizontal hydraulic gradient estimates (both in magnitude and direction) at a site.

This research provides a novel approach to track advective groundwater flow in real-time and determine the effect that uncertainty in head measurements and anisotropy values have on model results. A limitation of all the aforementioned methods used to determine advective groundwater flow is that the need for manual data downloads and data processing results in increased time before usable results are reached. As previously mentioned this can miss adverse conditions that require a timely response and may lead to human health risks and costly cleanup. Additionally, the cost of data acquisition for manual data collection methods can be large. By designing and building affordable cellular connected data acquisition systems, data can be gathered and transformed in real-time. This leads to advantages such as reduced cost both in terms of equipment and labor/maintenance as well as decreasing the time to recognize adverse conditions. Automated data collection and analysis also allows for more short-lived and dynamic events to be resolved more accurately due to increased data density. In addition, by modeling the

uncertainty associated with measurement error and anisotropy uncertainty the possible range of flow directions can be modeled with higher confidence at sites.

1.2 Research Objectives

The first objective of this research is to use continuous head data to determine the effects of measurement error and anisotropy uncertainty on groundwater flow direction and seepage velocity at four field sites. For each site, analyses are conducted assuming A) homogeneous, isotropic conditions with measurement error and B) homogeneous conditions with uncertainty in horizontal anisotropy and no measurement error. This allows the effects of each source of error to be considered individually and then compared for each site. The cumulative effects of measurement error and anisotropy uncertainty are also considered. In addition, field testing of low-cost, modified pressure transducers is conducted and field results are compared to model results to analyze how the model preforms when using low-cost sensors.

The second objective of this study is to develop an affordable, cellular connected data acquisition system to collect and send data to a cloud based dashboard for real-time data transformations depicting the path of advective groundwater flow. Data transformations assume homogenous, isotropic conditions, and no vertical hydraulic gradient. Data transformations are displayed without the effects of measurement error or anisotropy uncertainty.

In this research, the parameters assumed at each site may not be truly representative of site conditions. Assumed inputs will not influence the objective of this research as the aim is to demonstrate the methods and analyses described in the paragraphs above. The research is not intended to rigorously make predictions about processes at the chosen sites.

1.3 Organization and Content

This Thesis is divided into four parts. First, a literature review is presented in Chapter 2. Next, methods are presented in Chapter 3. Results are discussed in Chapter 4. Lastly, conclusions and suggestions for future work are advanced in Chapter 5.

CHAPTER 2 - LITERATURE REVIEW

The following provides background information relevant to the forthcoming chapters.

2.1 Head

Following Schwartz and Zhang (2002), hydraulic head represents the energy of an incompressible fluid. Hydraulic head is often defined as a water level above a chosen datum (e.g. feet above mean sea level). Mathematically the hydraulic head (h [L]) for groundwater can be defined as

$$h = z + \frac{P}{p_w g} \tag{2.1}$$

where, z is the elevation [L], P is the pressure exerted by the water column [M/LT^2], p_w is the fluid density [M/L^3], and g is the gravitational acceleration [L/T^2].

2.2 Methods for Obtaining Head Values

Hydraulic head is typically a transient property, making it potentially important to continuously collect head measurements over time to understand groundwater flow. The following sections discuss methods and instrumentation used to obtain and record head values.

2.2.1 Sensors Used to Gain Head Values

2.2.1.1 Water Level Sounder

Water level sounders are devices used to gather head readings by-hand. Water level sounders work using a probe attached to the end of a tape measure on a spool. The user lowers the probe down to the surface of the water at which time the water level sounder will emit a noise and/or light to let the user know contact with water has been made. At this time the user is able to read

the value on the tape measure to see how far down the probe contacted water and therefore determine the depth to the air-water interface below a known reference point.

2.2.1.2 Pressure Transducers

When not using a water level sounder, a common method to measure head is by using pressure transducers. Pressure transducers measure the pressure of the water column above them which can be used to calculate hydraulic head using Equation 2.1. Typically pressure transducers consist of a sensing diaphragm located at the end of the sensor whose electrical resistance changes according to changes in pressure. The change in electrical resistivity can be measured using a data logger (further discussed in Sections 2.2.2.2, 2.2.2.3, and 3.1.1-3.1.3).

The pressure observed by a pressure transducer is a function of both the height of fluid above the sensor, density of the fluid, and local barometric pressure. Fluctuations in barometric pressure cause changes in sensor output that are not representative of the hydraulic head. Therefore changes in barometric pressure must be accounted for to ensure accurate resolution of hydraulic head.

Vented pressure transducers compensate for barometric fluctuations by including a tube that connects the reference end of the pressure transducer to the atmosphere. This allows for the barometric pressure on the sensing side of the sensor and reference side of the sensor to be the same. Vented pressure transducers are the most accurate form of pressure transducers since a second measurement and associated error is not required to gain an accurate head value. The downside of vented pressure transducers is that the vent line is pathway for moisture to enter the sensor, potentially damaging the sensor or causing inaccurate readings (TE Connectivity, 2016). A common requirement for vented pressure transducers is to place desiccant at the end of the

vent tube to absorb moisture that may enter the tube. This raises cost and requires extra maintenance to replace expended desiccant through time.

Sealed pressure transducers do not incorporate a vent tube into their design. This allows for sealed pressure transducers to avoid issues associated moisture intrusion; however, the sensor reading will fluctuate with both a change in hydraulic head and change in barometric pressure. As a result an additional sensor is required to gain barometric pressure measurements, ultimately leading to increased cost and error in measured head. Barometric pressure readings are usually consistent across a region which allows for single barometric pressure sensor to be used for correcting head measurements within a 10-mile range (Onset, 2019).

2.2.1.3 Other Sensors for Gaining Head Values

In addition to water level sounders and pressure transducers there are many other sensors that can be used to measure head. Table 2.1 gives an overview of four other common sensors used to measure head. The table discusses how these sensors operate as well as some common advantages and disadvantages of each sensor.

Table 2.1: An overview of other common water level sensing instruments and their pros and cons. This is not an exhaustive list.

	How it Operates	Pros	Cons
Bubbler	**Pushes air through an airline submerged underwater. The amount of pressure required to push a bubble out of the airline is directly proportional to the height of water above the airline.**	**•Less prone to corrosion and other damage compared to submerged sensors (only tube is submerged). •Minimal drift •High Accuracy**	**•High cost •Potential safety concerns regarding gas migration up tube.**
Ultrasonic/ Radar	**Emit either an ultrasonic or radar wave and measures the amount of time it takes for the wave to bounce off the surface of the water and return to the sensor.**	**•Less prone to corrosion and other damage compared to submerged sensors. •Can be used to gain measurements where water may become frozen.**	**•Low accuracy •Low resolution •Must be mounted at top of well (increases the required range of the sensor therefore decreasing its accuracy). •For narrow wells or long ranges, sides of well may interfere with emitted signal.**
Float and Pulley	**Consists of a buoyant float which moves up and down with the rise and fall of the water level. The float is attached to a pulley at the top of the well which rotates as the pulley moves up and down. This rotation can be converted into water level.**	**•High Accuracy •Minimal drift**	**•Requires a large (> 3") still well. •Requires housing on top of still well. •High cost**
Capacitive Rod	**Measures the change in capacitance along a rod partially submerged in water. The difference in the capacitance between water and air allows for the water level to be obtained.**	**•Inexpensive**	**•Low accuracy •Low resolution •Limited range**

2.2.2 Data Acquisition

2.2.2.1 By-Hand Data Acquisition

Water level sounders require someone to physically visit wells to take and record a depth to water (DTW) measurement. The benefits of water level sounders are that they are accurate and lose little accuracy over time, they require little maintenance, and only one is needed to measure head at multiple locations. The downfall is that due to time and cost restraints water level sounder measurements are often taken on a quarterly to annual basis. As a result small data sets are used to make inferences about large time periods which can miss dynamic aspects of groundwater flow. In addition, the time between sampling events results in delayed reaction times to adverse conditions the gathered data may identify. At select facilities there may also be concerns with both worker safety and site security.

2.2.2.2 Data Loggers Without Automatic Uploads

When using a pressure transducer or other automated head sensor a method to store data is required. This involves using either an external or integrated data logger such as the CR-1000 (Campbell Scientific) or Levelogger (Solinst), respectively. This provides a continuous data set, overcoming the issues associated with more infrequent data collection methods (i.e. by-hand data collection). However this still requires someone to physically visit the site and manually download the data which again results in delayed observation of potentially adverse conditions.

2.2.2.3 Data Loggers With Automatic Uploads and Emerging Technologies

Data loggers such as the CR-1000 (Campbell Scientific) can be paired with cellular modems such as the RAVEN XT (Sierra Wireless) which can be programmed to remotely and automatically upload data to a third-party device (e.g. desktop computer). This method provides continuous data and continuous data uploads, overcoming the issues associated with the methods

mentioned in Sections 2.2.2.1 and 2.2.2.2. The downside to this method is that the cumulative price of commercially available data loggers, cellular modems, and pressure transducers are often large, making site wide deployment of such devices impractical.

The Internet of Things (IoT) involves systems of interrelated computing devices which have the ability to transfer data over a network without any human interaction. Recent advancements in IoT technology have made sensor networks cheaper and more user friendly than ever before allowing scientists in fields such as agriculture (Subanshini, 2018) to create their own IoT-based data acquisition systems for a fraction of the price of their commercial counterparts. Overall, IoT technologies are reducing costs while also providing continuous, real-time data.

2.3 Advective Transport

Advection can be defined as "mass transport due simply to the flow of water" (Schwartz and Zhang, 2002). Advection is the dominant process in which groundwater contaminants are transported long distances in the subsurface through transmissive zones. Mathematically, advective transport in 1D for homogeneous, isotropic conditions can be described using Darcy's seepage velocity (v [L/T]) equation

$$v = \frac{q}{n_e} = \frac{-K\frac{\partial h}{\partial l}}{n_e} \tag{2.2}$$

where, q [L/T] is the Darcy velocity, n_e [dimensionless] is the effective porosity, K [L/T] is the hydraulic conductivity, and $\frac{\partial h}{\partial l}$ [L/L] is the gradient of head driving advection.

When considering homogeneous, anisotropic conditions hydraulic conductivity values vary with direction resulting in (Domenico and Schwartz, 1997)

$$q_x = -K_{xx}\frac{\partial h}{\partial x} - K_{xy}\frac{\partial h}{\partial y} - K_{xz}\frac{\partial h}{\partial z} \tag{2.3}$$

$$q_y = -K_{yx}\frac{\partial h}{\partial x} - K_{yy}\frac{\partial h}{\partial y} - K_{yz}\frac{\partial h}{\partial z} \quad (2.4)$$

$$q_z = -K_{zx}\frac{\partial h}{\partial x} - K_{zy}\frac{\partial h}{\partial y} - K_{zz}\frac{\partial h}{\partial z} \quad (2.5)$$

where,

$$q_x \neq q_y \neq q_z \quad (2.6)$$

$$v_x \neq v_y \neq v_z \quad (2.7)$$

here, *x*, *y*, and *z* are the positions [L].

2.4 Methods for Determining Advective Transport

The following sections provide background for methods used to determine the magnitude and direction of advection for groundwater and contaminants. The first section reviews current methods commonly used for resolving advective transport. The second section discusses emerging methods for resolving advective transport.

2.4.1 Current Methods for Resolving Advective Transport

The current methods commonly used to determine advective flow involve either analytical methods or numerical models. Analytical methods involve using closed form mathematical models that provide an exact solution to the stated mathematical problem. Their simplicity and ability to gain an exact solution give them an advantage over numerical models, however they often require assumptions to be made that may not be realistic of the system they are modeling (steady state, homogeneous, isotropic, etc.).

Numerical models involve using computer software and user entered information to estimate advective transport. The benefit of numerical models is that they spatially and temporally discretize a system, allowing for them to handle more complex aquifer systems than analytical

models. Using the method of particle tracking, modeling codes such as MODFLOW or MODPATH can be used to define path lines of solute particles under purely advective transport (Jackson, 2002). Particle tracking is widely used in numerical modeling for tracking groundwater flow and contaminant paths (e.g. Yidana, 2011 and Shamsuddin et al., 2014.). A key disadvantage of numerical models is that the gradients driving advection are based on prescribed boundary conditions versus actual head data obtained from the study area. Another downside to numerical models is that they give an approximate answer based on the partial differential equation and discretization of the model. Additionally, analytical and numerical models use limited data to interpolate the conditions between the model cells defined by the discretization. Using limited data to interpolate the conditions between the model cells defined by the discretization can lead to discrepancies between the modeled and physical aquifer system, ultimately resulting in a decrease in model reliability.

2.4.2 Emerging Methods for Determining Advective Transport

In response to the pitfalls of the methods described above, new methods have emerged for determining advective transport. Using the least-squares fitting of plane surfaces to head data, Kelley and Bogardi (1989) developed a method that could be implemented into a spreadsheet to determine the direction of groundwater flow. Devlin (2003) utilized the matrix-solving functions of a modern spreadsheet program (Excel) to solve for the magnitude and direction of a water-table plane using head values from multiple wells. Beljin et al. (2014) created a spreadsheet tool named 3PE as an extension of the previously developed spreadsheet tools developed by Kelley and Bogardi (1989), Devlin (2003), and on-line calculators such as the Three Point Gradient Calculator (USEPA, 2012). Gao (2017) utilized the method of fitting a planar surface to gathered head data to track groundwater flow using continuous, dynamic head data. A downfall with the

methods mentioned in this section is that they require the user to manually input data into the model which increases the time required to transform head data into meaningful results.

2.5 Sources of Uncertainty in Groundwater Flow

The next two sections discuss measurement error and anisotropy uncertainty and their effect on groundwater flow. It should be noted that additional sources of uncertainty (e.g. heterogeneity) exist however these topics are beyond the scope of this study.

2.5.1 Uncertainty of Measurement Error in Head Values

Referring to Equation 2.1, it can be seen that hydraulic head is function of elevation (z), the pressure exerted by the water column (P), fluid density (p_w), and the gravitational acceleration (g). The elevation (z) is measured using surveying tools while the pressure exerted by the water column (P) can be measured using a sensor such as a pressure transducer (fluid density (p_w) and the gravitational acceleration (g) are assumed constant). Head values are used in analytical and numerical models making the accuracy of measured head values a factor in resolving the accuracy of the model.

Based on a series of analyses of published data sets, Silliman and Mantz (2000) observed a consistent problem in the estimation of the vertical component of the hydraulic gradient at multiple sites. Using a simple numerical study they concluded that measurement error was the primary cause of the observed variance. Devlin and McElwee (2007) used Monte Carlo simulations to examine the effect of measurement error on horizontal hydraulic gradient estimates. They concluded that for shallow hydraulic gradient sites, horizontal hydraulic gradients are susceptible to variability due to measurement error. For the site examined, they found the average hydraulic gradient to vary by ±25% in magnitude ±18^o in direction when the

effect of measurement error was considered. They also found the spacing of wells to have considerable effect on the influence of measurement error on hydraulic gradient estimates, concluding that the monitored area should be sufficiently large so that a head drop of at least three times the expected measurement error occurs from one end of the monitored area to the other. While the effects of measurement error on hydraulic gradient estimations have been explored, research has not yet been conducted exploring the effect that measurement error has on causing deviation from estimated groundwater flow path travel directions and seepage velocities over time.

2.5.2 Uncertainty in Hydraulic Conductivity

With hydraulic conductivity being a primary driver of groundwater flow and contaminant transport, the effects of uncertainty in hydraulic conductivity values can have considerable effects on estimated groundwater flow directions and seepage velocities. Field measurements indicate that hydraulic conductivity of aquifers consistently varies through space in an irregular manner (Dagan, 1986). In addition, hydraulic conductivity is also known to vary with direction (anisotropy).

Bright et al. (2002) examined the effect of increasing the amount of hydraulic conductivity data on the level of uncertainty about contaminant concentration predictions. They found that increasing the amount of hydraulic conductivity data used in predicting contaminant transport resulted in an improvement of the measure of confidence in the predicted contaminant concentration. In addition, Monte Carlo simulations were found to be a potentially useful tool in improving the measure of confidence when large hydraulic conductivity data sets are not available for a given site. While research has been conducted exploring the benefits of increasing hydraulic conductivity data, research has not yet been advanced to visualize the effect that

uncertainty in anisotropy estimates have on causing deviation from estimated groundwater flow path travel directions and seepage velocities over time.

CHAPTER 3 - METHODS

The following Chapter focuses on the methods associated with hardware, measurement validation, mathematics, and field sites used in this Thesis.

3.1 Hardware

3.1.1 Pressure Transducers

Pressure transducers convert pressure head into an electrical signal that can be read by a data logger or other data acquisition device. The pressure transducers used in this Thesis utilize a piezoresistive sensing element whose resistance changes linearly with an increase in pressure. The change in resistance is then converted to a current between 4-20 milliamps by the pressure transducer which can be measured and converted into a pressure. When paired with a surveyed height of the well where the pressure transducer is installed, a head elevation can be obtained. Pressure transducers were chosen to meet the following specifications

1. ±0.1%/FS (Full Scale) accuracy – Equivalent to a measured head accuracy of ±0.01 ft for pressure transducers with a range of 0-10 ft.
2. Approximately $100.00 or less in cost
3. Chemically resistant housing and wire – 316L stainless steel housing, PTFE/ETFE wire
4. Sealed pressure transducer design – to prevent issues with sensor damage due to moisture intrusion that can occur with vented pressure transducers.

Three pressure transducer models were found that meet specifications 1-3. Since these pressure transducers are only sold as vented models they were tested to see how they preform when unaltered. Additionally, one model was modified to meet specification 4 and determine if

modifying the pressure transducer affects its accuracy. Table 3.1 shows the pressure transducers considered in this Thesis.

Table 3.1: Pressure Transducer make, model, and test information.

Model:	Manufacturer:	Vented test?	Sealed test?
FYD-101	Xi'an Feng Yu Instrument Co.	YES	YES
YD322	Xi'an Yunyi Instrument Co.	YES	NO
LV800	Voltell	YES	NO

3.1.2 Transforming Pressure Head into Elevation Head

The following sections discuss equations used to gain head elevation data from pressure transducers as well as modifications of the pressure transducers used in this Thesis. Figure 3.1 illustrates the conceptual framework for converting pressure data into head elevations. Per Gao (2017), pressure head can be mathematically converted into a head elevation (W_{elev} [L]) using Equation 3.1.

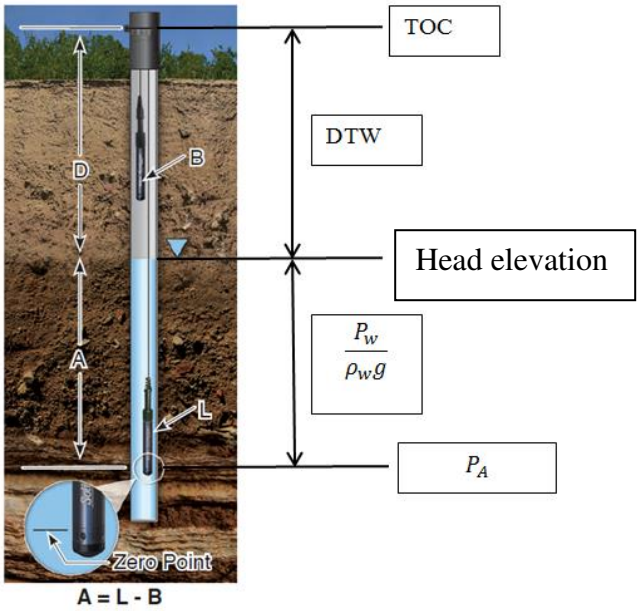

Figure 3.1: Level Logger measurement fundamentals (Solinst, 2014). (A = actual water column height, B = barometric pressure, L = level logger total pressure readings, and D = depth to water level, below reference datum).

$$W_{elev}(t) = TOC(t) - DTT_P + \frac{P_w(t)}{\rho_w g} \quad (3.1)$$

where, *TOC* is the elevation of the top of casing (TOC) [L], DTT_P [L] is the depth to the pressure transducer below the *TOC*, P_w [M/T^2/L] is the water pressure measured by the pressure transducer, ρ_w [M/L^3] is the density of water, and g is the gravitational acceleration [L/T^2].

3.1.3 Calculating Head Elevation from Pressure Transducer Milliamp Output

As previously mentioned, the pressure transducers used in this Thesis output a 4-20 milliamp signal. For the experiment the milliamp signal is transformed into a millivolt signal using a shunt resistor at the data logger. The addition of the shunt resistor results in voltages which can be read by the data logger and transformed into head elevations using Equations 3.2-3.5. Equations 3.2-3.5 assume a sealed pressure transducer design is being used.

To calculate a head elevation that is not compensated for fluctuations in barometric pressure

$$W_{elev}(t_i, t_o) = \frac{I(t_i) * \Omega_{shunt}}{Slope} + Offset(t_o) \quad (3.2)$$

where, *I* [Ampere] is the output of the pressure transducer, Ω_{shunt} [Ohm] is the value of the shunt resistor, *Slope* [Volt/L] is the calibration curve of the pressure transducer, and *Offset* [L] is the offset calibration which can be calculated as

$$Offset(t_o) = TOC(t_o) - DTW(t_o) - \frac{I(t_o) * \Omega_{shunt}}{Slope} \quad (3.3)$$

where, the depth to water (*DTW*) [L] is the distance from *TOC* to the water surface in the well.

If correcting the head elevation for fluctuations in barometric pressure

$$W_{elev}(t_i, t_o) = \frac{I(t_i) * \Omega_{shunt}}{Slope} + Offset(t_i) + Offset_{\rho}(t_i, t_o) \quad (3.4)$$

$$Offset_{\rho}(t_o, t_i) = \rho(t_o) - \rho(t_i) \quad (3.5)$$

where, $Offset_{\boldsymbol{\rho}}$ [Hydraulic Head as L] is the barometric pressure offset, $\rho_{\boldsymbol{int}}$ [Hydraulic Head as L] is the barometric pressure at the time the *Offset* [L] calibration was made, and $\rho_{current}$ [Hydraulic Head as L] is the current barometric pressure. By using Equation 3.4 an absolute head elevation is gained. Transformation of pressure transducer data into flow paths (Section 3.3) uses Equation 3.2, gaining relative head elevations for reasons subsequently explained in Section 3.4.1.1.

3.1.4 Pressure Transducer Modifications

All pressure transducers that meet the specifications of accuracy, cost, and chemical resistance are designed as vented sensors. FYD-101 pressure transducers (FYD-101, Xi'an Feng Yu Industry Co.) were purchased without wire so they could be modified into a sealed pressure transducer design prior to deployment (Figure 3.2). Sealing the sensors was achieved by splicing ETFE coated wire to the existing pressure transducer wire and then using electrically safe potting epoxy (DP270, 3M) to seal around the bare wire. The method was used to ensure that no airflow can reach the sensing end of the pressure transducer through the wire sheath and cause measurement error. A rubber stopper was custom made for each sensor to prevent the DP270 from seeping into the sensing end of the pressure transducer and damaging it. Finally, each pressure transducer was modified to allow for custom made stainless steel hangers to be added. The stainless-steel hangers allowed for the pressure transducers to be hung in wells from steel

hanging wire to avoid hanging the sensor from the ETFE cable, which could stretch over time and cause measurement error.

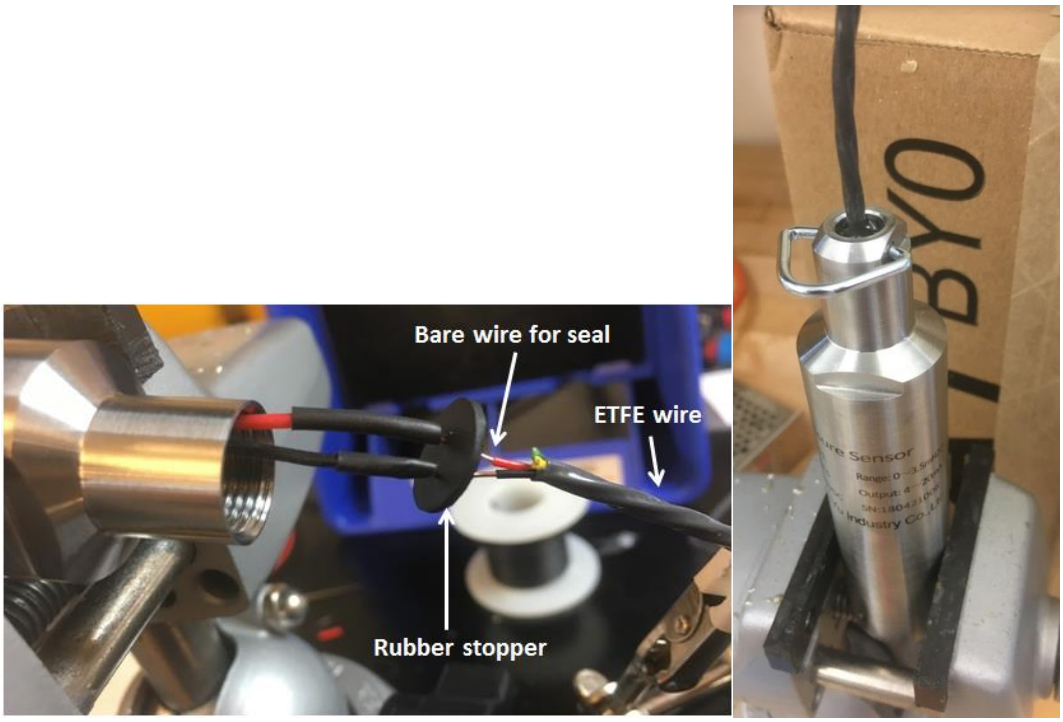

Figure 3.2: Pressure Transducer Modifications. Sealing process (left) and stainless steel hanger addition (right).

3.1.5 Data Logging and Transmission

3.1.5.1 Cellular Connected Microcontroller

A cellular enabled microcontroller (Electron, Particle io) is used to transmit data in real-time. The Electron microcontroller (Figure 3.3) was chosen based on its price, ease of use, and the large community able to provide assistance while trouble shooting the developed code and hardware.

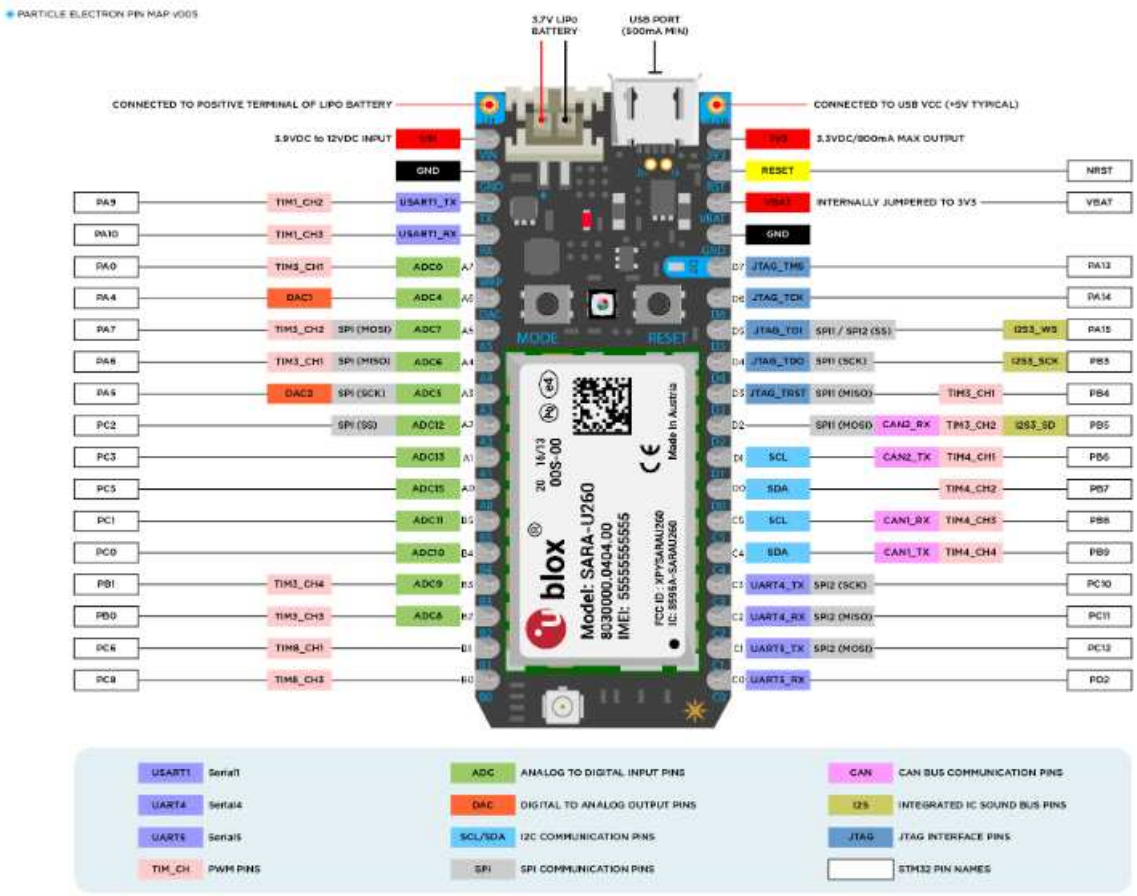

Figure 3.3: Particle Electron microprocessor layout.

The Electron microcontroller does not contain its own power source. Nor does it have the capacity to read the output signals from pressure transducers. The following sections discuss the hardware used to power the data acquisition system and transform pressure transducer outputs into signals that can be read by the Electron microcontroller.

3.1.5.2 Power Supply

Solar panels (2 Watt Solar Panel or 3.5 Watt Solar Panel, Voltaic) are used to power the Electron microcontrollers. Solar panels range from 6 volt, 2 watt to 6 volt, 3.5 watts depending on the available sunlight and power needs at each site. Charge regulators (USB/DC/Solar Lithium Ion/Polymer charger – v2, Adafruit) are used to charge 3.7 volt, 6600 milliamp hour, lithium ion batteries (Lithium Ion Battery Pack – 3.7V 6600mAh, Adafruit) to provide power during periods

of inadequate sunlight. The pressure transducers require 12 volts to operate which is greater than the solar panel can supply. A 12 volt step-up voltage regulator (U3V12F12, Polulu) is used to increase the voltage to pressure transducers. The U3V12F12 is turned off when not in use to reduce power consumption.

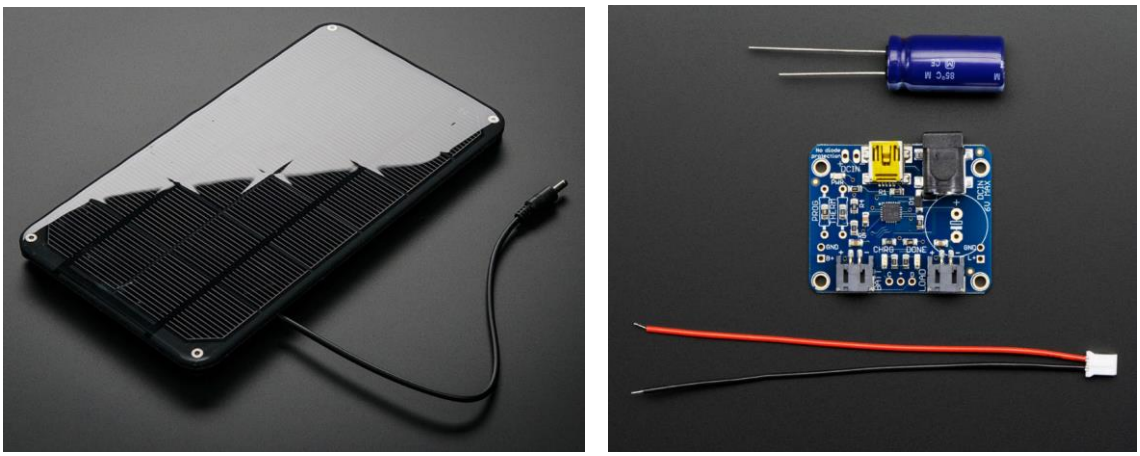

Figure 3.4: 6V, 3.5 W Voltaic solar panel (left) and Adafruit USB/DC/solar lithium ion/polymer charger (right).

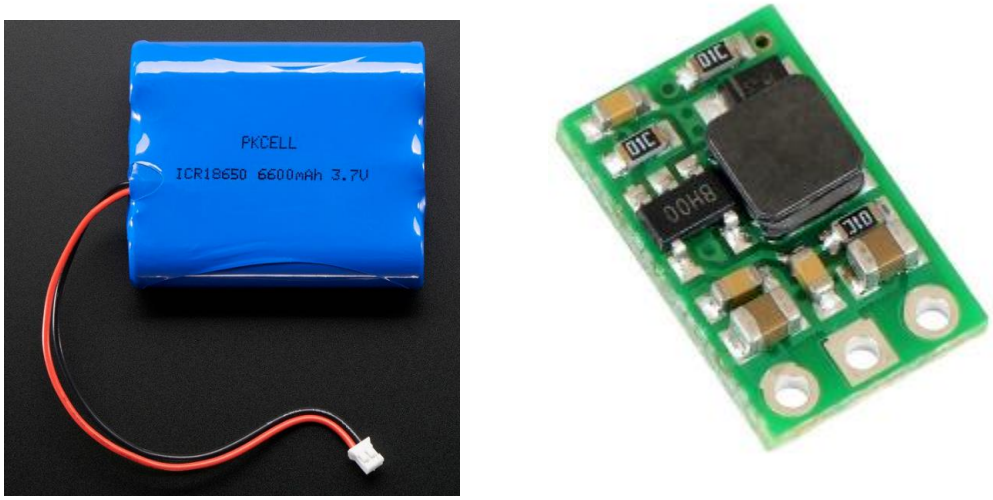

Figure 3.5: Adafruit 3.7V, 6600mAh lithium ion battery (left) and Polulu U3V12F12 12V step-up voltage regulator (right).

3.1.5.3 Analog to Digital (ADC) testing

To transform the output signal of the pressure transducer into a signal readable by the Electron microcontroller an analog to digital converter (ADC) is used. The ADS1115 (ADS1115, Texas Instruments) and MCP3424 (MCP3424, Microchip Technology) were chosen to test due to their low cost, high bit count (higher bit counts give more resolution), and availability of commercially made breakout boards (Figure 3.6).

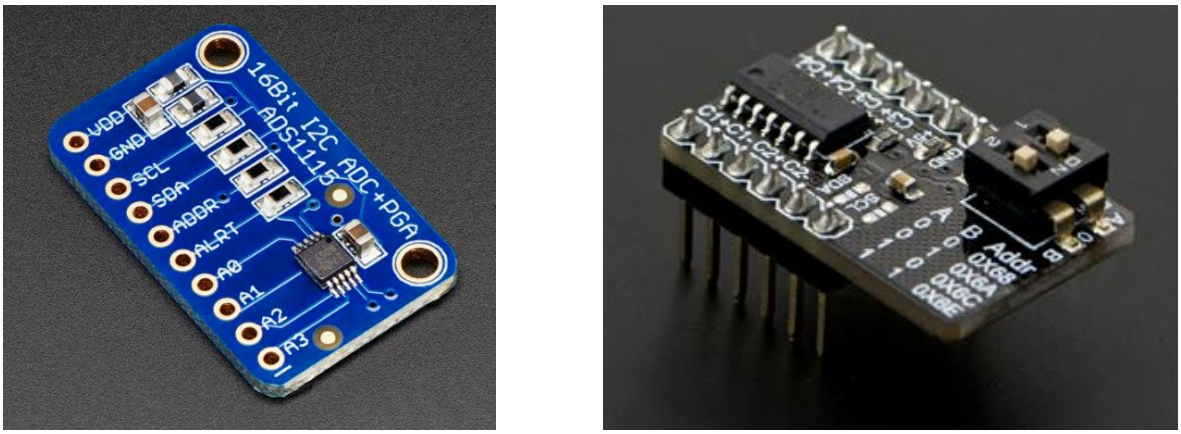

Figure 3.6: The ADS1115 breakout board (ADS1115 16-Bit ADC – 4 Channel with Programmable Gain Amplifier, Adafruit) is shown on the left and the MCP3424 breakout board (MCP3424 18-Bit ADC-4 Channel with Programmable Gain Amplifier for Raspberry Pi, DF Robot) is shown on the right.

To test the ADCs two identical, sealed pressure transducers were submerged in the same column of water and read with both ADCs. The pressure transducers were placed side-by-side and calibrated to read the DTW in the column for each ADC. Milliamp outputs of the pressure transducers were transformed into millivolt signals, readable by the ADCs using 100 Ohm, 0.1% tolerance shunt resistors. Differences in readings between each pressure transducer were compared over time for each ADC which allowed for the accuracy of the ADCs to be compared. Data from the ADC test can be found in Appendix A. Barometric pressure, room temperature, and water temperatures were also recorded during the experiment and examined afterwards to confirm stable testing conditions.

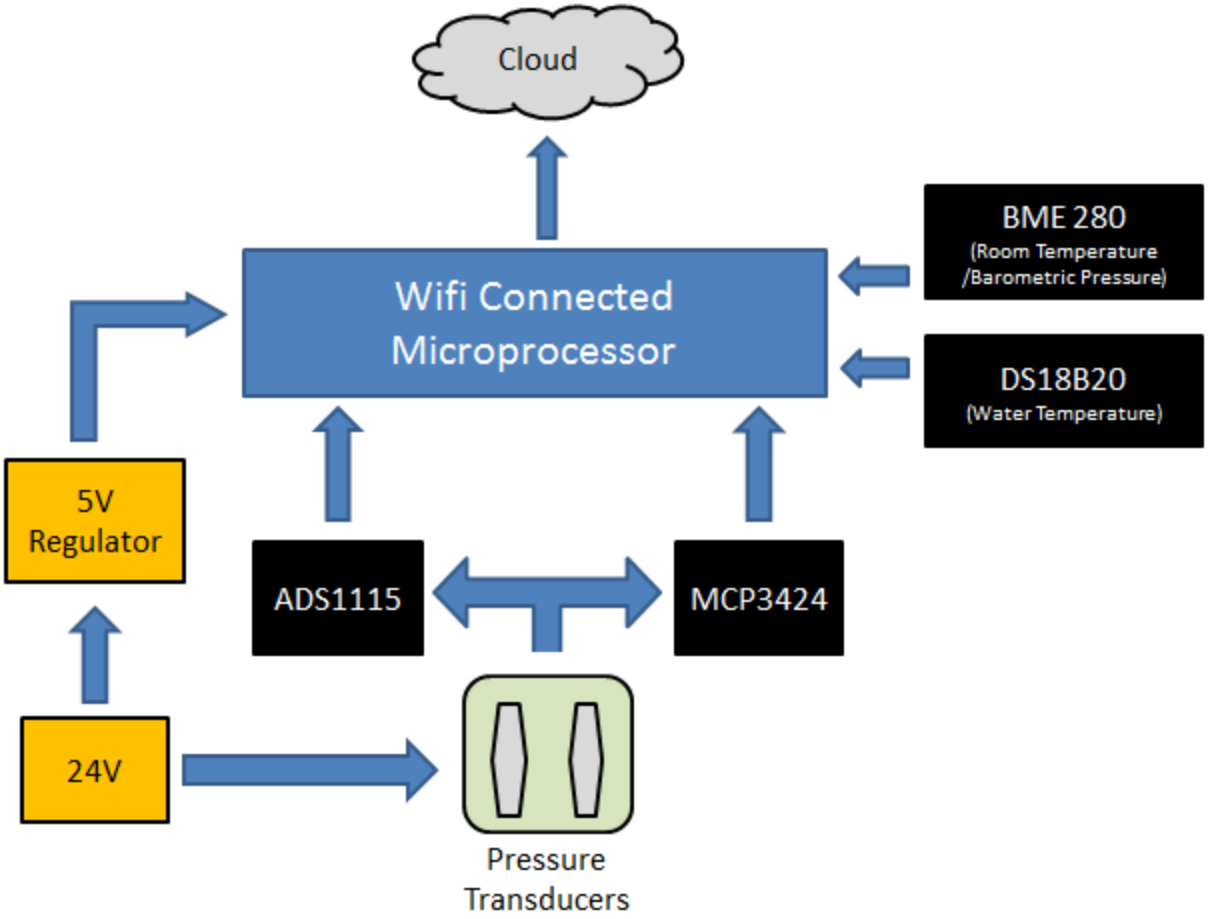

Figure 3.7: Block Diagram of circuit used for ADC testing and comparison.

3.1.5.4 Printed Circuit Board Development

Data from the ADC testing experiment shows the MCP3424 to out-perform the ADS1115 (this data available in Appendix A). The MCP3424 was therefore chosen to develop two printed circuit boards (PCBs) for reading pressure transducers with milliamp signal outputs. Each board uses an Electron microcontroller to send real-time data to the cloud. In addition, each board also stores data on a Micro SD Card for added data security and data backup. An on-board sensor (BME280, Bosh Sensortec) is used to gather barometric pressure data to correct sealed pressure transducers for barometric fluctuations. The BME280 is also used monitor enclosure temperature and humidity so alerts can be sent in real-time if enclosure conditions become adverse and

possibly lead to data logger damage. Figure 3.8 shows the *Cellular Connected PT Logger V2.1* which is designed to read up to four pressure transducers with milliamp signal outputs. Figure 3.9 shows the *Cellular Connected PT Logger V1.2* which is designed to read up to two pressure transducers with milliamp signal outputs. The *Cellular Connected PT Logger V1.2* also contains two I^2C ports to allow for the user to add additional sensors to the board which communicate via I^2C protocol. Both boards were designed using Eagle PCB design software. Designs were then sent to a PCB manufacturer (OSH Park) for fabrication.

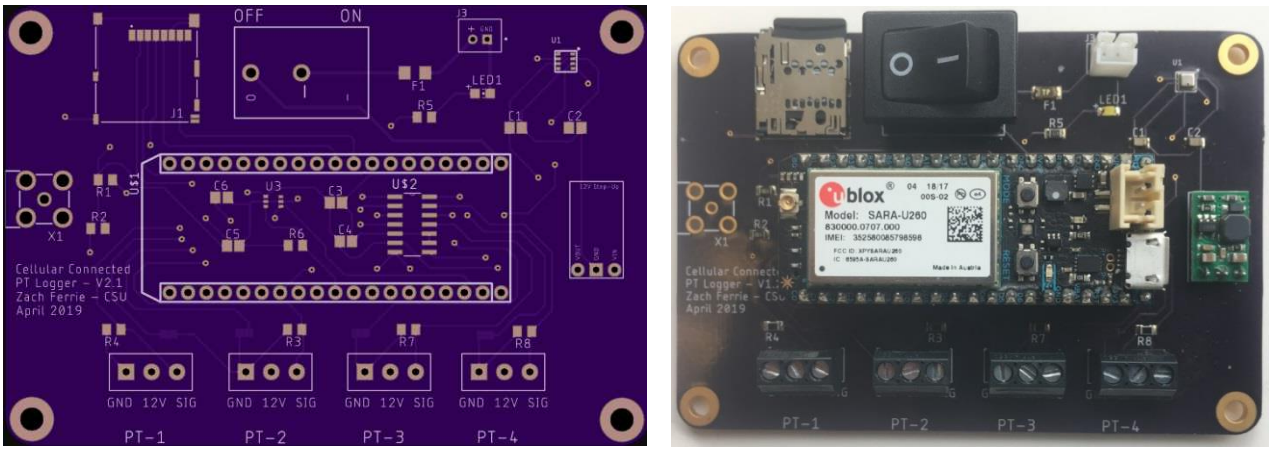

Figure 3.8: Cellular Connected PT Logger V2.1.

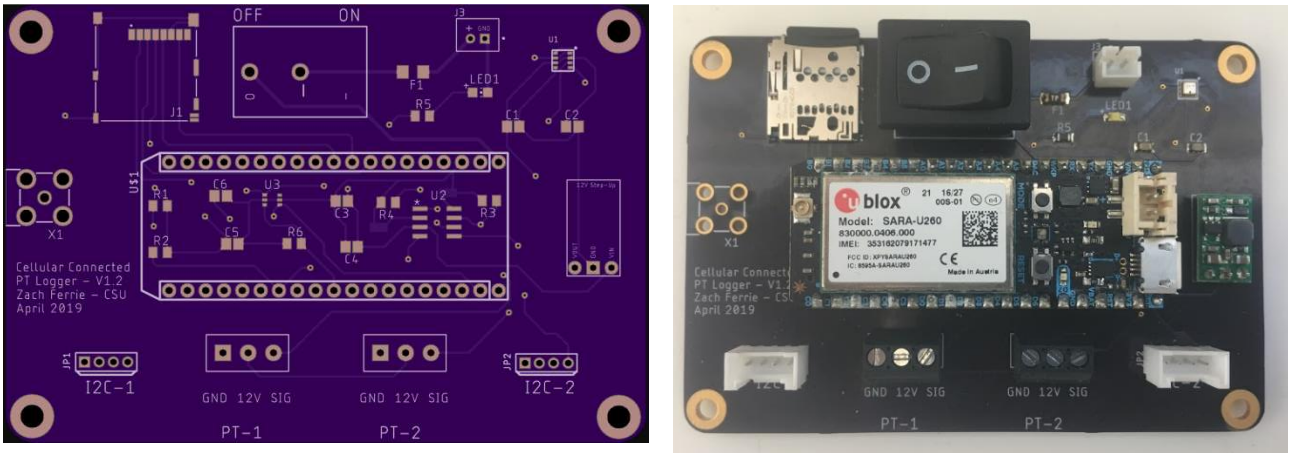

Figure 3.9: Cellular Connected PT Logger V1.2.

3.1.5.5 Cost Comparison for Custom Designed vs Commercially Available Data Acquisition Hardware

Table 3.2 provides a cost comparison for the cellular based data acquisition systems designed in this Thesis vs common, commercially available data acquisition systems for gathering groundwater head. The Cellular Connected PT Logger V1.2 provides a percent savings of approximately 30% when compared to the Onset pressure transducer and a percent savings of approximately 40% when compared to the Solinst pressure transducer. Additionally, the Onset and Solinst pressure transducers require manual data downloads of groundwater head unlike the Cellular Connected PT Logger V1.2 which sends groundwater head data to the cloud in real-time. The Cellular Connected PT Logger V1.2 provides a percent savings of approximately 90% when compared Campbell Scientific data acquisition system in Table 3.2 which is able to send groundwater head data via a cellular connection.

Table 3.2: Cost of components comparison of the Cellular Connected PT Logger V1.2 and Cellular Connected PT Logger V2.1 designed in this Thesis vs common, commercially available data acquisition systems for gathering groundwater head data. This is not an exhaustive list.

	Approximate Cost ($ US)	Equipment Included
Cellular Connected PT Logger V1.2	**340.00**	• **Modified FYD-101 Pressure Transducer with 17ft of cable** • **Cellular Connected PT Logger V1.2** • **Solar Panel, Battery, Solar Charge Regulator** • **Enclosure**
Cellular Connected PT Logger V2.1	**360.00**	• **Modified FYD-101 Pressure Transducer with 17ft of cable** • **Cellular Connected PT Logger V2.1** • **Solar Panel, Battery, Solar Charge Regulator Enclosure**
Campbell Scientific (Cellular Enabled Data Acquisition System)	**3,200.00**	• **CS451 Pressure Transducer with 17ft of cable** • **CR300 Cellular Enabled Data Logger and Antenna** • **Solar Panel and Battery** • **Enclosure**
Onset (Pressure Transducer Only)	**495.00**	• **HOBO Fresh Water Level Data Logger, Stainless Steel Housing (U2-001-0X)**
Solinst (Pressure Transducer Only)	**580.00**	• **Levelogger Edge (Model 3001)**

3.2 Measurement Validation and Reliability Testing

3.2.1 Pressure Transducer Calibration and Lab Testing

Before deployment each pressure transducer was calibrated and tested using a laboratory column where head can be systematically varied (Figure 3.10). A measuring tape was attached to the side of the column to allow for pressure transducer readings to be compared with visually determined head elevations. When calibration sheets were provided pressure transducers were tested against the provided calibration information to ensure the calibrations were correct. When not available, calibration was performed by fluctuating the head in the column and relating it to the pressure transducers output. In addition, before each installation, each set of pressure transducers were set in the same column of water and allowed to fluctuate with barometric pressure for a 24-hour period. Data was then compared among pressure transducers to ensure their outputs were in good agreement. Once deployed in the field, a manual head reading was taken at each well to apply a zero calibration (i.e. calculate Equation 3.3) to the pressure transducers.

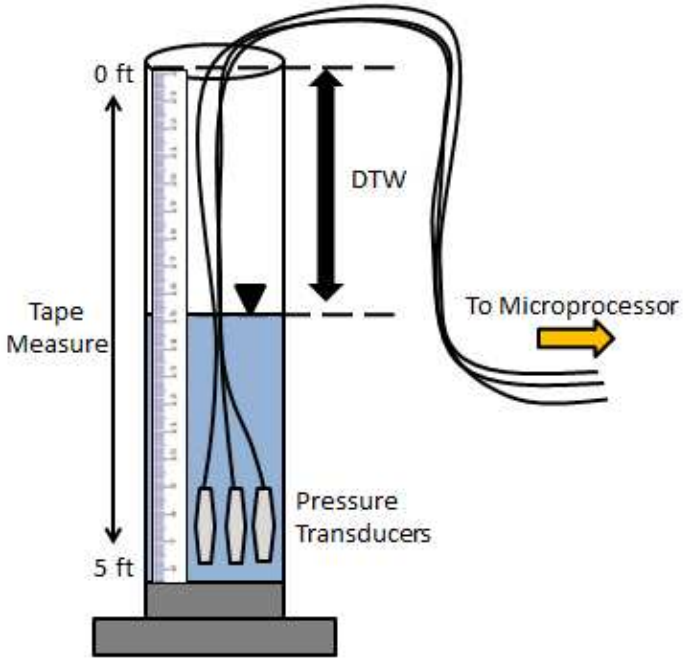

Figure 3.10: Pressure transducer calibration/testing column setup.

3.2.2 Field Testing Hardware

Two sites near Colorado State University were chosen to test the pressure transducers and supporting hardware. Table 3.3 shows the key attributes of each field site.

Table 3.3: Key attributes of hardware testing sites.

	Number of wells:	Number of pressure transducers per well:	Pressure transducer manufacturers:	Pressure transducer models:	Test type:
Gilcrest	**1**	**3**	**Volltel, Xi'an Feng Yu, Xi'an Yunyi**	**LV800, FYD-101, YD322**	**Vented pressure transducer drift testing**
ARDEC	**3**	**2**	**Xi'an Feng Yu, Solinst**	**FYD-101, Levelogger**	**Sealed pressure transducer drift testing**

Pressure transducer signal outputs can drift over time. Drifting occurs through drift in zero and/or span. A drift in zero occurs when the *Offset* value (Equation 3.3) changes. A drift in span occurs when the calibration curve changes (*Slope* in Equation 3.2).

Field testing was chosen over lab testing to asses long-term sensor drift since the effects of drift are often more significant in field settings than in lab settings. Temperature sensors were added to each testing system to measure water temperature at the location of the pressure transducers since temperature fluctuations can affect sensor output. (Sorensen and Butcher 2011)

3.2.2.1 Vented Pressure Transducer Testing

Research into pressure transducers revealed three vented models that met the desired specifications of accuracy, cost, and chemical resistance. To assess and compare the drift of these pressure transducers, all three pressure transducers were deployed in the same well (Figure 3.11) for a period of 6.5 months. For a period of 4.5 months during the study the head fell below the uppermost pressure transducer resulting in a period of unusable data. Usable sounder readings were obtained twice from the Gilcrest site to assess sensor drift in zero. Prior to

deployment a lab column of water was used to calibrate each pressure transducer. After field testing the pressure transducers were removed from the well and calibrated again using the same process to assess the sensors drift in span.

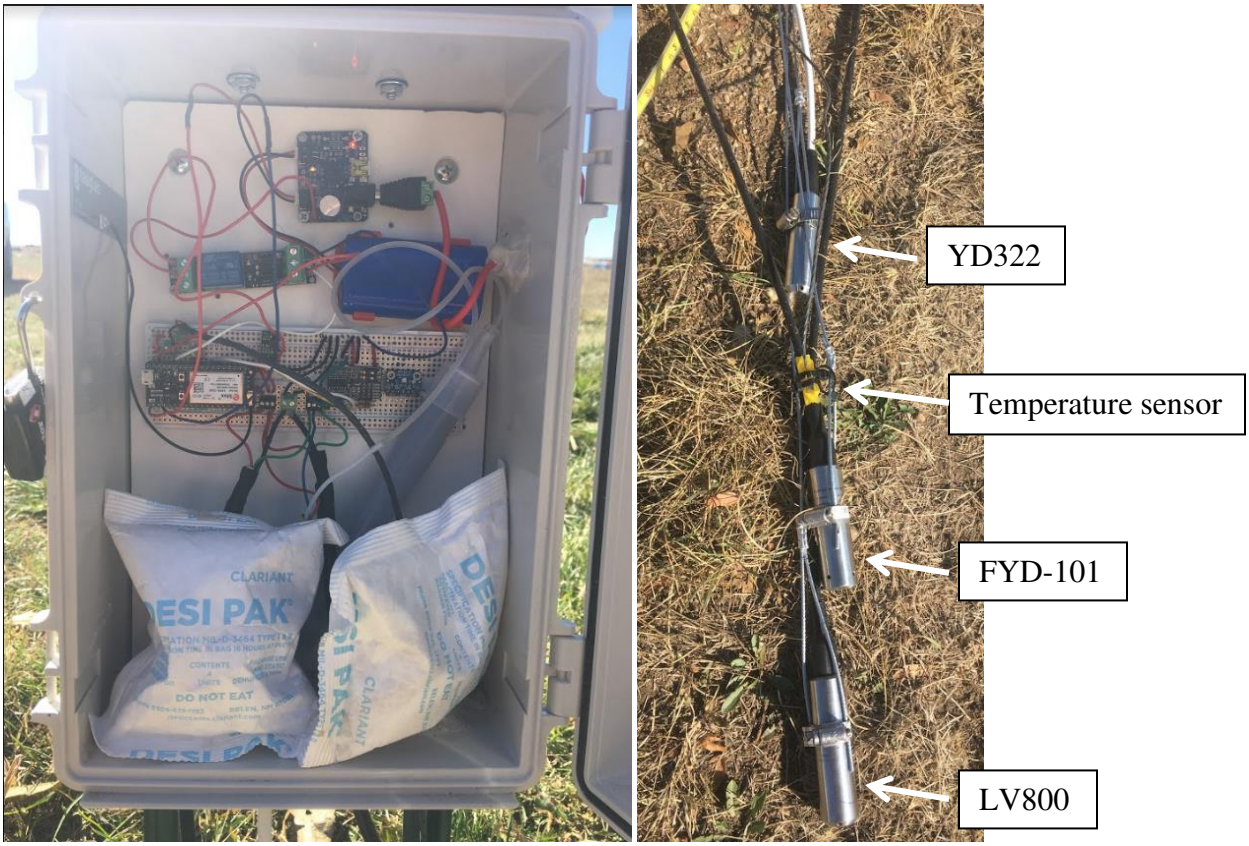

Figure 3.11: Installed testing system (left) and pressure transducer deployment (right) for the vented pressure transducer test.

3.2.2.2 Sealed Pressure Transducer Testing

The FYD-101 pressure transducer can be purchased without attached wire, allowing for the vented pressure transducer to be sealed following the processes described in Section 3.1.4. The YD322 (YD322, Xi'an Yunyi Instrument co.) and LV800 (LV800, Voltell) pressure transducers are not available to purchase without wire and therefore were not chosen for sealed testing. To assess the drift of the sealed/modified pressure transducers, three modified FYD-101s were placed in separate wells for a period of 6 months. Sounder readings were taken at the three wells on a monthly basis and then compared to the FYD-101 readings which were corrected for barometric pressure fluctuations using a BME280. In addition, a Levelogger (3001 LT F15/M5, Solinst) was placed in each well to compare the modified FYD-101s to a commercially designed, sealed pressure transducer (Figure 3.12). The Levelogger was also used to monitor water temperature in the well. At the end of the experiment the FYD-101s were submerged in a lab column of water to compare calibration curves of the pressure transducers before and after the field experiment.

Figure 3.12: Deployment of modified/sealed FYD-101 (top) and Leveloger (bottom).

3.3 Data Transforms

3.3.1 Transforming Head Data into Groundwater Flow Paths

Gathered head data is transformed into flow paths following the process described in Gao (2017). Using three head values a planar regression can be performed, resulting in a solution for the plane of elevation for the head surface (*Head* [L]) shown by Equation 3.6.

$$Head(x, y, t) = A(t)x + B(t)y + C \tag{3.6}$$

Here coefficients *A* [dimensionless] and *B* [dimensionless] represent the hydraulic gradients in the x and y-directions, respectively and *C* [L] is the head at the point when x and y are equal to zero. When stepping through time, the position of a groundwater flow path at a future time ($x_{(ti+1)}$ [L], $y_{(ti+1)}$ [L]) is estimated using Equations 3.7 and 3.8.

$$x_{(t_{i+1})} = \frac{-K * A(t_i)}{n_e} * (t_{i+1} - t_i) + x_{(t_i)} \tag{3.7}$$

and

$$y_{(t_{i+1})} = \frac{-K * B(t_i)}{n_e} * (t_{i+1} - t_i) + y_{(t_i)} \tag{3.8}$$

where, $(t_{i+1} - t_i)$ [T] represents the time step, *K* [L/T]

\is the hydraulic conductivity, n_e [dimensionless] is the effective porosity, and $x_{(t_i)}$ and $y_{(t_i)}$ represent the position of the end of the groundwater flow path at time step *i*.

The initial position of the groundwater flow path (x_o [L], y_o [L]) is set using Equation 3.9.

$$(x_o = \frac{x_{well1} + x_{well2} + x_{well3}}{3} \ , \ y_o = \frac{y_{well1} + y_{well2} + y_{well3}}{3}) \tag{3.9}$$

where, x_{well1} , x_{well2} , and x_{well3} [L] represent the x-coordinate locations of each well and y_{well1} , y_{well2} , and y_{well3} [L] represent the y-coordinate locations of each well.

3.3.2 Estimating the Effect of Measurement Error on Groundwater Flow Paths

Results from Devlin and McElwee (2007) revealed that errors in head measurements can have effects on hydraulic gradient estimates. Based on this research an algorithm was developed to determine the effect of measurement error on groundwater flow directions and seepage velocities.

Equation 3.10 shows that the water table elevation is both a function of the measurement of the DTW and the measurement of the elevation of the TOC reference point.

$$W_{elev}(t) = TOC(t) - DTW(t) \tag{3.10}$$

As such, there are two sources of measurement error when obtaining a head value to use in the advancement of the groundwater flow path. Following Devlin and McElwee's (2007) interpretation of Bevington (1992) error in DTW and TOC measurements can be combined into a single value (e_h [L]) using Equation 3.11.

$$e_h = \sqrt{(e_{TOC})^2 + (e_{DTW})^2} \tag{3.11}$$

where, e_{TOC} [L] represents the measurement accuracy quoted by the manufacturer for the survey equipment being used and e_{DTW} [L] represents the measurement accuracy quoted by the manufacturer for the pressure transducer being used. In this Thesis e_{TOC} values are obtained from the datasheet provided by Topcon for their HiPer VR survey instrument and e_{DTW} values

are obtained from the datasheet provided by Xi'an Feng Yu for their FYD-101 pressure transducers.

To estimate the effect of measurement error (e_h) on groundwater flow paths, a synthetic data set is created using the following steps. First, different random error values are generated at each of the three well locations (E_{rand1} [L], E_{rand2} [L], E_{rand3} [L]) where head data is being gathered. Random error values are constrained within the bounds of $\pm e_h$. Constraining the random error values within the bounds of $\pm e_h$ is achieved using Equations 3.12-3.14.

$$E_{rand1}(n) = e_h * rand_{z1}(n) \tag{3.12}$$

$$E_{rand2}(n) = e_h * rand_{z2}(n) \tag{3.13}$$

$$E_{rand3}(n) = e_h * rand_{z3}(n) \tag{3.14}$$

where, $rand_{z1}$, $rand_{z2}$, and $rand_{z3}$ [dimensionless] represent uniform random numbers generated between -1 and 1 and n [dimensionless] represents the desired number of values in the synthetic dataset.

For each n, a plane is fit to the random error values to acquire a solution for the planar surface (E_{surf} [L]).

$$E_{surf}(x, y, n) = A_e(n)x + B_e(n)y + C_e \tag{3.15}$$

Coefficients A_e and B_e are then stored in an array. This process repeated until n number of A_e and B_e values have been generated. In this study 1,000 values of A_e and B_e are generated (i.e. n = 1,000) so the data follows a normal distribution based on the Central Limit theorem. In order to

calculate the average ($\overline{A_e}$ [L], $\overline{B_e}$ [L]) and standard deviation (σ_{Ae} [L], σ_{Be} [L]) of the error based planar surfaces in the x and y-directions Equations 3.16 and 3.17 are used.

$$\overline{A_e} = \frac{1}{n}\sum_{i=1}^{n} A_{ei} \quad , \quad \overline{B_e} = \frac{1}{n}\sum_{i=1}^{n} B_{ei} \tag{3.16}$$

and

$$\sigma_{A_e} = \sqrt{\frac{1}{n-1} * \sum_{i=1}^{n} |A_{ei} - \overline{A_e}|^2} \quad , \quad \sigma_{B_e} = \sqrt{\frac{1}{n-1} * \sum_{i=1}^{n} |B_{ei} - \overline{B_e}|^2} \tag{3.17}$$

To account for the effect of e_h on hydraulic gradients in the x and y-directions ($A_{95.low}$/$A_{95.high}$ [L] and $B_{95.low}$/$B_{95.high}$ [L], respectively) Equations 3.18 and 3.19 are used. Equations 3.18 and 3.19 assume that the synthetic dataset is normally distributed.

$$A_{95.low} = -1.96 * \sigma_{A_e} \quad , \quad B_{95.low} = -1.96 * \sigma_{B_e} \tag{3.18}$$

and

$$A_{95.high} = +1.96 * \sigma_{A_e} \quad , \quad B_{95.high} = +1.96 * \sigma_{B_e} \tag{3.19}$$

In Equations 3.18 and 3.19 σ_{Ae} and σ_{Be} are multiplied by 1.96 in order to encompass 95% of the possible outcomes of the simulation. A model was created using Equations 3.12-3.19 to estimate effect of e_h on flow groundwater flow directions and seepage velocities. Figure 3.13 provides a flow chart that illustrates how the model operates.

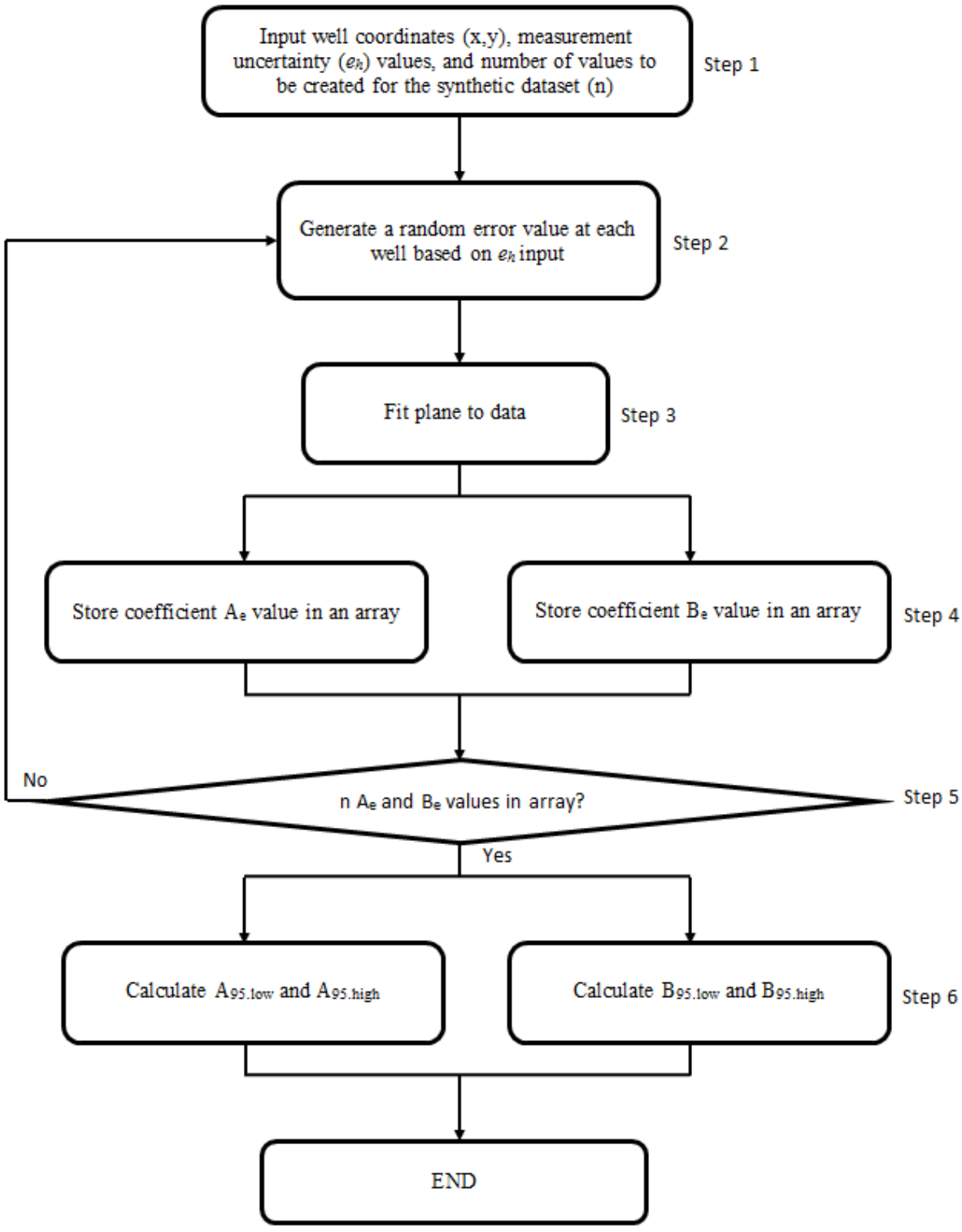

Figure 3.13: Flow chart outlining the steps needed to calculate the effect of measurement error on groundwater flow direction and seepage velocity.

After obtaining the 95% confidence interval results, the estimated and measurement error effected groundwater flow paths are advanced using the following equations. To advance the lower 95% confidence interval path ($x_{95.low(ti+1)}$ [L], $y_{95.low(ti+1)}$ [L]) Equations 3.20 and 3.21 are used.

$$x_{95.low(t_{i+1})} = \frac{-K*(A(t_i)+A_{95.low})}{n_e} * (t_{i+1} - t_i) + x_{95.low(t_i)} \quad (3.20)$$

and

$$y_{95.low(t_{i+1})} = \frac{-K*(B(t_i)+B_{95.low})}{n_e} * (t_{i+1} - t_i) + y_{95.low(t_i)} \quad (3.21)$$

where, $x_{95.low(t_i)}$ and $y_{95.low(t_i)}$ represent the current coordinates of the lower 95% confidence interval path.

To advance the upper 95% confidence interval path ($x_{95.high(ti+1)}$ [L], $y_{95.high(ti+1)}$ [L]) Equations 3.22 and 3.23 are used.

$$x_{95.high(t_{i+1})} = \frac{-K*(A(t_i)+A_{95.high})}{n_e} * (t_{i+1} - t_i) + x_{95.high(t_i)} \quad (3.22)$$

and

$$y_{95.high(t_{i+1})} = \frac{-K*(B(t_i)+B_{95.high})}{n_e} * (t_{i+1} - t_i) + y_{95.high(t_i)} \quad (3.23)$$

where, $x_{95.high(t_i)}$ and $y_{95.high(t_i)}$ represent the current coordinates of the upper 95% confidence interval path. A model was created that resolves the errors in groundwater flow directions and seepage velocity about the estimated groundwater flow path. Figure 3.14 provides a flow chart that illustrates the use of Equations 3.7, 3.8, and 3.20-3.23 to advance the estimated, lower, and upper 95% confidence interval flow paths.

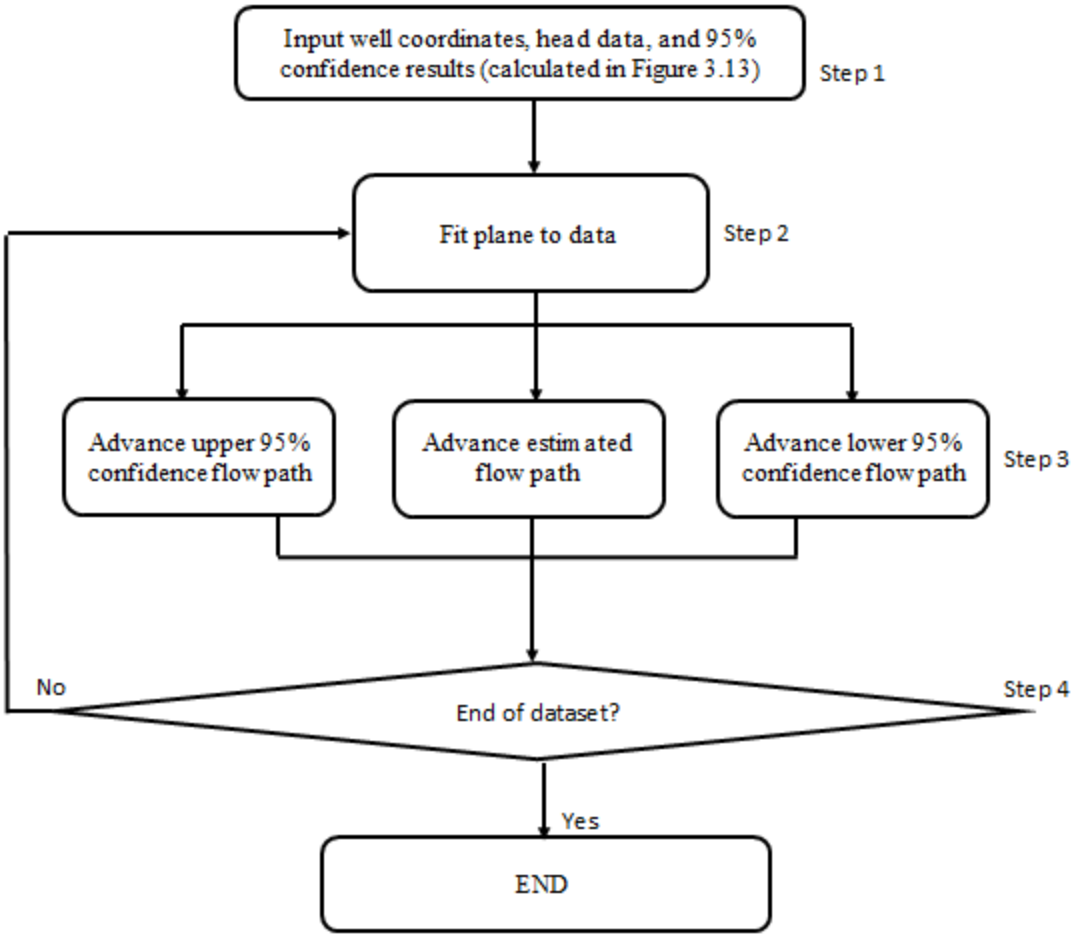

Figure 3.14: Flow chart outlining the steps to advance the estimated and measurement error affected flow paths.

To check the model for validity, hand calculations were performed using Kramer's rule and a synthetic dataset to compare modeled vs expected results. The results confirmed model validity and can be found in Appendix A.

To determine the angle between the estimated and 95% confidence interval flow paths (Θ [degrees]) Equation 3.24 is used.

$$\theta = tan^{-1}\left|\frac{m_{est}-m_{95}}{1+m_{est}*m_{95}}\right| \tag{3.24}$$

where, m_{est} [L/L] is the x/y slope of the estimated flow path and m_{95} [L/L] is the x/y slope of the 95% confidence interval path (Equation 3.24 is valid for both the upper and lower 95% confidence interval paths for measurement error and anisotropy uncertainty effected flow paths – further explained in Section 3.3.3). Note that to gain the angle between both 95% confidence interval paths and the estimated path Equation 3.24 must be used twice to account for the angle variation on each side of the estimated (without error) flow path.

3.3.3 Estimating the Effect of Uncertainty in Horizontal Anisotropy on Flow Paths

Getzen (1983) studied anisotropy in different sedimentary environments finding a horizontal anisotropy factor [dimensionless] of 1.19:1.0, where 1.19 is assumed to be in the direction of deposition and 1.0 is perpendicular to the direction of deposition. Using 1.19 as the estimated anisotropy factor, a synthetic data set is created to account for the possible error in this estimation. This synthetic data set is created using the following steps.

First, the smoothing factor (p [dimensionless]) is chosen. The smoothing factor determines the number of randomly generated values of the anisotropy factor that will be averaged together to create each n value in the synthetic dataset. The purpose of the smoothing factor is to create a normally distributed synthetic dataset. Without the smoothing factor the synthetic dataset would be uniformly distributed. Using Equation 3.25, p number of random, synthetic anisotropy factors (λ_{rand} [dimensionless]) are created and averaged.

$$\lambda_{rand}(p) = 1.0 + 0.38 * \frac{1}{p}\sum_{i=1}^{p} rand_i \tag{3.25}$$

where, $rand$ [dimensionless] represents a uniformly distributed, randomly generated number between 0-1. In Equation 3.25 the numbers 1.0 and 0.38 function to set 1.0 and 1.38 as the minimum and maximum values of the anisotropy factor that can be randomly generated for the

synthetic dataset. The numbers 1.0 and 0.38 were chosen so the average value of the anisotropy factor represents the estimated value of 1.19 and no synthetic anisotropy factor is simulated below 1.0.

After an array of n (n = 1,000 – same as the measurement error synthetic dataset) number of synthetic anisotropy factors are created, the average ($\bar{\lambda}$ [dimensionless]) and standard deviation (σ_λ [dimensionless]) of the anisotropy factor array are calculated using Equations 3.26 and 3.27.

$$\bar{\lambda} = \frac{1}{n}\sum_{i=1}^{n}\lambda_i \tag{3.26}$$

and

$$\sigma_\lambda = \sqrt{\frac{1}{n-1}\sum_{i=1}^{n}\left|\lambda_i - \bar{\lambda}\right|^2} \tag{3.27}$$

Equations 3.28 and 3.29 are used to gain the lower ($\lambda_{95.low}$ [dimensionless]) and upper ($\lambda_{95.high}$ [dimensionless]) 95% confidence intervals for the synthetic dataset of normally distributed anisotropy factors.

$$\lambda_{95.low} = \bar{\lambda} - 1.96 * \sigma_\lambda \tag{3.28}$$

and

$$\lambda_{95.high} = \bar{\lambda} + 1.96 * \sigma_\lambda \tag{3.29}$$

In Equations 3.28 and 3.29 σ_λ is multiplied by 1.96 in order to encompass 95% of the possible outcomes of the simulation. A model was created to use Equations 3.25-3.29 to estimate the effect of uncertainty in anisotropy on groundwater flow directions and seepage velocities. Figure 3.15 provides a flow chart that illustrates how the model operates.

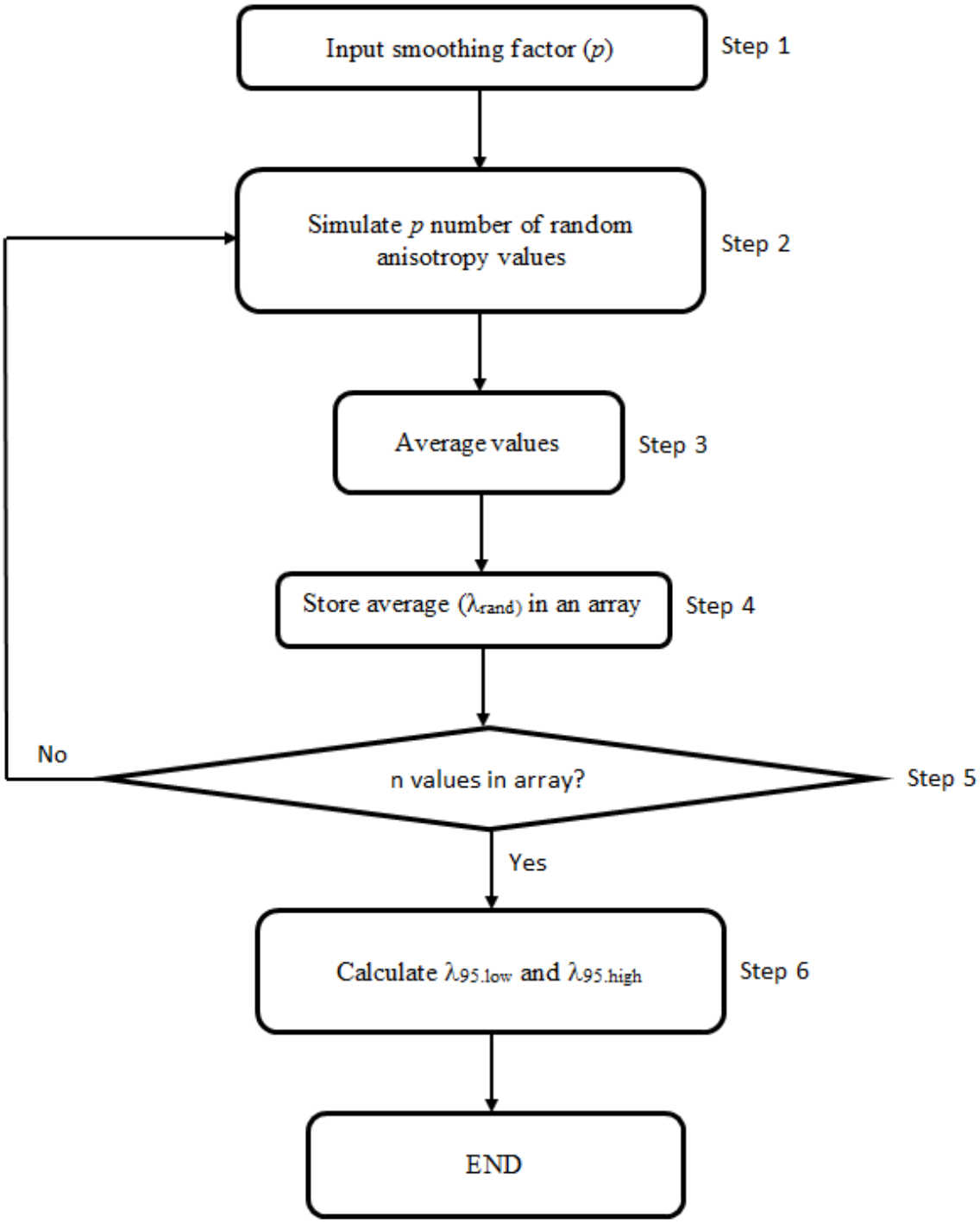

Figure 3.15: Flow chart outlining the steps taken to calculate the effect of horizontal anisotropy uncertainty on groundwater flow directions and seepage velocities.

After obtaining the 95% confidence interval results, the estimated and anisotropy uncertainty effected flow paths can be advanced. The anisotropy factor is only applied to flow in the primary direction of deposition (either the x or y direction) at a given site. If the primary direction of deposition is in the x-direction Equations 3.30 and 3.31 are used.

$$x_{Aniso.95.low(t_{i+1})} = \frac{-K * \lambda_{95.low} * A(t_i)}{n_e} * (t_{i+1} - t_i) + x_{Aniso.95.low(t_i)} \quad (3.30)$$

and

$$x_{Aniso.95.high(t_{i+1})} = \frac{-K * \lambda_{95.high} * A(t_i)}{n_e} * (t_{i+1} - t_i) + x_{Aniso.95.high(t_i)} \quad (3.31)$$

where, $x_{Aniso.95.low(t_i)}$ [L] and $x_{Aniso.95.high(t_i)}$ [L] represent the current x-coordinates of the lower and upper 95% confidence interval paths, respectively.

If the primary direction of deposition is in the y-direction Equations 3.32 and 3.33 are used.

$$y_{Aniso.95.low(t_{i+1})} = \frac{-K * \lambda_{95.low} * B(t_i)}{n_e} * (t_{i+1} - t_i) + y_{Aniso.95.low(t_i)} \quad (3.32)$$

and

$$y_{Aniso.95.high(t_{i+1})} = \frac{-K * \lambda_{95.high} * B(t_i)}{n_e} * (t_{i+1} - t_i) + y_{Aniso.95.high(t_i)} \quad (3.33)$$

where, $y_{Aniso.95.low(t_i)}$ [L] and $y_{Aniso.95.high(t_i)}$ [L] represent the current y-coordinates of the lower and upper 95% confidence interval paths, respectively.

The flow path with the estimated anisotropy is advanced using Equation 3.34 or 3.35.

$$x_{Aniso(t_{i+1})} = \frac{-K * \overline{\lambda} * A(t_i)}{n_e} * (t_{i+1} - t_i) + x_{Ansio(t_i)} \quad (3.34)$$

or

$$y_{Aniso(t_{i+1})} = \frac{-K * \bar{\lambda} * B(t_i)}{n_e} * (t_{i+1} - t_i) + y_{Aniso(t_i)} \quad (3.35)$$

where, $x_{Aniso(t_i)}$ [L] and $y_{Aniso(t_i)}$ [L] represent the current x and y-coordinates of the estimated flow path, respectively. A model was created that resolves the errors in groundwater flow directions and seepage velocity about the groundwater flow path advanced using the estimated anisotropy factor (1.19:1.00). This model operates just as the measurement error model (Figure 3.14) except it uses the 95% confidence interval results calculated in Figure 3.15 instead of the 95% confidence interval results calculated in Figure 3.13. Table 3.4 shows which equations are used to advance the groundwater flow paths that use the estimated anisotropy factor and 95% confidence interval anisotropy factors (i.e. accounts for anisotropy uncertainty) given the primary direction of deposition at a given site.

Table 3.4: Table illustrating equations used to advance the estimated and 95% confidence interval anisotropy uncertainty paths, based on the primary direction of deposition at a site.

	Primary Direction of Deposition in the X-Direction	**Primary Direction of Deposition in the Y-Direction**
Estimated Groundwater Flow Path	**Equation 3.34 and Equation 3.8**	**Equation 3.7 and Equation 3.35**
Low 95% Confidence Interval Anisotropy Uncertainty Effected Flow Path	**Equation 3.30 and Equation 3.8**	**Equation 3.7 and Equation 3.32**
High 95% Confidence Interval Anisotropy Uncertainty Effected Flow Path	**Equation 3.31 and Equation 3.8**	**Equation 3.7 and Equation 3.33**

3.3.4 Colored Visualizations of Flow Path Seepage Velocity

To visualize the seepage velocity of the groundwater flow path a color gradient based on the colors of a stoplight is used. This color gradient is used to color the plotted coordinates of the

estimated flow path, based on the average daily seepage velocity. Table 3.5 shows the seepage velocities associated with each color of the stoplight. This velocity to color scheme is standard across all sites and can be seen in Figure 3.16. Note that the color gradient fades based on a log scale between the values in Table 3.5.

Table 3.5: Table of colors used for visualizing seepage velocities.

Color	Seepage Velocity (ft/day):
Green	10
Yellow	1
Red	10^{-1}

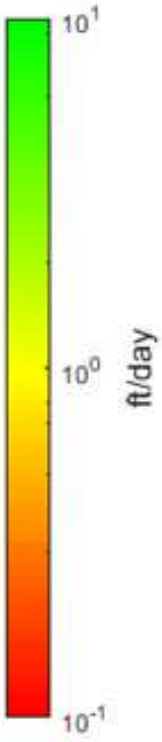

Figure 3.16: Color gradient bar used for visualizing groundwater flow path seepage velocity.

Average daily seepage velocity ($\bar{v}$ [L/T]) is calculated using Equation 3.36.

$$\bar{v} = \frac{1}{k}\sum_{i=1}^{k}\sqrt{v_x^2 + v_y^2} \tag{3.36}$$

where, k [dimensionless] represents the number of samples taken over the course of the day and v_x [L/T] and v_y [L/T] represent the seepage velocities in the x and y-directions, respectively. Note that $\bar{V}$ has dimensions of [L/T] but must have units of [ft/day] in order to compare it to the color gradient bar in Figure 3.16.

3.4 Field Sites and Monitoring Well Networks for Data Transformations

3.4.1 Monitoring Well Networks

Work by Devlin and McElwee (2007) revealed that the placement of wells in a monitoring network has an effect on the accuracy of hydraulic gradient estimates. Here the primary well layouts and assumptions used for the chosen field sites are covered. More information on the results of Devlin and McElwee (2007) can be found in Section 2.5.1.

Figure 3.17 shows the simplest form of a monitoring well network. In Figure 3.17 three wells are laid out in a single triangle. The well locations and head values from each well are used to estimate the gradient magnitude and direction for the area inside the triangle.

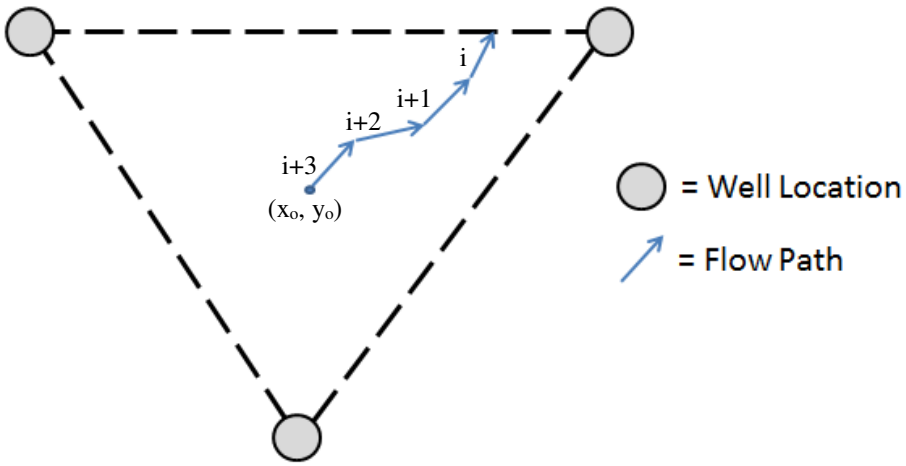

Figure 3.17: Single triangle monitoring well network.

By adding more monitoring wells to the monitoring well network, additional flow paths can be drawn. When using more than three wells, the three wells that make up the points of each triangle are used to obtain the gradient inside that triangle. Figure 3.18 shows an example of this concept. Since groundwater gradients are a continuum, flow paths are terminated if they exit either the monitored area or enter a triangle different form their origin.

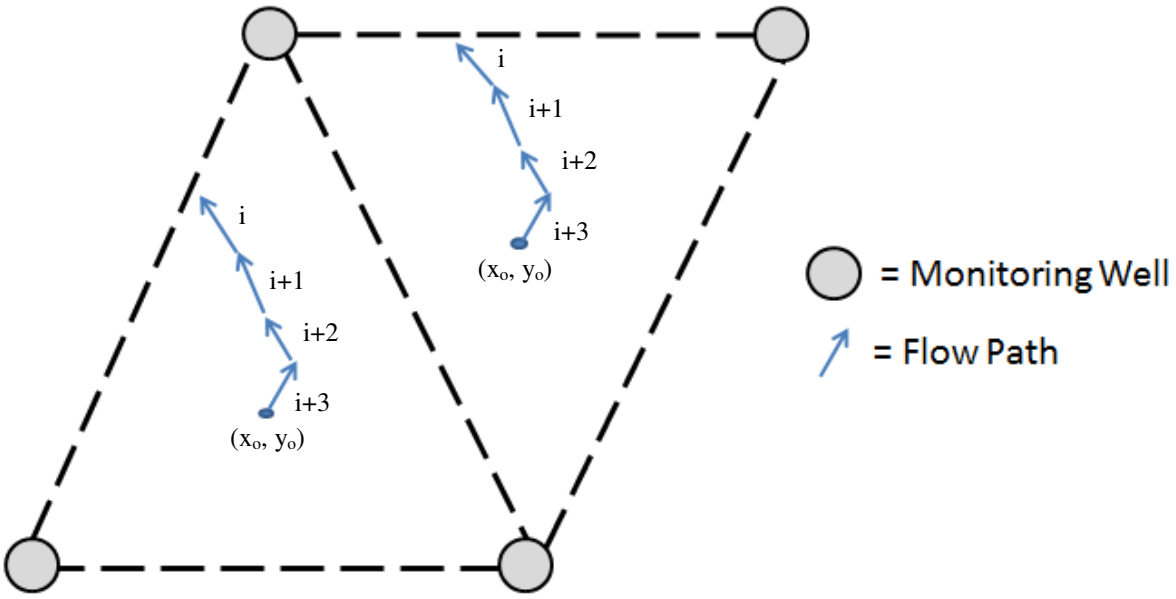

Figure 3.18: Two flow paths created by adding an additional well to the monitoring well network shown in Figure 3.17.

3.4.1.1 Assumptions for Monitoring Well Networks

When advancing the flow paths the following assumptions are made

1. Homogenous aquifer
2. Aquifer is either isotropic or anisotropic in the x and y-directions
3. Vertical flow is not significant
4. Flow conditions are steady state between sampling events

5. The fitting of a plane across head values accurately describes the head gradient in the x and y-directions
6. The effects of barometric pressure are common at all wells at each site, negating the need for barometric correction of head values (done to avoid additional measurement error associated with barometric pressure sensors)
7. The accuracy of the pressure transducers and surveying equipment accurately depict the possible measurement error in head
8. The density of the fluid is essentially equal to the density of freshwater

3.4.2 Field Sites for Data Transformations

Four field sites were used to demonstrate the described techniques. Key attributes of these sites are presented in Table 3.6.

Table 3.6: Key attributes of field sites used for demonstrating techniques to visualize the effects of measurement error and anisotropy uncertainty on groundwater flow direction.

	Geologic setting:	Number of wells:	Pressure transducer range (ft):	Hydraulic conductivity (ft/day):	Effective porosity (dimensionless):	Monitoring well network type:	Measurement Error Range (ft):	Anisotropy Uncertainty Range (dimensionless):
ARDEC	**Braided Stream**	**3**	**0-11.5**	**288**	**0.25**	**Single triangle**	**± 0.039**	**1.0 – 1.38**
ERC	**Eolian**	**3**	**0-11.5**	**0.288**	**0.40**	**Single triangle**	**± 0.039**	**1.0 – 1.38**
Site A	**Glacial-Fluvial**	**3**	**0-20/0-15**	**28.8**	**0.30**	**Single triangle**	**± 0.04 (for 0-20ft range)/ ± 0.038 (for 0-15ft range)**	**1.0 – 1.38**
Site B	**Braided Stream**	**4**	**0-11.5**	**28.8**	**0.25**	**Two triangles**	**± 0.039**	**1.0 – 1.38**

3.5 Dashboard Functionality and Visualization of Raw and Transformed Field Data

Raw data is sent from the Electron microprocessors to Ubidots (IoT platform) for visualization. Using Windows Task Scheduler (Microsoft) a computer was programmed to pull raw data in from Ubidots every hour and run a MATLAB program which transforms and sends data back to Ubidots for visualization. Additionally, dashboard features include videos of flow flags and automated alerts. The code mentioned in Section 3.5 can be found in Appendices A and B.

3.5.1 Dashboard Video Visualization of Data

For the ARDEC site videos of flow paths are uploaded to Ubidots (Figure 3.19). Creating and uploading videos of flow paths is achieved using MATLAB to create GIF files of the flow paths and then manually upload them to a free GIF hosting website (giphy.com). Videos are then linked to Ubidots so they can be viewed on the ARDEC dashboard. In order to be able to view the videos on Ubidots they have to be made publicly available on giphy.com. For this reason videos are not displayed on Ubidots dashboards where site data is considered private.

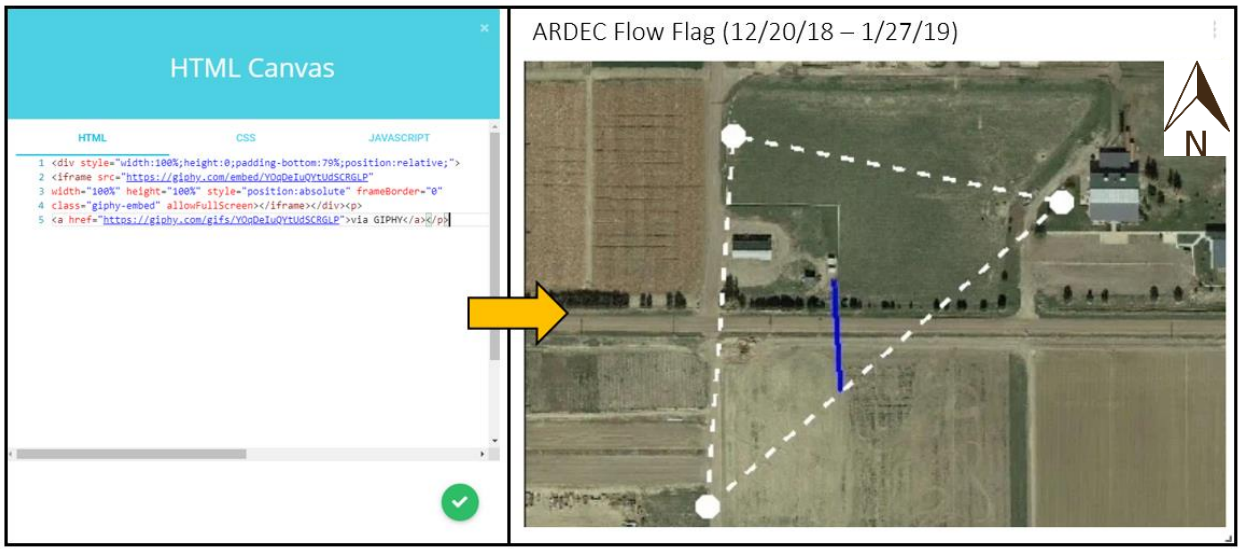

Figure 3.19: Ubidots HTML canvas *Widget* (left) used to upload flow flag videos (right) to the dashboard from a third party website (giphy.com).

3.5.2 Automated Alerts

Figure 3.20 shows an example of the Ubidots *Events* functionality for sending real-time alerts. The uppermost box in Figure 3.20 shows a hydrograph of groundwater head elevation at location where real-time groundwater head data is collected at Site B. Site B is an active oil and gas refinery where groundwater contaminants are present. A containment barrier wall has been built around the site to prevent groundwater contaminants from reaching public water supplies. If the groundwater head elevation rises above the height of the contaminant barrier wall, groundwater contaminants can potentially be transported out of the site boundaries and reach public water supplies. The red line in the hydrograph represents a hypothetical height of the contaminant barrier wall. Using the Ubidots *Events* functionality an alert was set to send an email if the groundwater head elevation rose above the hypothetical height of the contaminant barrier wall. The bottom box in Figure 3.20 shows the resulting email that was sent in real-time to warn users of potentially adverse site conditions.

Figure 3.20: Example of a real-time alert using the Ubidots *Events* functionality. The uppermost box shows a hydrograph at a real-time data acquisition location at Site B. The red line in the hydrograph shows a hypothetical height of the contaminant barrier wall at Site B used to prevent the groundwater contaminants at Site B from reaching the public water supply. The bottom graph shows an example of an email that was sent in real-time as a result of the groundwater head elevation exceeding the hypothetical height of the containment barrier wall at Site B.

CHAPTER 4 – RESULTS AND DISCUSSION

The following chapter provides results and discussion for this study. First, insights from pressure transducer field testing are reviewed. Next, the effects errors in head measurements and anisotropy have on groundwater flow directions and seepage velocities are addressed. Lastly, a dashboard display is presented.

4.1 Pressure Transducer Comparison Test Results

Section 4.1 provides results and discussion for the pressure transducer field tests. First, the results for drift in the unmodified vented pressure transducers are covered. Next, the results for drift in the modified sealed pressure transducers are discussed. Finally, the effects of pressure transducer drift on predicted groundwater flow directions and seepage velocities are addressed.

4.1.1 Vented Pressure Transducer Drift Testing Results

At the end of the 6.5 month study at Gilcrest a water level sounder reading was taken and compared to the head read by the pressure transducers to determine their drift in zero (deviation from true head). To determine the drift in pressure transducer span (the slope of the calibration curve) the pressure transducers were removed at the end of the study and re-calibrated following the steps outlined in Section 3.2.1. The new calibration slopes were then compared to the original calibration slopes to assess the drift in span. The results of vented pressure transducer drift study are found in Table 4.1.

Table 4.1: A comparison of the drift in zero and span for the three, vented pressure transducer models over a 6.5 month period.

	Drift in Zero (ft)	Drift in Span (mV/ft)
YD322 (Xian Yunyi)	**0.056**	**2.66**
LV800 (Voltell)	**0.028**	**0.95**
FYD-101 (Xian Feng Yu)	**0.018**	**0.36**

The FYD-101 drifted the least out of the three pressure transducers both in drift in zero and drift in span. These results support the continued use of the FYD-101 over the other pressure transducers tested. As mentioned in Section 3.2.2.1 the water table fell below the uppermost pressure transducer resulting in 4.5 months of unusable data during the 6.5 month study. As a result the dataset used to determine the drift in zero for the vented pressure transducers is too small to reach definitive conclusions. The Gilcrest results are included because they aid in understating the results presented in the following section.

4.1.2 Sealed Pressure Transducer Drift Field Testing Results

Additional tests were conducted at ARDEC to assess drift in the FYD-101s to see if the modification of sealing the pressure transducers caused an increase in their tendency to drift. These results were compared to the drift of Solinst Levelogger pressure transducers to test the performance of the modified FYD-101s to a well-known commercial standard. Using barometric pressure data from the sensor (BME280) integrated into the data acquisition system sealed pressure transducer readings were corrected for fluctuations in barometric pressure. Corrected heads were then compared to water level sounder readings which are considered to represent the true head. The BME280 has an accuracy of ±0.03 ft H_2O. The BME280 accuracy was subtracted from the drift in readings to get a more representative result of the drift of the pressure transducers and not the effect of the accuracy of the BME280. If subtracting the BME280 accuracy from the pressure transducer drift resulted in a negative number (i.e. a better than 100% accuracy) the drift was assumed to be zero. Figures 4.1-4.3 show a comparison between pressure transducer and water level sounder readings.

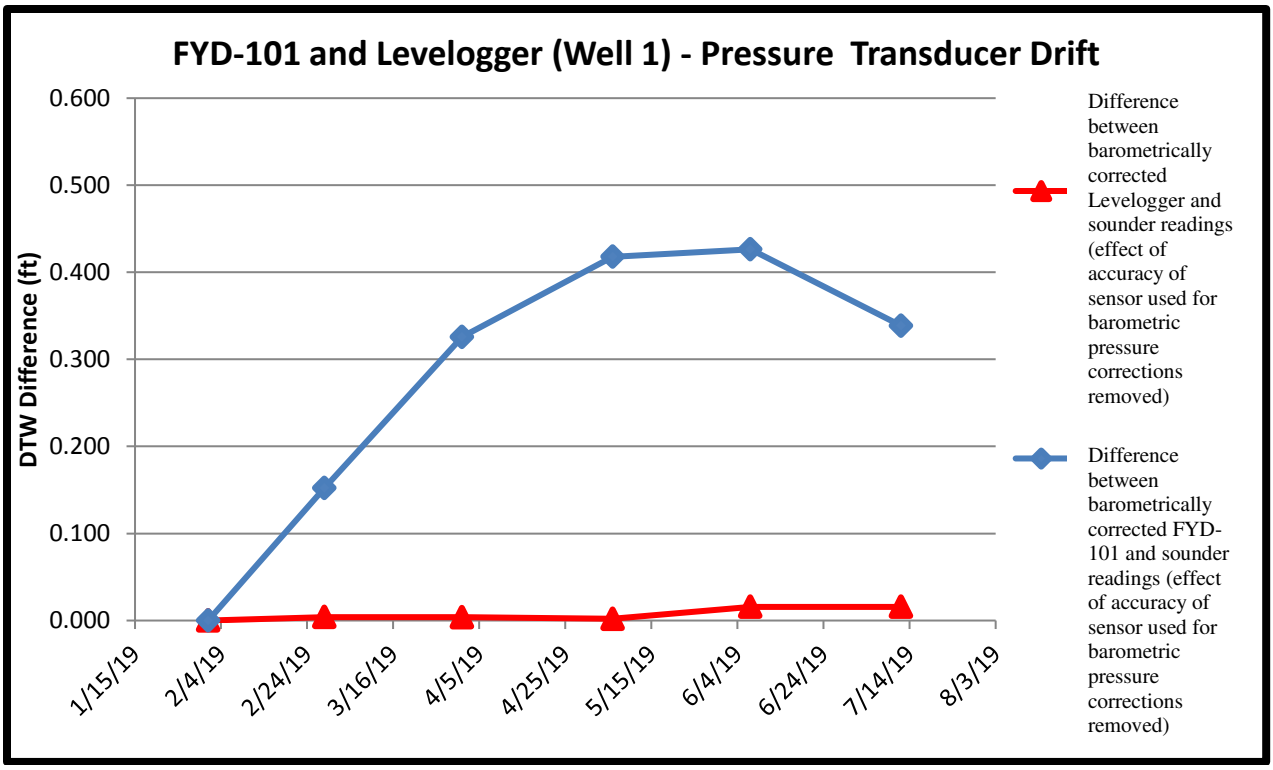

Figure 4.1: Drift in depth to water for the modified FYD-101 and Levelogger compared to water level sounder readings over time at ARDEC well location 1.

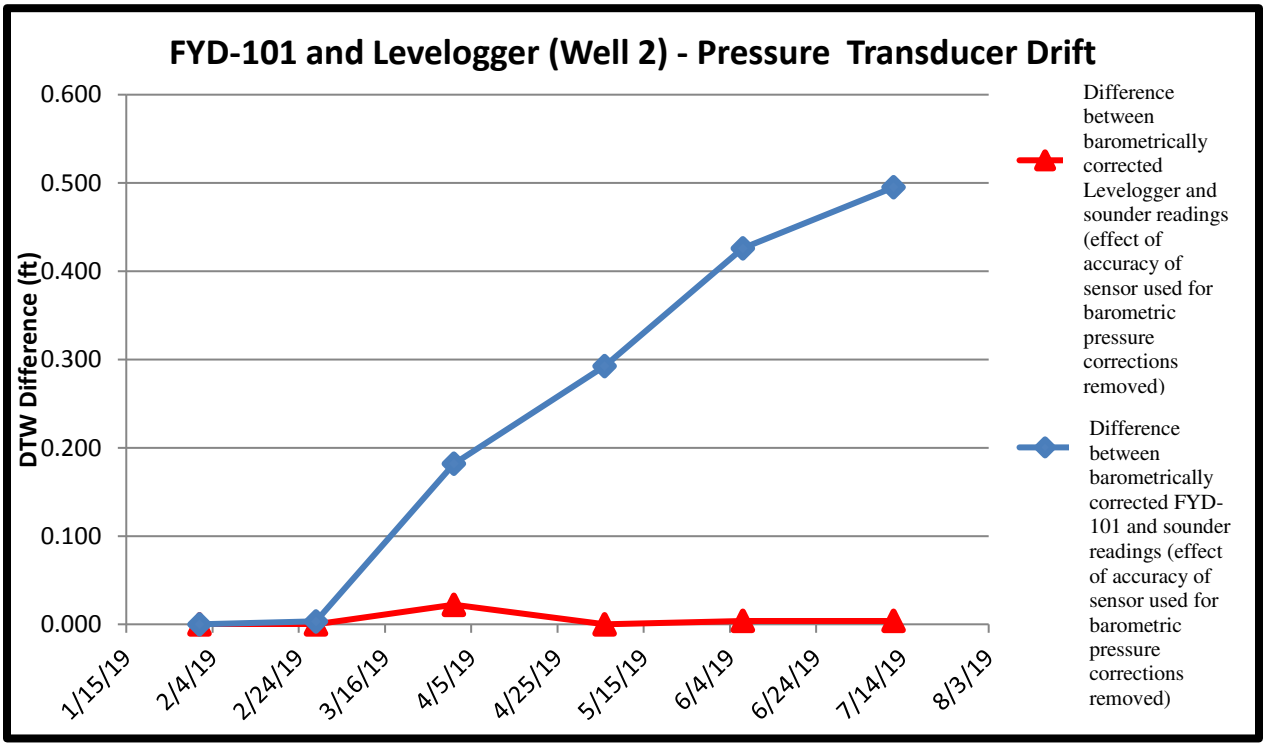

Figure 4.2: Drift in depth to water for the modified FYD-101 and Levelogger compared to water level sounder readings over time at ARDEC well location 2.

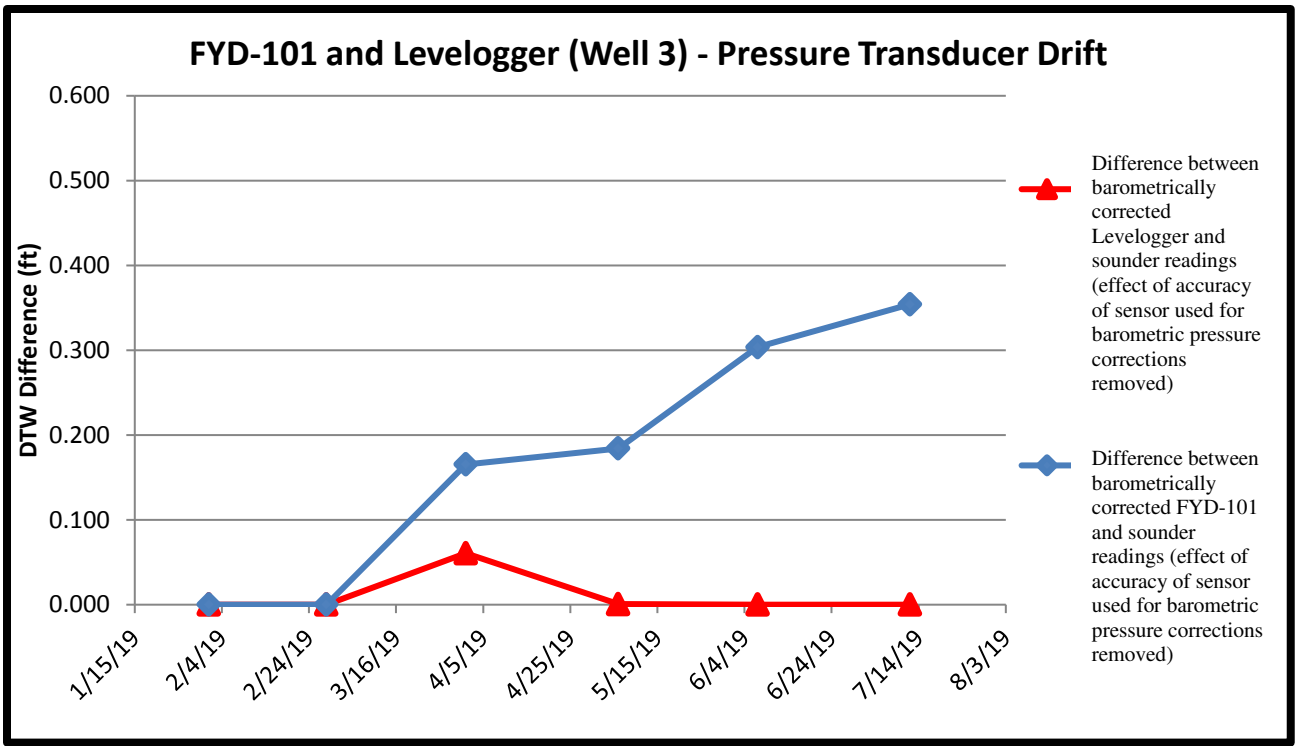

Figure 4.3: Drift in depth to water for the modified FYD-101 and Levelogger compared to water level sounder readings over time at ARDEC well location 3.

Depending on the pressure transducer errors between 0.354-0.495 feet are seen for the FYD-101s over the course of the experiment. These results indicate that the modification of sealing the FYD-101s does increase their tendency to drift when compared to the drift of 0.018 feet seen in the vented sensor study. In addition, the maximum drift for the Leveloggers ranged from 0.016-0.061 feet, showing that the sealed FYD-101s drifted more than the Leveloggers by an order of magnitude. The reason for the increased drift in FYD-101 readings is most likely due to changes in temperature causing a change in pressure in the sealed headspace in the pressure transducers. Supporting evidence for temperature changes casing pressure changes in the sealed headspace in the pressure transducers are found in Figure 4.4.

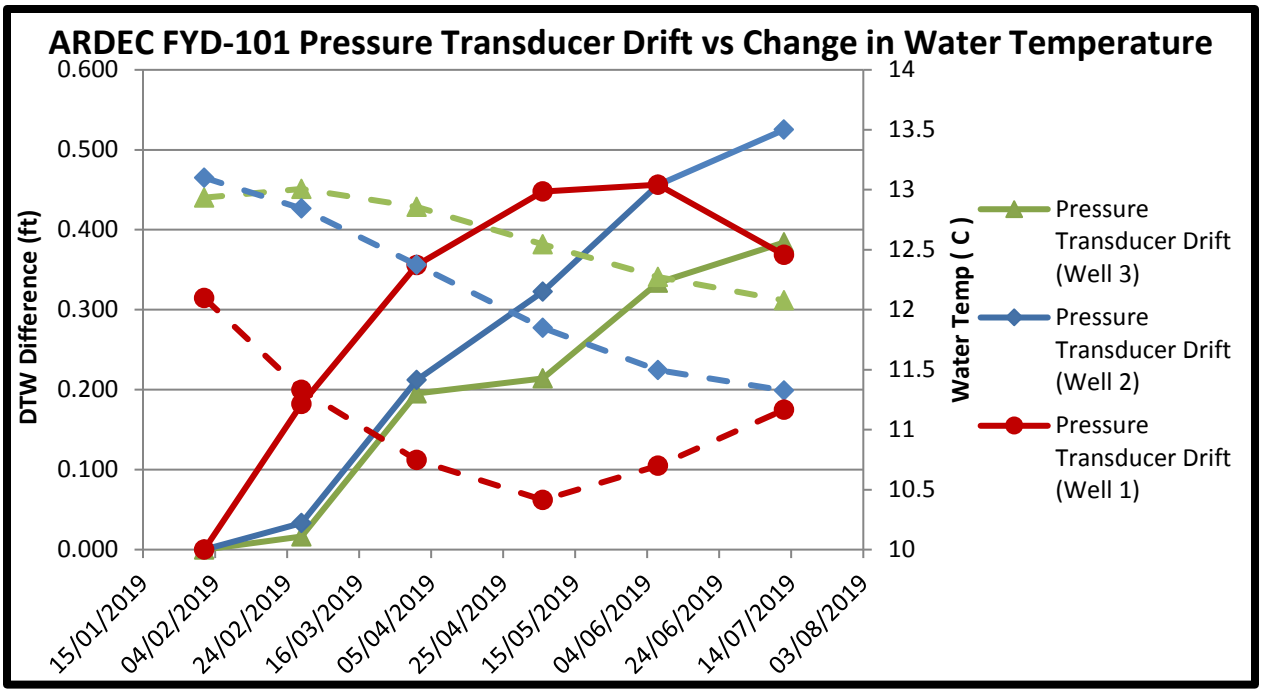

Figure 4.4: Change in pressure transducer drift vs change in water temperature at each well at ARDEC.

When looking at Figure 4.4, careful attention should be paid to the relation between temperature and pressure transducer drift at Well 1. While the water temperature at Well 1 decreased, moving away from the initial water temperature at the time of the field calibration (first measurement) the pressure transducer drift increased. Towards the end of the experiment the water temperature began to increase, moving back towards the initial temperature. As water temperature moved back towards the initial temperature, the pressure transducer drift decreased (i.e. experienced an increase in pressure transducer accuracy).

4.1.3 Sealed FYD-101 Calibration Comparison

Table 4.2 shows the results of the sealed FYD-101 calibration comparison which was used to assess the pressure transducers drift in span. At the end of a six-month testing period each pressure transducer was removed, recalibrated, and compared to its initial calibration. Pressure Transducer 3 had the greatest difference between calibration slopes with an initial calibration slope of 136.25 mV/ft versus a final calibration slope of 134.97 mV/ft, resulting in a <1%

difference in the calibration slope. The small change between initial and final calibration slopes show that although the sealed pressure transducers experienced a large drift in their zero reading when compared to the water level sounder measurements, their drift in span is largely negligible. As a result, the drift in sealed pressure transducer readings can be offset by periodically taking manual head measurements and using them to re-calibrate the pressure transducer(s) in the field. The frequency of manual head measurements taken to re-calibrate the pressure transducers in the field would need to be determined on a site-by-site basis, depending on the goals a site has for using the pressure transducer data.

Table 4.2: Comparison of calibration slopes for pressure transducers 1-3 at ARDEC.

	Initial Calibration Slope (mV/ft)	Final Calibration Slope (mV/ft)	Difference (mV/ft)
Pressure Transducer 1	**136.49**	**135.82**	**0.67**
Pressure Transducer 2	**136.61**	**136.02**	**0.59**
Pressure Transducer 3	**136.25**	**134.97**	**1.28**

4.1.4 Sealed FYD-101 vs Levelogger and Water Level Sounder Readings – Effect on Variability in Groundwater Flow at ARDEC

The Leveloggers experienced minimal drift compared to the sealed FYD-101s over the course of the study. For this reason the Leveloggers were used to determine the effect that the increased error (drift) in sealed FYD-101 readings would have on model results when compared to a well-known, commercial standard at the ARDEC site. The seepage velocities and directions of groundwater flow were compared for the sealed FYD-101 vs Levelogger datasets. This comparison was then used to assess the effect that the increased drift of the sealed FYD-101 would have on model results.

The average seepage velocity is 6.76 ft/day for the FYD-101 dataset and 6.81 ft/day for the Levelogger dataset. The difference in average seepage velocity between the FYD-101 and Levelogger datasets is 5.0×10^{-2} ft/day or 0.73% indicating good agreement between datasets. Comparison of the seepage velocities for the FYD-101 and Levelogger datasets is shown in Figure 4.5. The average direction of groundwater flow (measured clockwise from the positive x-axis) is 84.05° for the FYD-101 dataset and 84.97° for the Levelogger dataset. The average difference in direction of groundwater flow is 0.92° which also indicates good agreement between datasets. Comparison of groundwater flow directions for the FYD-101 and Levelogger datasets is shown in Figure 4.6. The reason for the small differences in model results for the sealed FYD-101 vs Levelogger datasets is that the sealed FYD-101s experienced a similar drift magnitude and direction (Figures 4.1-4.3). The small differences in model results shows that although the absolute head became more inaccurate over time the relative head at the three wells remained similar. Common drifts in all pressure transducers allow for the model to continue providing reasonable results even when subjected to pressure transducer drift. Based on these results the following models assume that simulating the effects of the initial pressure transducer accuracy provide a reasonable range of possible groundwater flow directions, even when subject to pressure transducer drift.

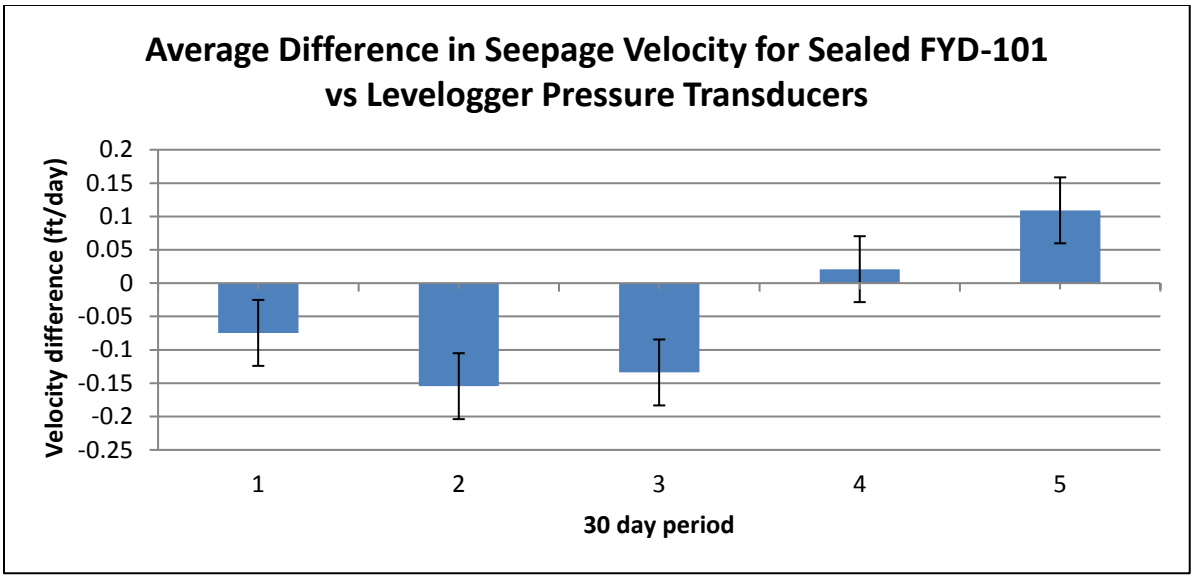

Figure 4.5: Comparison of sealed FYD-101 vs Levelogger average seepage velocities for five 30-day periods.

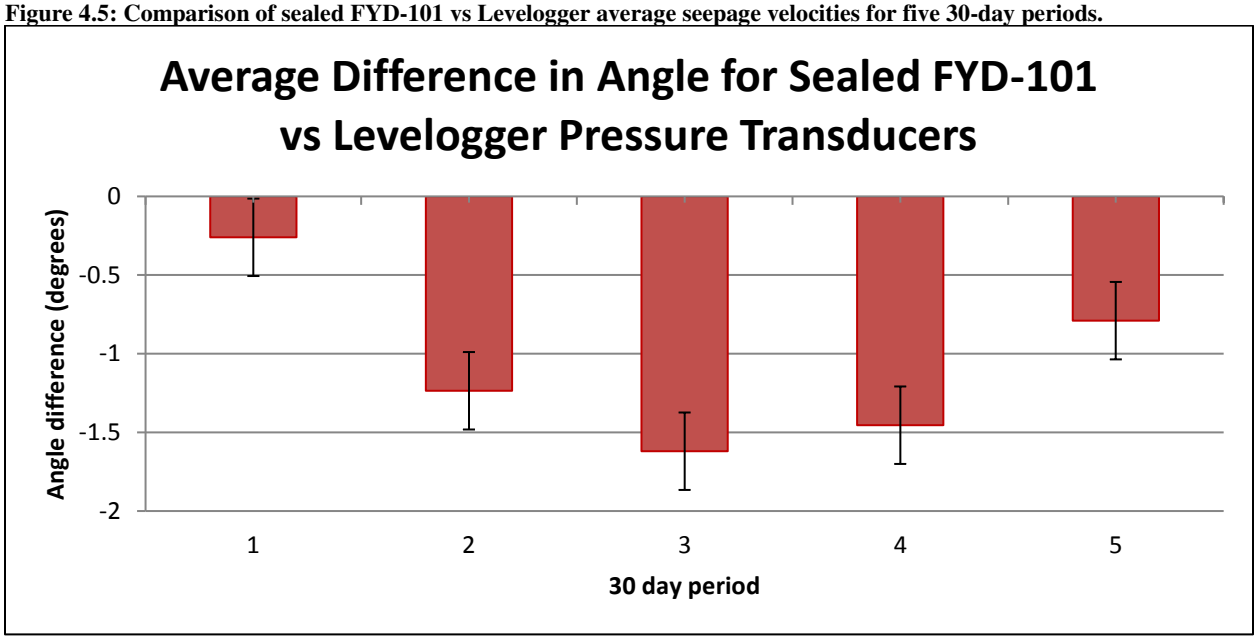

Figure 4.6: Comparison of sealed FYD-101 vs Levelogger average direction of groundwater flow for five 30-day periods.

As an additional confirmation of the observation that the model provides reasonable results even when subject to pressure transducer drift, the sealed FYD-101 and water level sounder readings (assumed to represent the true head) were compared. Seepage velocity and direction of groundwater flow were compared for five sealed FYD-101s and water level sounder readings taken at each well over the study. The average seepage velocity is 6.81 ft/day for the FYD-101 dataset and 6.85 ft/day for the water level sounder dataset. The difference in average seepage

velocity between the FYD-101 and water level sounder datasets is 4.0 x 10^{-2} ft/day, or 0.58% indicating good agreement between datasets. The average direction of groundwater flow (measured clockwise from the positive x-axis) is 83.98^{o} for the FYD-101 dataset and 84.99^{o} for the water level sounder dataset. The average difference in direction of groundwater flow is 1.01^{o} which also indicates good agreement between datasets. The results of FYD-101 and water level sounder datasets comparison are presented in Appendix B.

It should be mentioned that the ARDEC site had an average hydraulic gradient of 5.9 x 10^{-3} ft/ft during the study. It can be assumed if the site had a flatter hydraulic gradient the effects of pressure transducer drift on model results would have been greater (Devlin and McElwee, 2007).

4.2 ARDEC

Sections 4.2-4.5 contain figures depicting the summed hourly groundwater flow vectors, hereafter referred to as flow flags. All flow flags all follow a common display. The white circles represent the monitoring well locations where data is being collected. Wells are connected with white dashed lines outlining the monitoring area considered. The path colored using the log-based, color gradient of a stoplight (red, yellow, green) represents the estimated flow flag. The blue paths represent the 95% confidence interval flow flags.

4.2.1 ARDEC – Effect of Measurement Error on Variability in Groundwater Flow Direction and Seepage Velocity

Figures 4.7 and 4.8 show the results of the synthetic dataset simulation for estimating the effect of measurement error on hydraulic gradient estimations in the x and y-directions at ARDEC. Both histograms show a normal distribution of data, supporting the use of the method described in Section 3.3.2 for determining the effect of measurement error on groundwater flow direction and seepage velocity. The effect of measurement error on estimated hydraulic gradients at the

ARDEC site is ±8.51 x 10^{-5} (ft/ft) about estimated hydraulic gradients in the x-direction and ±8.36 x 10^{-5} (ft/ft) about estimated hydraulic gradients in the y-direction. The effects of measurement error represent a 95% confidence interval about the estimated hydraulic gradients.

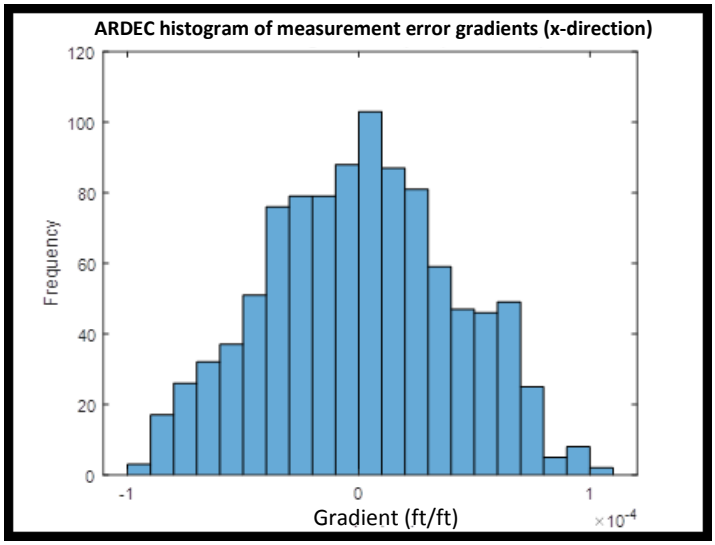

Figure 4.7: Histogram of synthetic dataset simulation results for measurement error based gradients in the x-direction at ARDEC.

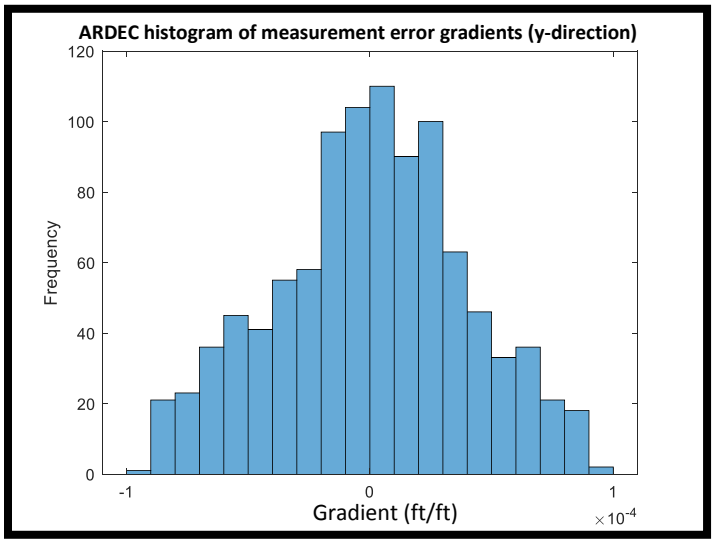

Figure 4.8: Histogram of synthetic dataset simulation results for measurement error based gradients in the y-direction at ARDEC.

During a 182-day study, the measurement error effected flow flag simulation at ARDEC results in five flow flags that exit the monitored area and one that is still in motion inside the monitored area when the study ends. Figure 4.9 shows the results of the estimated and measurement error based flow flags for the 182-day study. During the study the average direction of travel is south

for all flow flags. The average seepage velocity (not considering the effects of measurement error) is 6.74 ft/day causing the flow flags to fall in the green section of the velocity color gradient. The variability in the direction of travel is small (+0.89º/-0.91º about the estimated direction of travel) between the estimated and measurement error effected flow flags indicating that the direction of groundwater flow is largely unaffected by measurement error. The variability in seepage velocity is also small (±0.09 ft/day about the estimated seepage velocity) between the estimated and measurement error effected flow flags indicating that the seepage velocity is also largely unaffected by measurement error.

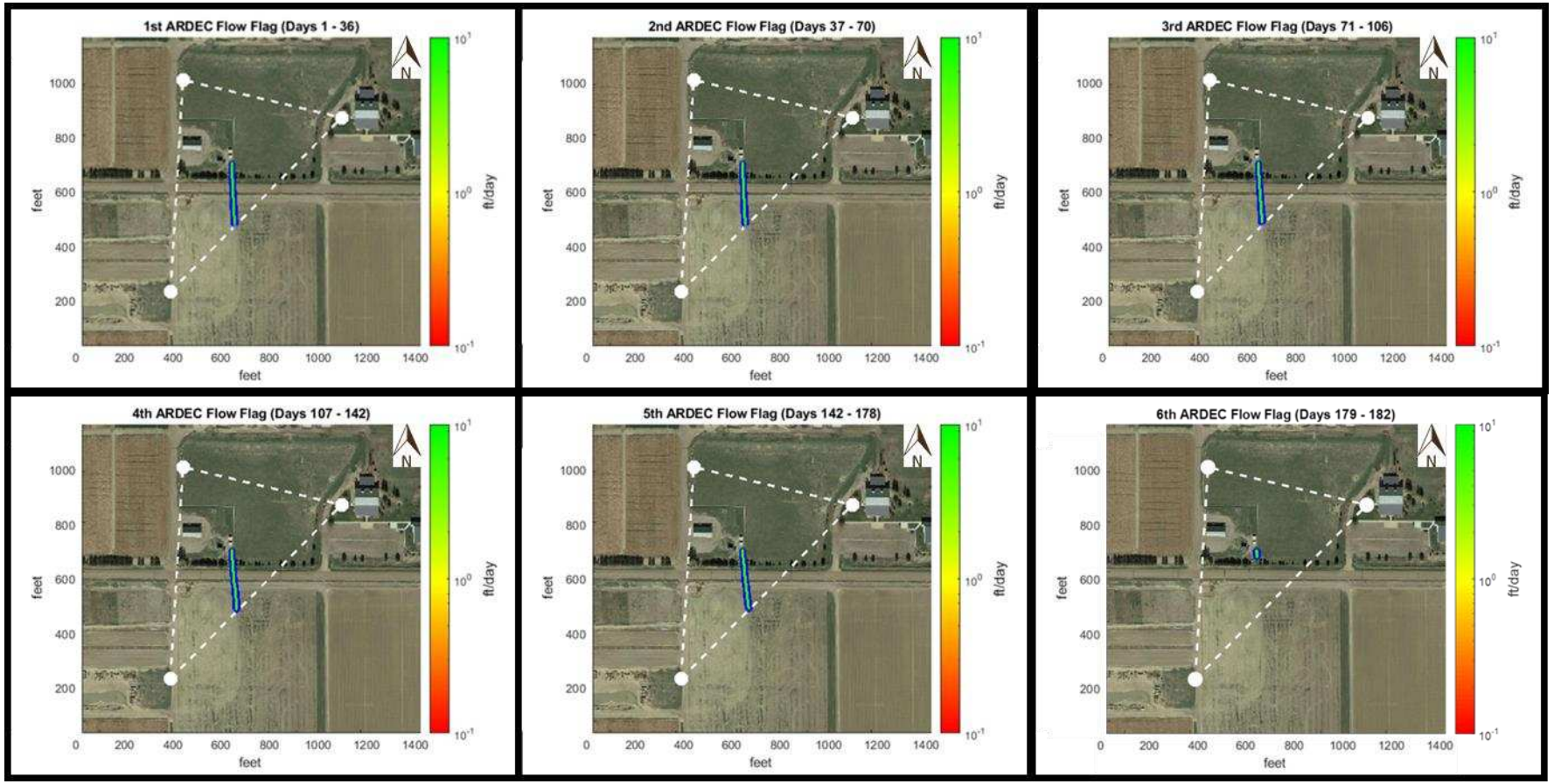

Figure 4.9: Results of the estimated and measurement error based ARDEC flow flags over a 182-day period. The white dashed lines outline the monitoring area, the white circles show where head data is being gathered, the blue lines show the 95% confidence interval when affected by measurement error, and the green line shows the estimated flow flag. Note that due to the large monitored area and narrow 95% confidence interval about the estimated flow flag, the blue and green lines are very close to one another making it difficult to discern the different lines from one another.

4.2.2 ARDEC – Effect of Anisotropy Uncertainty on Variability in Groundwater Flow Direction and Seepage Velocity

Figure 4.10 shows the results of the synthetic dataset simulation for estimating the effect of uncertainty in anisotropy on groundwater flow directions and seepage velocities for a smoothing factor of $p = 6$. Multiple synthetic datasets were created, increasing the value of the smoothing factor until a normally distributed dataset was reached that this researcher deemed satisfactory. It should be noted that by increasing the value of the smoothing factor, the histograms yielded smoother normal type curves, however fewer values of the anisotropy factor were estimated at the extreme upper and lower bounds. The histogram in Figure 4.10 shows a normal type curve, supporting use of the method described in Section 3.3.3 for determining the effect of uncertainty in anisotropy on groundwater flow directions and seepage velocities.

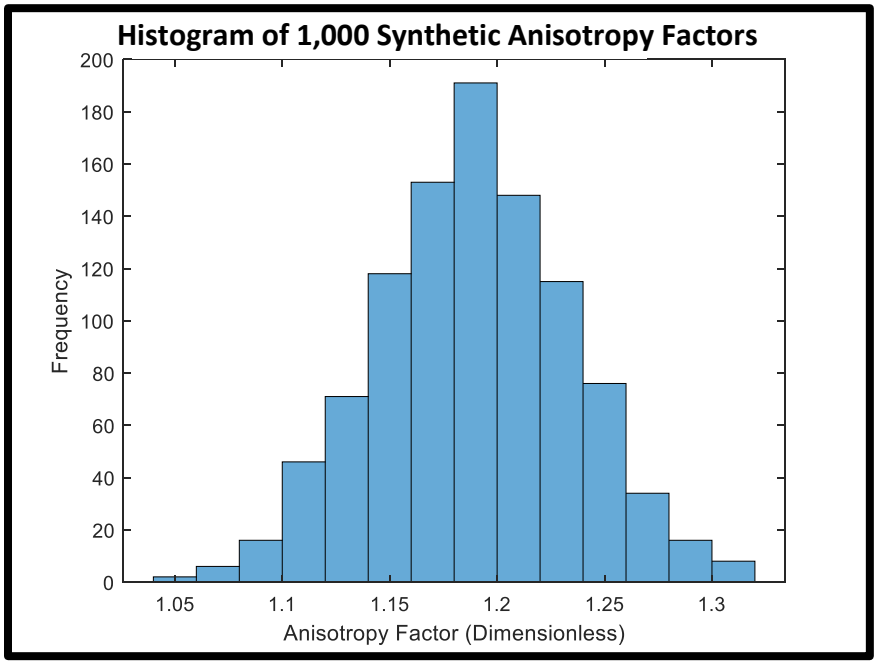

Figure 4.10: Histogram of the synthetic dataset simulation results for the Anisotropy Factor (p = 6).

The values for the anisotropy factor are not site-specific. Therefore the average and low and high 95% confidence interval values for the anisotropy factor calculated using the synthetic dataset in

Section 4.2.2 remain the same in the anisotropy uncertainty models for all sites. The results of the anisotropy factor synthetic dataset are found in Table 4.3.

Table 4.3: Resulting anisotropy factors (dimensionless) from the synthetic dataset simulation. The $\lambda_{Average}$ anisotropy factor is hereafter referred to as the estimated anisotropy factor in this Thesis.

λ_{Low}	**1.10 : 1.0**
$\lambda_{Average}$	**1.19 : 1.0**
λ_{High}	**1.28 : 1.0**

It should be noted that when possible data from pumping tests can be used to determine the values of anisotropy (e.g., Hantush, 1966; Way and McKee, 1982; Neuman et al., 1984) as anisotropy values are often site-specific. A general constraint of resolving anisotropy at field sites is the complexity of pumping tests required to resolve anisotropy.

Figure 4.11 shows the anisotropy uncertainty effected flow flag simulation for the 182-day study at ARDEC. For this simulation the principal direction of deposition (i.e. the direction to apply the uncertainty in anisotropy) is assumed to be from north to south following Boxelder Creek. The anisotropy uncertainty effected flow flag simulation also results in five flow flags that exit the monitored area and one still in motion inside the monitored area when the study ends. During this time the average direction of travel is south for all flags. The average seepage velocity for the flow flag that uses the estimated anisotropy factor ($\lambda_{Average}$ = 1.19:1.0) is 8.01 ft/day causing the flow flags to fall in the green section of the velocity color gradient. The variability in the direction of travel is small (+0.29º/-0.33º about the estimated direction of travel) between the estimated and anisotropy uncertainty effected flow flags indicating that the direction of groundwater flow is largely unaffected by uncertainty in anisotropy. The variability in seepage velocity between the estimated and anisotropy uncertainty effected flow flags is ±0.58 ft/day

about the estimated seepage velocity, indicating that the magnitude of the seepage velocity is moderately affected by uncertainty in anisotropy.

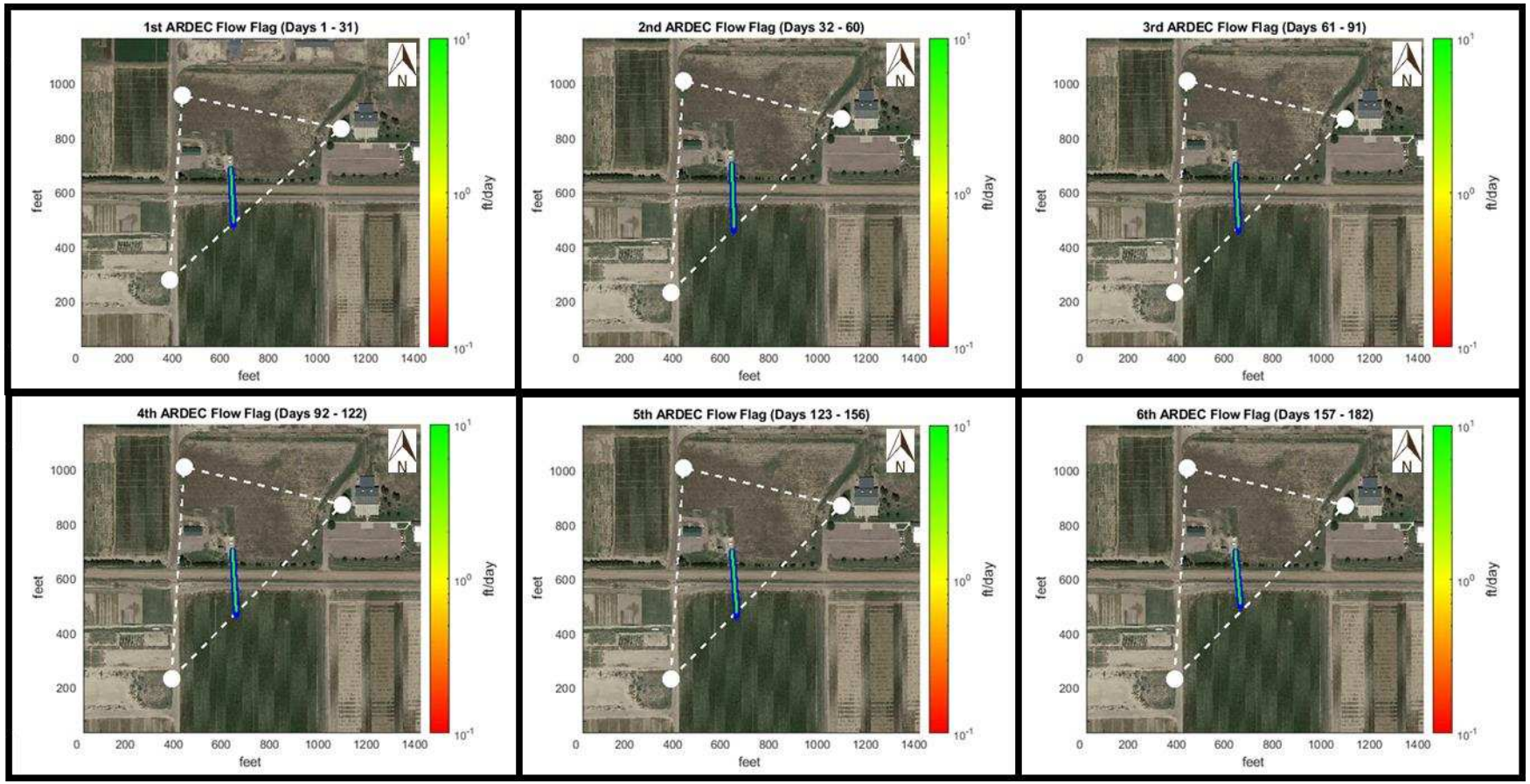

Figure 4.11: Results of the estimated and anisotropy uncertainty based ARDEC flow flags over a 182-day period. The white dashed lines outline the monitoring area, the white circles show where head data is being gathered, the blue lines show the 95% confidence interval when affected by anisotropy uncertainty, and the green line shows the estimated flow flag. Note that due to the large monitored area and narrow 95% confidence interval about the estimated flow flag, the blue and green lines are very close to one another making it difficult to discern the different lines from one another.

4.2.3 ARDEC – Comparison of Measurement Error vs Anisotropy Uncertainty

Comparing the results of the measurement error and anisotropy uncertainty flow flag simulations the difference in the average, estimated direction of travel is 0.86°. The cumulative deviation from the estimated direction of travel is nearly three times greater in the measurement error flow flag simulation versus the anisotropy uncertainty flow flag simulation (1.80° vs 0.62°, respectively). Considering the cumulative effects of measurement error and anisotropy uncertainty on groundwater flow direction, a +1.18°/-1.24°, 95% confidence interval about the estimated groundwater flow direction is seen.

Comparing the results of the measurement error and anisotropy uncertainty flow flag simulations the difference between the average, estimated seepage velocities is 1.29 ft/day. The 1.29 ft/day difference causes the estimated flow flag for the anisotropy uncertainty simulation to travel nearly 500 ft/yr faster than the estimated flow flag for the measurement error simulation. Comparing the 95% confidence intervals about the estimated seepage velocities, the anisotropy uncertainty simulation has a ±0.58 ft/day 95% confidence interval about the estimated seepage velocity while the measurement error simulation has a ±0.09 ft/day 95% confidence interval about the estimated seepage velocity. The larger 95% confidence interval for the anisotropy uncertainty simulation compared to the measurement error simulation shows that although anisotropy uncertainty does not affect the direction of travel for the flow flags as much as measurement error, it does have a greater effect on the possible range of seepage velocities for the flow flags. Considering the cumulative effects measurement error and anisotropy uncertainty have on seepage velocities, a ±0.67 ft/day, 95% confidence interval about the estimated seepage velocity is seen. Table 4.4 presents the results of the measurement error and anisotropy uncertainty affected flow flag studies.

Table 4.4: Comparable results of flow flags at ARDEC for the measurement error and anisotropy uncertainty simulations. Values in the table above are averaged over the entire study (except for the monitored area). The average directions of travel for the flow flags are measured counter clockwise from the positive x-axis.

	Numerical Results of Measurement Error Flow Flag Simulation	Numerical Results of Anisotropy Uncertainty Flow Flag Simulation
Direction of Travel for Estimated Flow Flag (degrees)	-84.87	-85.73
Difference in Direction of Travel Between Estimated and High 95% Confidence Interval Flow Flag (degrees)	+0.89	+0.29
Difference in Direction of Travel Between Estimated and Low 95% Confidence Interval Flow Flag (degrees)	-0.91	-0.33
Cumulative Deviation from Estimated Flow Direction (degrees)	1.80	0.62
Effects of Measurement Error and Anisotropy Uncertainty on Flow Direction (degrees)	+1.18 (high), -1.24 (low), -2.42 (cumulative)	
Seepage Velocity for Estimated Flow Flag (ft/day)	6.74	8.01
Difference in Seepage Velocity Between Estimated and High 95% Confidence Interval Flow Flag (ft/day)	+0.09	+0.58
Difference in Seepage Velocity Between Estimated and Low 95% Confidence Interval Flow Flag (ft/day)	-0.09	-0.58
Cumulative Deviation from Estimated Seepage Velocity (ft/day)	0.18	1.16
Effects of Measurement Error and Anisotropy Uncertainty on Seepage Velocity (ft/day)	+0.67 (high), -0.67 (low), 1.34 (cumulative)	
Monitored Area (ft^2)	264,650	

4.2.4 ARDEC – Hydrograph

Figure 4.12 shows a hydrograph of the data used for the study at ARDEC. The groundwater flow directions and seepage velocities remain relatively constant during the measurement error and anisotropy uncertainty simulations at ARDEC. Although the head data in Figure 4.12 varies over time most variations are similar at each well. The similar variations at each well support the relatively constant groundwater flow directions and seepage velocities for the measurement error and anisotropy uncertainty simulations at ARDEC. Data for the month of June provides evidence of groundwater pumping at ARDEC. Since the aquifer at ARDEC has a high hydraulic

conductivity the effects of pumping are similar at each well. It can be assumed that if the aquifer at ARDEC has a lower hydraulic conductivity pumping would have led to more noticeable changes in groundwater flow direction and seepage velocity. It should also be noted that the 182-day study period may miss seasonal changes in head that could cause changes in groundwater flow directions and/or seepage velocities.

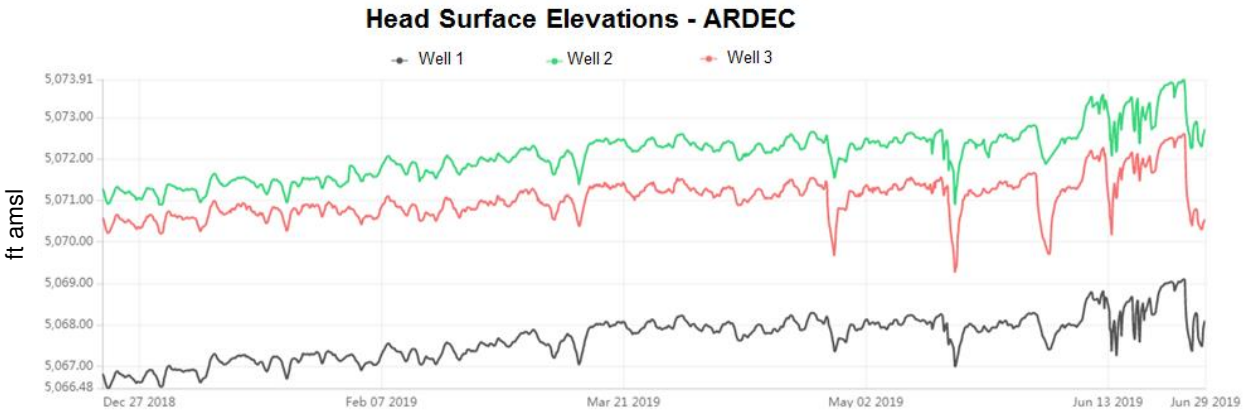

Figure 4.12: Hydrograph of head data used in the measurement error and anisotropy uncertainty simulations at ARDEC. This data has not been corrected for fluctuations in barometric pressure since the measurement error and anisotropy uncertainty models assume the effects of barometric pressure are common at all wells at each site, negating the need for barometric correction of head values.

4.3 ERC

When considering the results from Section 4.3 it should be noted that the saturated zone at the ERC field site consists entirely of silt (wind-blown loess). During the study at the ERC there was an average difference in head of 13 feet between wells 1 and 2 which are located 79 feet apart from one another. Based on the large change in head over a short distance, the ERC is thought to be subject to vertical groundwater flow which violates the assumption that the groundwater flow in the vertical direction is negligible. The possibility of vertical groundwater flow should be kept in mind when considering the results from the ERC site.

4.3.1 ERC – Effect of Measurement Error on Variability in Groundwater Flow Direction and Seepage Velocity

Figures 4.13 and 4.14 show the results of the synthetic dataset simulation for estimating the effect of measurement error on hydraulic gradient estimations in the x and y-directions at the ERC. Both histograms show a normal distribution of data, supporting the use of the method described in Section 3.3.2 for determining the effect of measurement error on groundwater flow direction and seepage velocity. The effect of measurement error on estimated hydraulic gradients at the ERC is ±2.00 x 10^{-3} (ft/ft) about estimated hydraulic gradients in the x-direction and ±1.10 x 10^{-3} (ft/ft) about estimated hydraulic gradients in the y-direction. The effects of measurement error represent a 95% confidence interval about the estimated hydraulic gradients.

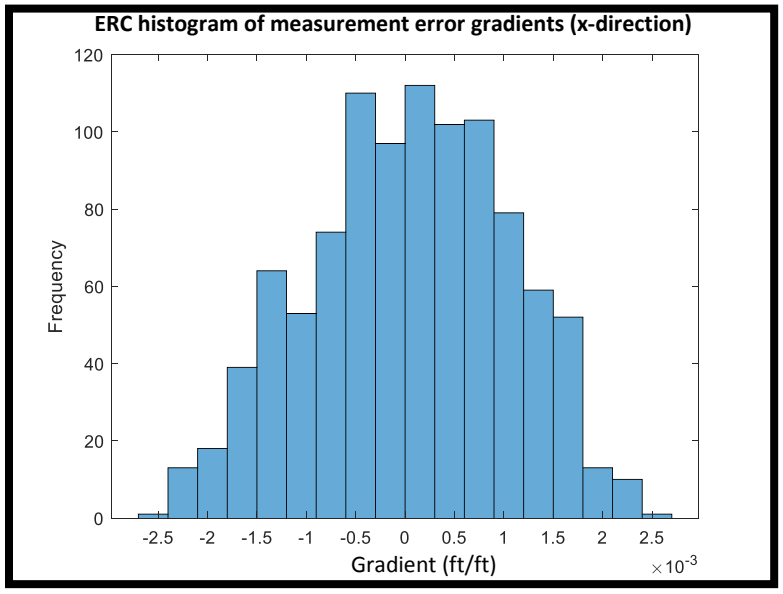

Figure 4.13: Histogram of synthetic dataset simulation results for measurement error based gradients in the x-direction at the ERC.

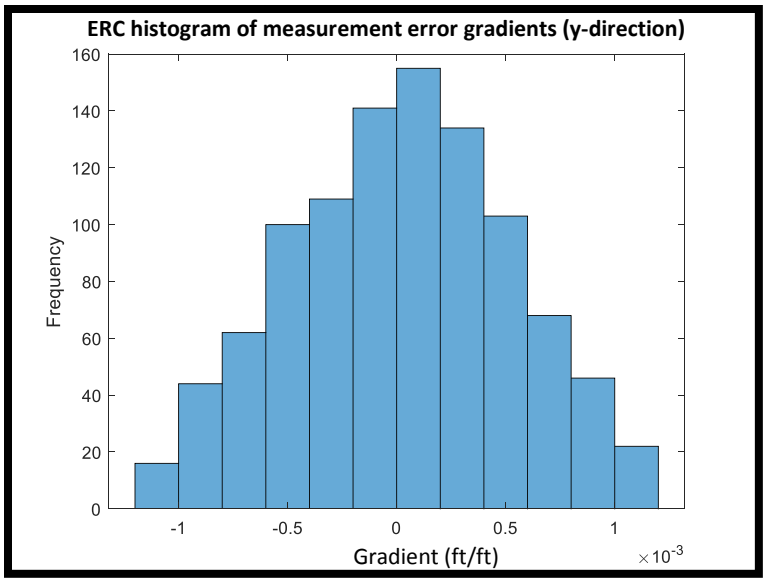

Figure 4.14: Histogram of synthetic dataset simulation results for measurement error based gradients in the y-direction at the ERC.

During a 90-day study, the measurement error effected flow flag simulation at the ERC results in three flow flags that exit the monitored area and one that is still in motion inside the monitored area when the study ends. Figure 4.15 shows the estimated and measurement error based flow flags for the 90-day period. During the study the primary direction of travel is east for all flow flags. During this time the average seepage velocity (not considering the effects of measurement error) is 0.22 ft/day causing the flow flags to fall in the red/orange section of the velocity color gradient. The variability in direction of travel is small (+0.15°/-0.14° about the estimated direction of travel) between the estimated and measurement error effected flow flags indicating that the direction of groundwater flow is largely unaffected by measurement error. The variability in seepage velocity is also small (+1.7 x 10^{-3}/-1.4 x 10^{-3} ft/day about the estimated seepage velocity) between the estimated and measurement error effected flow flags indicating that the seepage velocity is also largely unaffected by measurement error. As time progresses, the average seepage velocity decreases while the range of uncertainty in the direction of travel increases. This is a result of the gradient becoming flatter over time, indicating a direct relationship between the two variables.

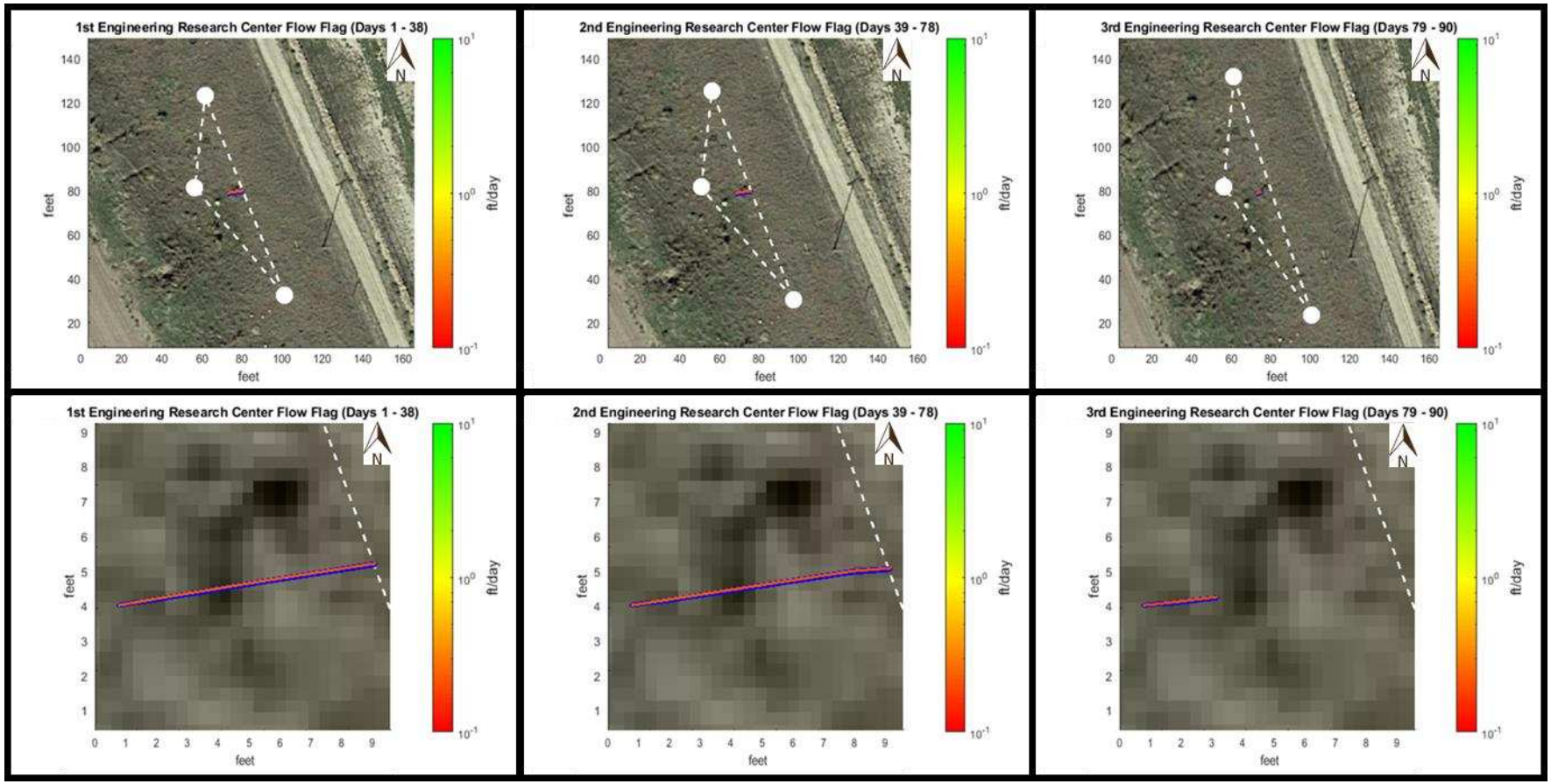

Figure 4.15: Results of the estimated and measurement error based ERC flow flags over a 90-day period. The top layer of the panel shows the three flow flags over the course of the study where the entire monitoring area is shown. The bottom layer of the panel shows the same three flow flags over the course of the study but are zoomed in only on the flow flag. The white dashed lines outline the monitoring area, the white circles show where head data is being gathered, the blue lines show the 95% confidence range when affected by measurement error, and the reddish line shows the estimated flow flag. Note that due to the narrow 95% confidence interval about the estimated flow flag, the blue and reddish lines are very close to one another making it difficult to discern the different lines from one another.

4.3.2 ERC – Effect of Anisotropy Uncertainty on Variability in Groundwater Flow Direction and Seepage Velocity

Figure 4.16 shows the anisotropy uncertainty effected flow flag simulation for the 90-day study at the ERC. For the ERC anisotropy uncertainty simulation the principal direction of deposition is assumed to be from the east to west based on wind direction which would have deposited the wind-blown loess at the site. The anisotropy uncertainty simulation also results in two flow flags that exit the monitored area and one still in motion inside the monitored area when the study ends. Again, the primary direction of travel is east for all flow flags. During this time the average seepage velocity for the flow flag that uses the estimated anisotropy factor is 0.26 ft/day causing the flow flags to fall in the red/orange section of the velocity color gradient. The variability in direction of travel is small (+0.45º/-0.52º about the estimated direction of travel) between the estimated and anisotropy uncertainty effected flow flags indicating that the direction of groundwater flow is largely unaffected by uncertainty in anisotropy. The variability in seepage velocity is also small ($\pm 2.0 \times 10^{-2}$ ft/day about the estimated seepage velocity) between the estimated and anisotropy uncertainty effected flow flags, indicating that the seepage velocity of the flow flag is also largely unaffected by uncertainty in anisotropy.

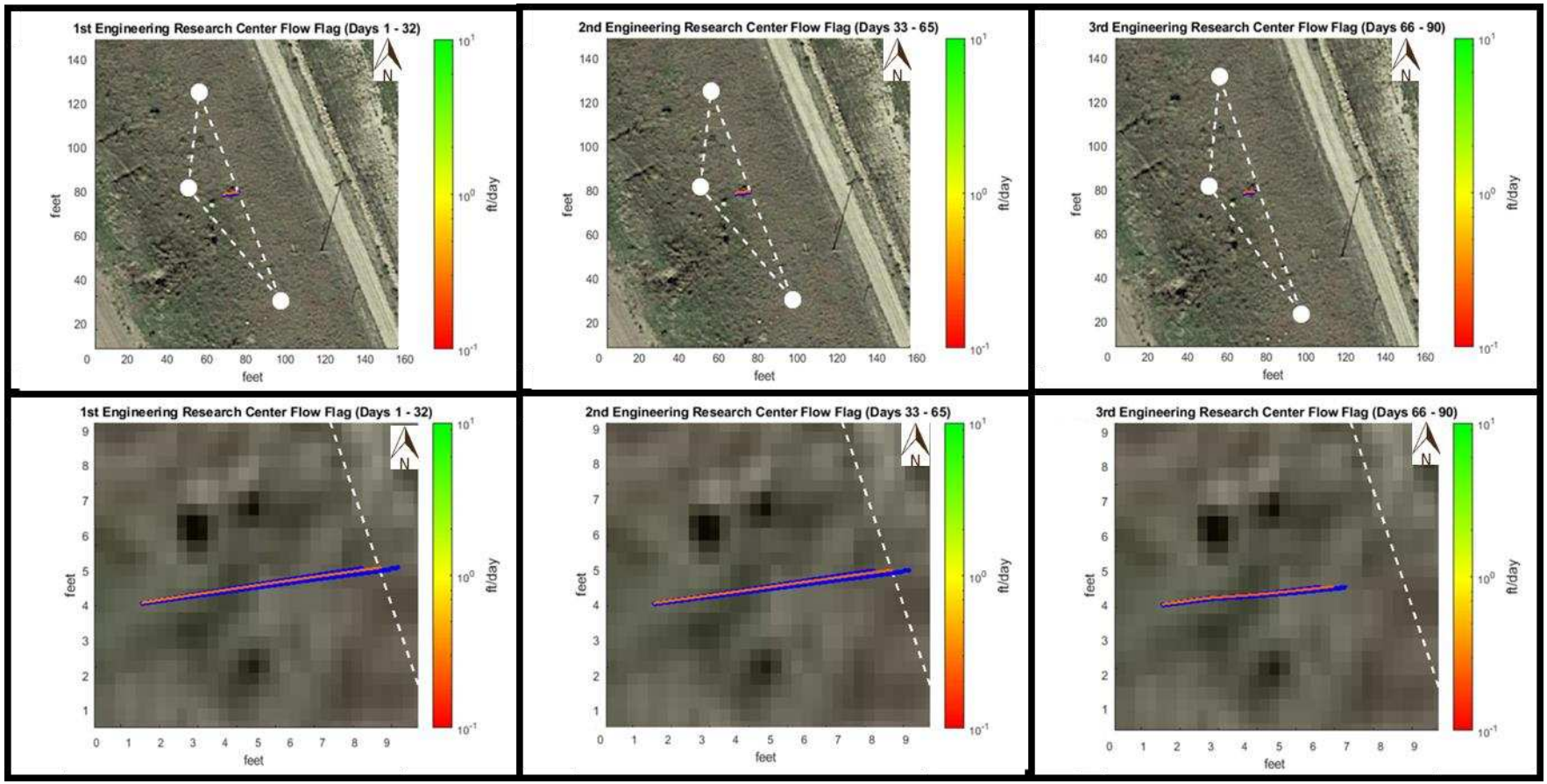

Figure 4.16: Results of the estimated and anisotropy uncertainty based ERC flow flags over a 90-day period. The top layer of the panel shows the three flow flags over the course of the study where the entire monitoring area is shown. The bottom layer of the panel shows the same three flow flags over the course of the study but are zoomed in only on the flow flag. The white dashed lines outline the monitoring area, the white circles show where head data is being gathered, the blue lines show the 95% confidence interval when affected by anisotropy uncertainty, and the reddish line shows the estimated flow flag. Note that due to the narrow 95% confidence interval about the estimated flow flag, the blue and reddish lines are very close to one another making it difficult to discern the different lines from one another.

4.3.3 ERC – Comparison of Measurement Error vs Anisotropy Uncertainty

Comparing the results of the measurement error and anisotropy uncertainty flow flag simulations the difference in the average, estimated direction of travel is 1.22°. The cumulative deviation from the estimated direction of travel is more than three times greater in the anisotropy uncertainty flow flag simulation versus the measurement error flow flag simulation (0.97° vs 0.29°, respectively). Considering the cumulative effects measurement error and anisotropy uncertainty have on groundwater flow direction, a +0.60°/-0.66°, 95% confidence interval about the estimated groundwater flow direction is seen.

Comparing the results of the measurement error and anisotropy uncertainty flow flag simulations the difference between the average, estimated seepage velocities is 0.04 ft/day. However, the 95% confidence interval for seepage velocity in the anisotropy uncertainty flow flag simulation is greater by one order of magnitude compared to the 95% confidence interval for seepage velocity in the measurement error flow flag simulation. The larger 95% confidence intervals for groundwater flow direction and seepage velocity in the anisotropy uncertainty simulation show that at the ERC site, uncertainty in anisotropy affects both the possible range of direction of travel and seepage velocity of the flow flag more than measurement error. When considering the cumulative effects measurement error and anisotropy uncertainty have on seepage velocity, a $\pm 2.2 \times 10^{-2}$ ft/day, 95% confidence interval about the estimated seepage velocity is seen. Table 4.5 presents the results of the measurement error and anisotropy uncertainty affected flow flags.

Table 4.5: Comparable results of flow flags at the ERC for the measurement error and anisotropy uncertainty simulations. Values in the table above are averaged over the entire study (except for the monitored area). The average directions of travel for the flow flags are measured counter clockwise from the positive x-axis.

	Numerical Results of Measurement Error Flow Flag Simulation	Numerical Results of Anisotropy Uncertainty Flow Flag Simulation
Direction of Travel for Estimated Flow Flag (degrees)	7.72	6.50
Difference in Direction of Travel Between Estimated and High 95% Confidence Interval Flow Flag (degrees)	+0.15	+0.45
Difference in Direction of Travel Between Estimated and Low 95% Confidence Interval Flow Flag (degrees)	-0.14	-0.52
Cumulative Deviation from Estimated Flow Direction (degrees)	0.29	0.97
Effects of Measurement Error and Anisotropy Uncertainty on Flow Direction (degrees)	+0.60 (high), -0.66 (low), 1.26 (cumulative)	
Seepage Velocity for Estimated Flow Flag (ft/day)	0.22	0.26
Difference in Seepage Velocity Between Estimated and High 95% Confidence Interval Flow Flag (ft/day)	$+1.7 \times 10^{-3}$	$+2.0 \times 10^{-2}$
Difference in Seepage Velocity Between Estimated and Low 95% Confidence Interval Flow Flag (ft/day)	-1.4×10^{-3}	-2.0×10^{-2}
Cumulative Deviation from Estimated Seepage Velocity (ft/day)	3.1×10^{-3}	4.0×10^{-2}
Effects of Measurement Error and Anisotropy Uncertainty on Seepage Velocity (ft/day)	$+2.2 \times 10^{-2}$ (high), -2.2×10^{-2} (low), 4.4×10^{-2} (cumulative)	
Monitored Area (ft^2)	1,487	

4.3.4 ERC – Hydrograph

Figure 4.17 shows a hydrograph of the data used for the study at the ERC. The groundwater flow directions and seepage velocities remain relatively constant during the measurement error and anisotropy uncertainty simulations at the ERC. Although the head data in Figure 4.17 varies over time most variations are similar at each well. The similar variations at each well support the relatively constant groundwater flow directions and seepage velocities for the measurement error and anisotropy uncertainty simulations at the ERC. It should be noted that although the groundwater flow directions and seepage velocities remain relatively constant during the study at

the ERC the 90-day study period may miss seasonal changes in head that could cause changes in groundwater flow directions and/or seepage velocities.

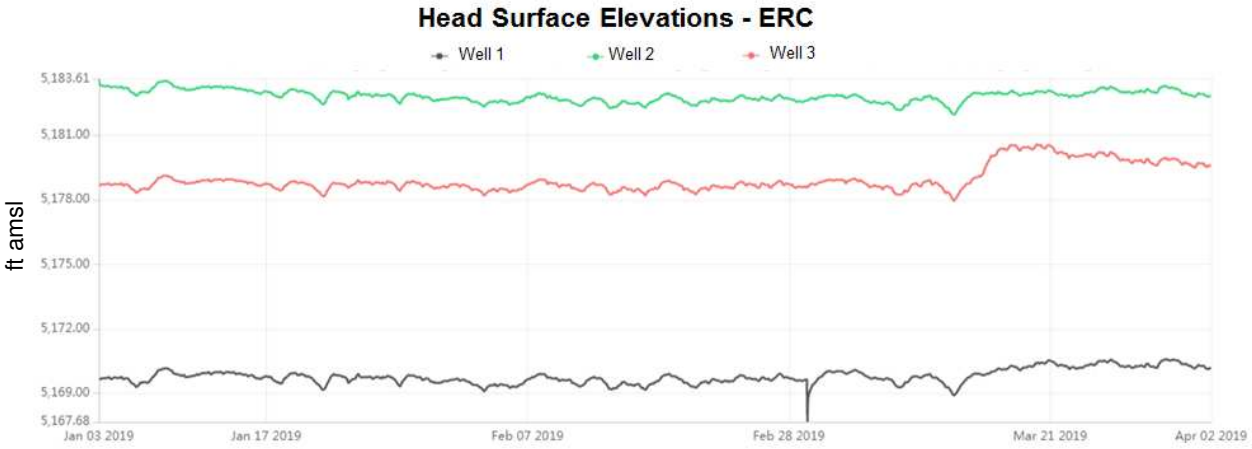

Figure 4.17: Hydrograph of head data used in the measurement error and anisotropy uncertainty simulations at the ERC. This data has not been corrected for fluctuations in barometric pressure since the measurement error and anisotropy uncertainty models assume the effects of barometric pressure are common at all wells at each site, negating the need for barometric correction of head values.

4.4 Site A

4.4.1 Site A – Effect of Measurement Error on Variability in Groundwater Flow Direction and Seepage Velocity

Figures 4.18 and 4.19 show the results of the synthetic dataset simulation for estimating the effect of measurement error on hydraulic gradient estimations in the x and y-directions at Site A. Both histograms show a normal distribution of data, supporting the use of the method described in Section 3.3.2 for determining the effect of measurement error on groundwater flow direction and seepage velocity. The effect of measurement error on estimated hydraulic gradients at the Site A site is $\pm 4.61 \times 10^{-4}$ (ft/ft) about estimated hydraulic gradients in the x-direction and $\pm 4.35 \times 10^{-4}$ (ft/ft) about estimated hydraulic gradients in the y-direction. The effects of measurement error represent a 95% confidence interval about the estimated hydraulic gradients.

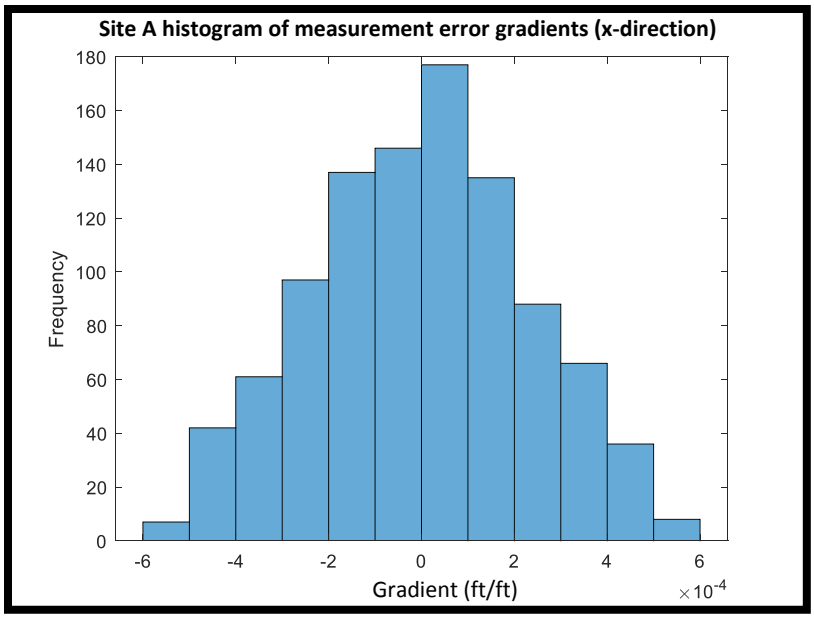

Figure 4.18: Histogram of synthetic dataset simulation results for measurement error based gradients in the x-direction at Site A.

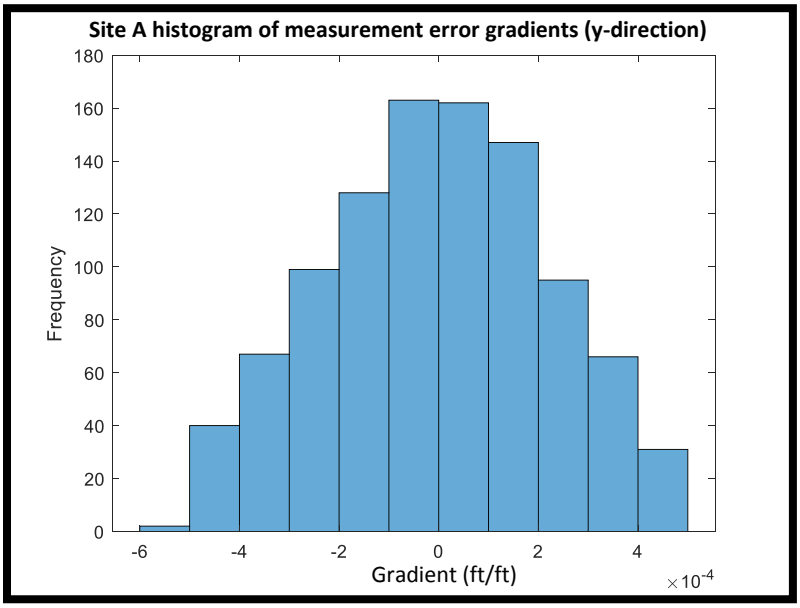

Figure 4.19: Histogram of synthetic dataset simulation results for measurement error based gradients in the y-direction at Site A.

Figure 4.20 shows the results of the estimated and measurement error based flow flags for a 158-day study. The principal direction of groundwater flow is west with groundwater flow turning north-west as the study progresses. During this time the average seepage velocity (not considering the effects of measurement error) is 0.42 ft/day causing the flow flag to fall in the red/orange section of the velocity color gradient. The variability in direction of travel is large

(+11.46º/ -9.08º about the estimated direction of travel) between the estimated and measurement error effected flow flags indicating that the direction of groundwater flow is greatly affected by measurement error. The variability in seepage velocity is small (+4.6 x 10^{-2}/-3.7 x 10^{-2} ft/day about the estimated seepage velocity) between the estimated and measurement error effected flow flags indicating that the seepage velocity is largely unaffected by measurement error.

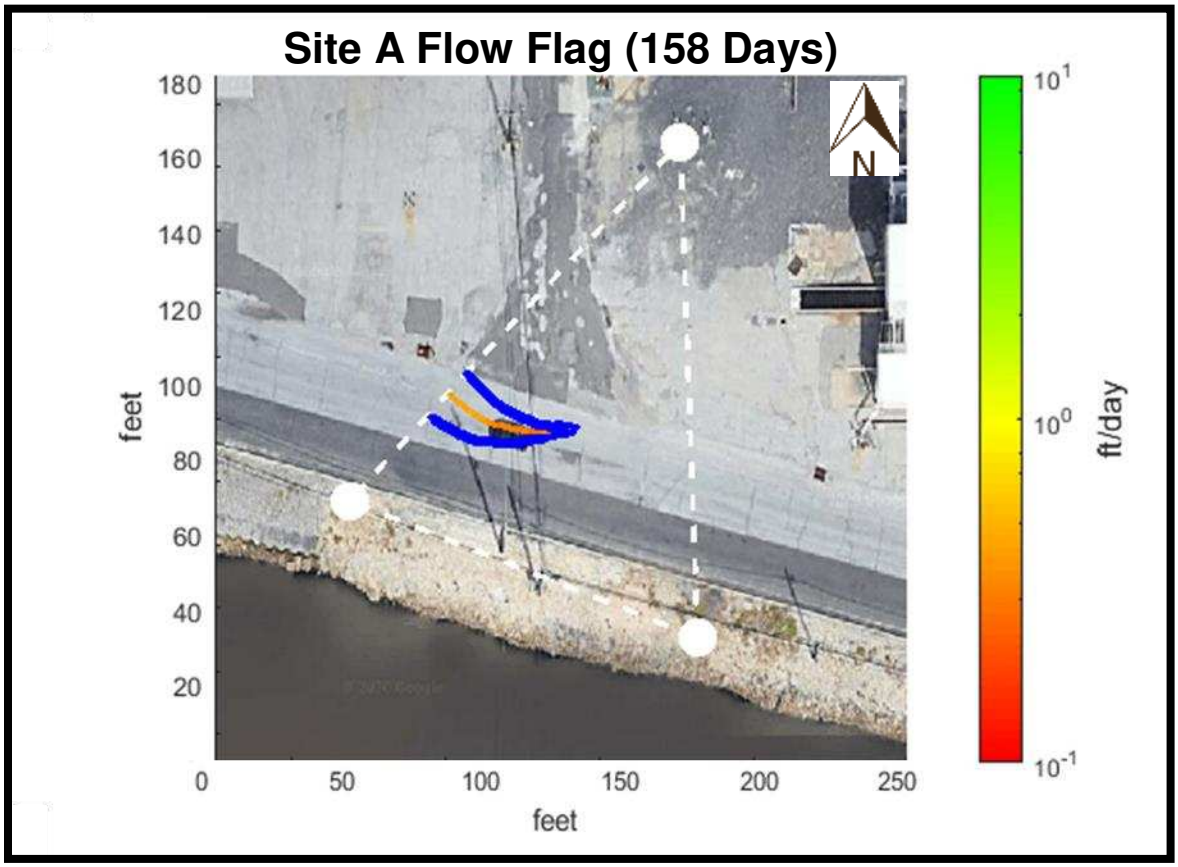

Figure 4.20: Results of the estimated and measurement error based Site A flow flag over a 158-day period. The white dashed lines outline the monitoring area, the white circles show where head data is being gathered, the blue lines show the 95% confidence interval when affected by measurement error, and the red/orange line shows the estimated flow flag.

4.4.2 Site A – Effect of Anisotropy Uncertainty on Variability in Groundwater Flow Direction and Seepage Velocity

Figure 4.21 shows the anisotropy uncertainty effected flow flag simulation for the 158-day study at Site A. For the anisotropy uncertainty simulation the principal direction of deposition is

assumed from north to south following the Delaware River. Again the principal direction of groundwater flow is west for the period of study with groundwater flow turning north-west as the study progresses. During this time the average seepage velocity for the flow flag that uses the estimated anisotropy factor is 0.43 ft/day causing the flow flag to fall in the red/orange section of the velocity color gradient. The variability in direction of travel is small ($+1.48^{o}/-1.25^{o}$ about the estimated direction of travel) between the estimated and anisotropy uncertainty effected flow flags indicating that the direction of groundwater flow is largely unaffected by uncertainty in anisotropy. The variability in seepage velocity is also small ($+9.6 \times 10^{-3}/-7.2 \times 10^{-3}$ ft/day about the estimated seepage velocity) between the estimated and anisotropy uncertainty effected flow flags indicating that the magnitude of the seepage velocity is also largely unaffected by uncertainty in anisotropy.

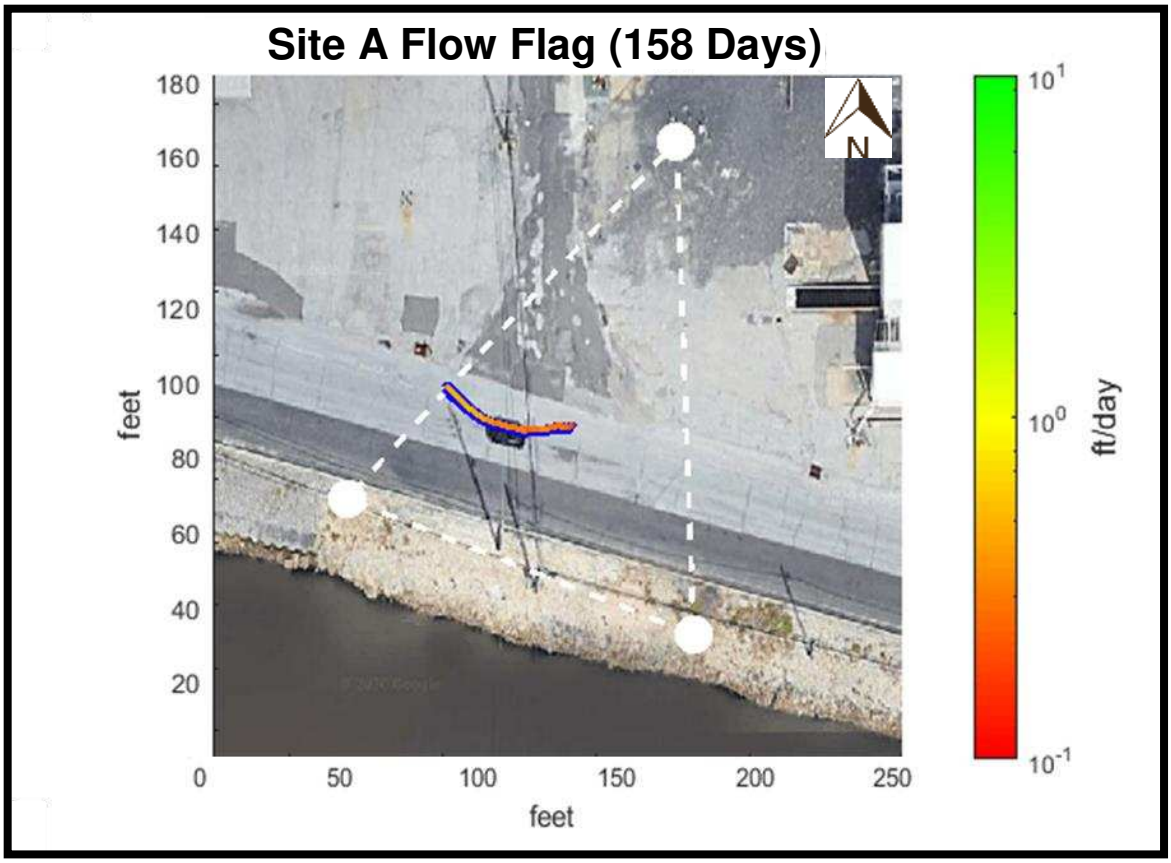

Figure 4.21: Result of the estimated and anisotropy uncertainty based Site A flow flag over a 158-day period. The white dashed lines outline the monitoring area, the white circles show where head data is being gathered, the blue lines show the 95% confidence interval when affected by anisotropy uncertainty, and the red/orange line shows the estimated flow flag. Note that due to the narrow 95% confidence interval about the estimated flow flag, the blue and red/orange lines are very close to one another making it difficult to discern the different lines from one another.

4.4.3 Site A – Comparison of Measurement Error vs Anisotropy Uncertainty

Comparing the effects of measurement error vs anisotropy uncertainty flow flag simulations the difference in the average, estimated direction of travel is 1.34°. The cumulative deviation from the estimated direction of travel is more than seven times greater in measurement error flow flag simulation versus the anisotropy uncertainty flow flag simulation (20.54° vs 2.73°, respectively). Considering the cumulative effects measurement error and anisotropy uncertainty have on groundwater flow direction, a +12.94°/-10.33°, 95% confidence interval about the estimated groundwater flow direction is seen.

Comparing the effects of measurement error vs anisotropy uncertainty flow flag simulations the difference between the average, estimated seepage velocities is 1.0×10^{-2} ft/day. The 95% confidence interval in seepage velocity for the measurement error flow flag simulation is nearly five times larger when compared to the 95% confidence interval in seepage velocity for anisotropy uncertainty flow flag simulation (8.3×10^{-2} ft/day vs 1.7×10^{-2} ft/day, respectively). The larger 95% confidence intervals for groundwater flow direction and seepage velocity for the measurement error simulation show that at the Site A site, measurement error affects both the possible range of direction of travel and seepage velocity of the flow flag more than anisotropy uncertainty. Considering the cumulative effects measurement error and anisotropy uncertainty have on seepage velocities, a $+5.6 \times 10^{-2}/-4.4 \times 10^{-2}$ ft/day, 95% confidence interval about the estimated seepage velocity is seen. Table 4.8 presents the results of the measurement error and anisotropy uncertainty affected flow flags.

Table 4.8: Comparable results of flow flags at Site A for the measurement error and anisotropy uncertainty simulations. Values in the table above are averaged over the entire study (except for the monitored area). The average directions of travel for the flow flags are measured counter clockwise from the positive x-axis.

	Numerical Results of Measurement Error Flow Flag Simulation	Numerical Results of Anisotropy Uncertainty Flow Flag Simulation
Direction of Travel for Estimated Flow Flag (degrees)	153.34	152.00
Difference in Direction of Travel Between Estimated and High 95% Confidence Interval Flow Flag (degrees)	+11.46	+1.48
Difference in Direction of Travel Between Estimated and Low 95% Confidence Interval Flow Flag (degrees)	-9.08	-1.25
Cumulative Deviation from Estimated Flow Direction (degrees)	20.54	2.73
Effects of Measurement Error and Anisotropy Uncertainty on Flow Direction (degrees)	+12.94 (high), -10.33 (low), 23.27(cumulative)	
Seepage Velocity for Estimated Flow Flag (ft/day)	0.42	0.43
Difference in Seepage Velocity Between Estimated and High 95% Confidence Interval Flow Flag (ft/day)	$+4.6 \times 10^{-2}$	$+9.6 \times 10^{-3}$
Difference in Seepage Velocity Between Estimated and Low 95% Confidence Interval Flow Flag (ft/day)	-3.7×10^{-2}	-7.2×10^{-3}
Cumulative Deviation from Estimated Seepage Velocity (ft/day)	8.3×10^{-2}	1.7×10^{-2}
Effects of Measurement Error and Anisotropy Uncertainty on Seepage Velocity (ft/day)	$+5.6 \times 10^{-2}$ (high), -4.4×10^{-2} (low), 0.10 (cumulative)	
Monitored Area (ft^2)	9,030	

4.4.4 Site A – Hydrograph

Figure 4.22 shows a hydrograph of the data used for the study at Site A. The head elevation at Well 105-M02B initially shows very similar values to the head elevation at Well 105-M01B. As time progresses the head elevation at Well 105-M02B becomes lower in elevation than the head elevation at Well 105-M01B. As a result the groundwater flow direction turns from west to north-west as the study progresses for the measurement error and anisotropy uncertainty simulations at Site A. It should be noted that since the Site A study uses 158 days of data the

study may miss seasonal changes in head that could cause more changes in groundwater flow directions and/or seepage velocities.

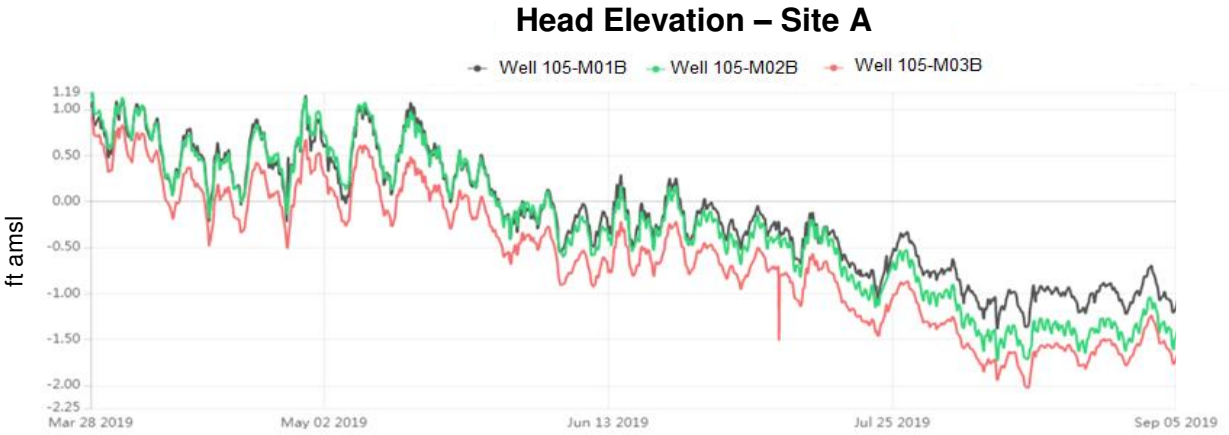

Figure 4.22: Hydrograph of head data used in the measurement error and anisotropy uncertainty simulations at Site A. This data has not been corrected for fluctuations in barometric pressure since the measurement error and anisotropy uncertainty models assume the effects of barometric pressure are common at all wells at each site, negating the need for barometric correction of head values.

4.5 Site B

Site B site consists of four monitoring wells allowing for two flow flags to be drawn. Hereafter the western flow flag is referred to as Flag A and the eastern flow flag is referred to as Flag B.

4.5.1 Site B – Effect of Measurement Error on Variability in Groundwater Flow Direction and Seepage Velocity

Figures 4.23 and 4.24 show the results of the synthetic dataset simulation for estimating the effect of measurement error on hydraulic gradient estimations in the x and y-directions for Flags A and B at Site B. All histograms show a normal distribution of data, supporting the use of the method described in Section 3.3.2 for determining the effect of measurement error on groundwater flow direction and seepage velocity. For Flag A the effect of measurement error on estimated hydraulic gradients is $\pm 9.32 \times 10^{-5}$ (ft/ft) about estimated hydraulic gradients in the x-direction and $\pm 8.36 \times 10^{-5}$ (ft/ft) about estimated hydraulic gradients in the y-direction. For Flag

B the effect of measurement error on estimated hydraulic gradients is ±1.38 x 10^{-4} (ft/ft) about estimated hydraulic gradients in the x-direction and ±8.70 x 10^{-5} (ft/ft) about estimated hydraulic gradients in the y-direction.

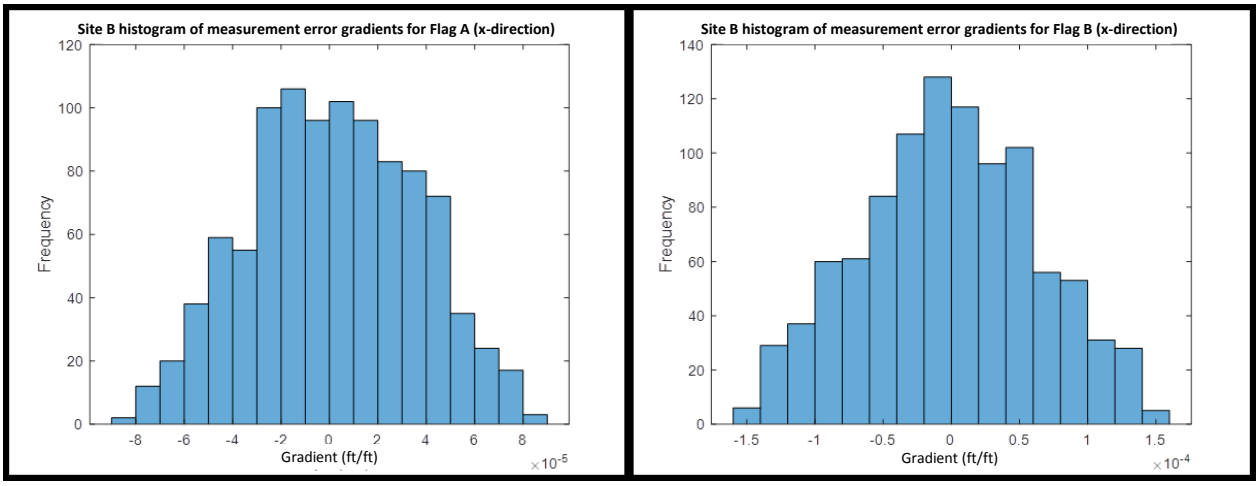

Figure 4.23: Histograms of the synthetic dataset simulation results for measurement error based gradients in the x-direction for Flag A and B at Site B.

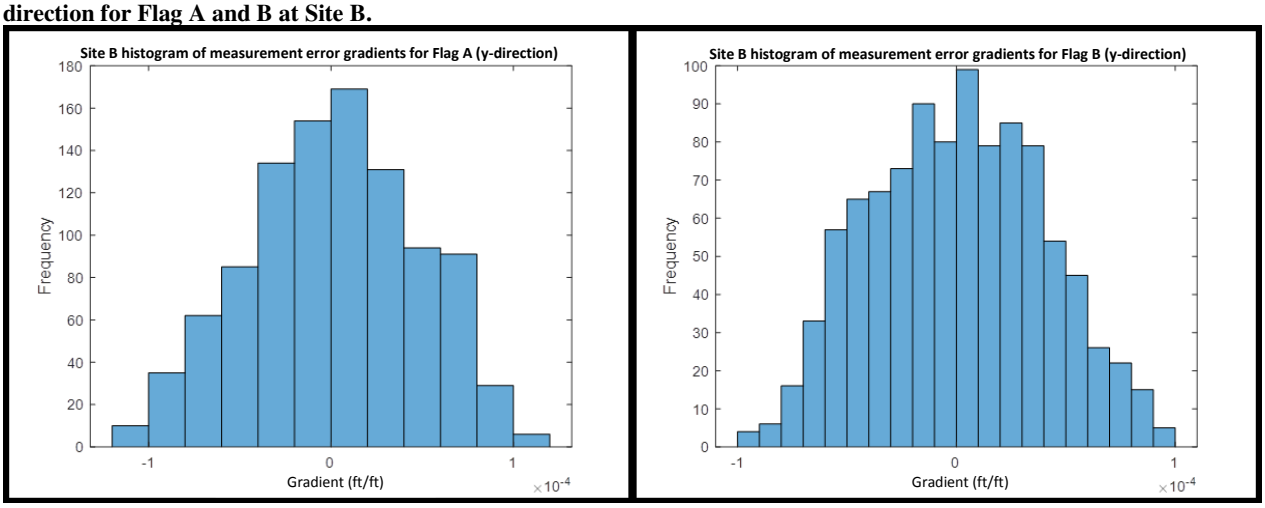

Figure 4.24: Histograms of the synthetic dataset simulation results for measurement error based gradients in the y-direction for Flag A and B at Site B.

Figure 4.25 shows the measurement error effected flow flag simulation (shows both Flag A and B) for a 150-day study at Site B. During the 150-day study Flag A primarily flows in the northern direction. Flag A moves towards Sand Creek and the edge of the site indicating a possibility of contaminant loading against the northern barrier wall that surrounds the site. The average seepage velocity (not considering the effects of measurement error) is 0.64 ft/day

causing Flag A to fall in the orange section of the velocity color gradient. The variability in the direction of travel is small (+0.67°/-0.79° about the estimated direction of travel) between the estimated and measurement error effected flow flags indicating that the direction of groundwater flow at Flag A is largely unaffected by measurement error. The variability in seepage velocity is also small (±1.1 x 10^{-2} ft/day about the estimated seepage velocity) between the estimated and measurement error effected flow flags indicating that the seepage velocity of the Flag A is also largely unaffected by measurement error.

Flag B primarily flows in the north-west direction during the 150-day study. Flag B also moves towards Sand Creek and the edge of the site, providing further evidence for the possibility of contaminant loading against the northern barrier wall that surrounds the site. The average seepage velocity (not considering the effects of measurement error) is 0.54 ft/day causing Flag B to fall in the orange section of the velocity color gradient. The variability in the direction of travel is small (+2.02°/-2.03° about the estimated direction of travel) between the estimated and measurement error effected flow flags indicating that the direction of groundwater flow at Flag B is largely unaffected by measurement error. The variability in seepage velocity is also small (+1.9 x 10^{-3}/-1.2 x 10^{-3} ft/day about the estimated seepage velocity) between the estimated and measurement error effected flow flags indicating that the seepage velocity of the Flag B is also largely unaffected by measurement error.

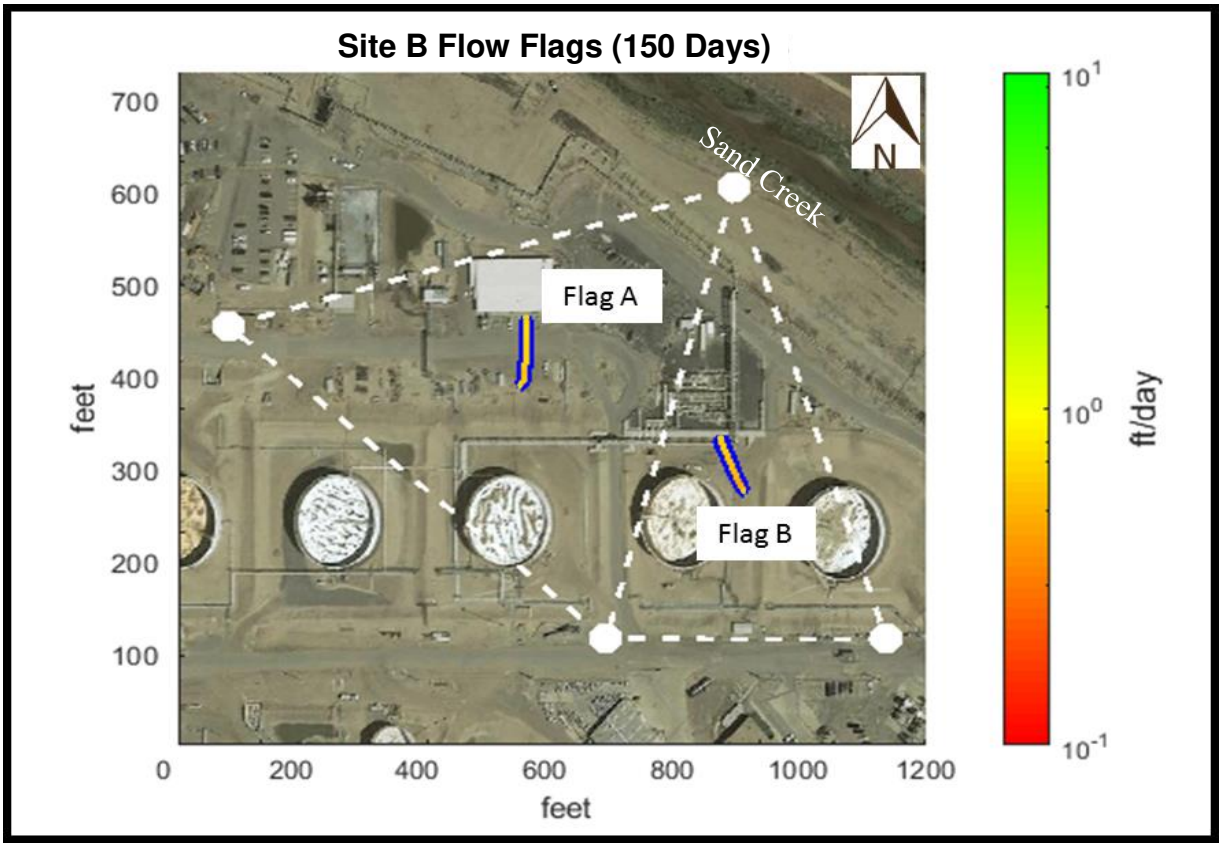

Figure 4.25: Results of the estimated and measurement error affected Site B flow flags over a 150-day period. The white dashed lines outline the monitoring area, the white circles show where head data is being gathered, the blue lines show the 95% confidence interval when affected by measurement error, and the orange line shows the estimated flow flag. Note that due to the large monitored area and narrow 95% confidence interval about the estimated flow flag, the blue and orange lines are very close to one another making it difficult to discern the different lines from one another.

4.5.2 Site B – Effect of Anisotropy Uncertainty on Variability in Groundwater Flow Direction and Seepage Velocity

Figure 4.26 shows the anisotropy uncertainty effected flow flag simulation (shows both Flag A and B) for a 150-day study at Site B. For the anisotropy uncertainty simulation the principal direction of deposition is assumed to be from east to west following Sand Creek. Again, during the 150-day period Flag A primarily flows in the northern direction. The average seepage velocity for the flow flag that uses the estimated anisotropy factor is 0.64 ft/day causing Flag A to fall in the orange section of the velocity color gradient. The variability in the direction of travel is small (±0.31^o about the estimated direction of travel) between the estimated and

anisotropy uncertainty effected flow flags indicating that the direction of groundwater flow at Flag A is largely unaffected by anisotropy uncertainty. The variability in seepage velocity is also small (±5.0 x 10^{-4} ft/day about the estimated seepage velocity) between the estimated and anisotropy uncertainty effected flow flags indicating that the seepage velocity of the Flag A is also largely unaffected by anisotropy uncertainty.

Again, Flag B primarily flows in the north-west direction during the 150-day study. The average seepage velocity for the flow flag that uses the estimated anisotropy factor is 0.56 ft/day causing Flag B to fall in the orange section of the velocity color gradient. The variability in the direction of travel is small (+1.97°/-1.89° about the estimated direction of travel) between the estimated and anisotropy uncertainty effected flow flags indicating that the direction of groundwater flow at Flag B is largely unaffected by anisotropy uncertainty. The variability in seepage velocity is also small (+1.2 x 10^{-2}/-1.1 x 10^{-2} ft/day about the estimated seepage velocity) between the estimated and anisotropy uncertainty effected flow flags indicating that the seepage velocity of the Flag B is also largely unaffected by anisotropy uncertainty.

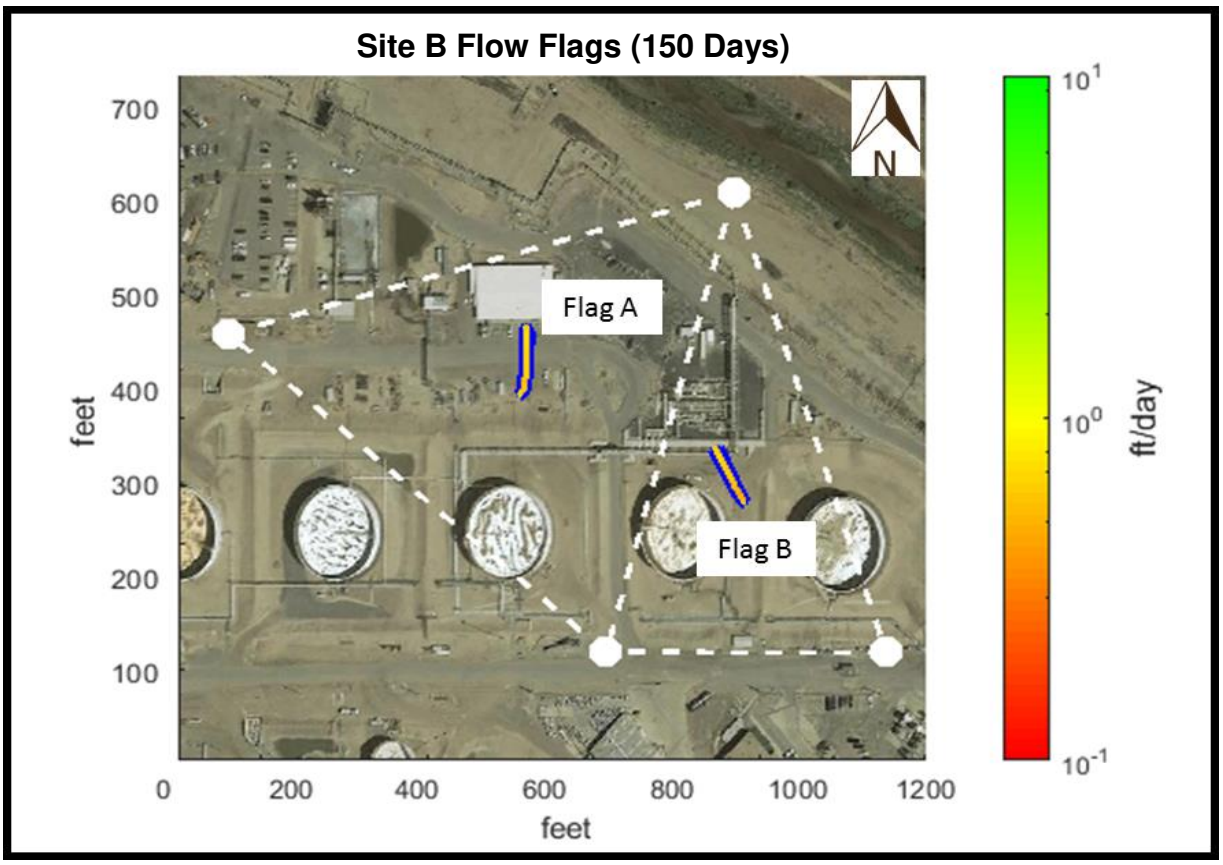

Figure 4.26: Results of the estimated and anisotropy uncertainty affected Site B flow flags over a 150-day period. The white dashed lines outline the monitoring area, the white circles show where head data is being gathered, the blue lines show the 95% confidence interval when affected by anisotropy uncertainty, and the orange line shows the estimated flow flag. Note that due to the large monitored area and narrow 95% confidence interval about the estimated flow flag, the blue and orange lines are very close to one another making it difficult to discern the different lines from one another.

4.5.3 Site B – Comparison of Measurement Error vs Anisotropy Uncertainty

Comparing the results of the measurement error and anisotropy uncertainty flow flag simulations at Flag A the difference in the average, estimated direction of travel is 0.67°. The cumulative deviation from the estimated direction of travel is more than twice as large in the measurement error flow flag simulation versus the anisotropy uncertainty flow flag simulation (1.46° vs 0.62°, respectively). When considering the cumulative effects measurement error and anisotropy uncertainty have on groundwater flow direction at Flag A, a +0.98°/-1.10°, 95% confidence interval about the estimated groundwater flow direction is seen.

Comparing the results of the measurement error and anisotropy uncertainty flow flag simulations at Flag B the difference in the average, estimated direction of travel is 4.25°. The difference in average velocity between the two sources of uncertainty is 0.02 ft/day which is small. The difference in cumulative deviation from the estimated direction of travel is also small (0.19°). When considering the cumulative effects measurement error and anisotropy uncertainty have on groundwater flow direction at Flag B, a +3.99°/-3.92°, 95% confidence interval about the estimated groundwater flow direction is seen.

There is no difference between the average seepage velocities for the measurement error and anisotropy uncertainty simulations for Flag A. However, the 95% confidence interval in seepage velocity for the measurement error flow flag is greater by one order of magnitude compared to the 95% confidence interval in seepage velocity for the anisotropy uncertainty flow flag simulation (2.2×10^{-2} vs 1.0×10^{-3}, respectively). The larger 95% confidence intervals for groundwater flow direction and seepage velocity for the measurement error simulation show that for Flag A, measurement error affects both the possible range of direction of travel and range of seepage velocity more than anisotropy uncertainty. When considering the cumulative effects measurement error and anisotropy uncertainty have on seepage velocity, a $\pm 1.2 \times 10^{-2}$ ft/day, 95% confidence interval about the estimated seepage velocity is seen.

For Flag B, the difference between the average seepage velocities for the measurement error and anisotropy uncertainty simulations is 0.02 ft/day. The 95% confidence interval in seepage velocity for the measurement error flow flag simulation is smaller by one order of magnitude compared to the 95% confidence interval in seepage velocity for the anisotropy uncertainty flow flag simulation (3.1×10^{-3} vs 2.3×10^{-2}, respectively). The larger 95% confidence intervals for seepage velocity in the anisotropy uncertainty simulation shows that at Flag B, anisotropy

uncertainty affects the possible range of seepage velocities of the flow flag more than measurement error. When considering the cumulative effects measurement error and anisotropy uncertainty have on seepage velocities, a $+1.4 \times 10^{-2}/-1.2 \times 10^{-2}$ ft/day, 95% confidence interval about the estimated seepage velocity is seen. Table 4.9 presents the results of the measurement error and anisotropy uncertainty affected flow flag simulations for Flags A and B.

Table 4.9: Comparable results of flow flags at Site B for the measurement error and anisotropy uncertainty simulations. Values in the table above are averaged over the entire study (except for the monitored area). The average directions of travel for the flow flags are measured counter clockwise from the positive x-axis

	Flag A		Flag B	
	Numerical Results of Measurement Error Flow Flag Simulation	Numerical Results of Anisotropy Uncertainty Flow Flag Simulation	Numerical Results of Measurement Error Flow Flag Simulation	Numerical Results of Anisotropy Uncertainty Flow Flag Simulation
Direction of Travel for Estimated Flow Flag (degrees)	86.42	85.75	117.54	121.79
Difference in Direction of Travel Between Estimated and High 95% Confidence Interval Flow Flag (degrees)	+0.67	+0.31	+2.02	+1.97
Difference in Direction of Travel Between Estimated and Low 95% Confidence Interval Flow Flag (degrees)	-0.79	-0.31	-2.03	-1.89
Cumulative Deviation from Estimated Flow Direction (degrees)	1.46	0.62	4.05	3.86
Effects of Measurement Error and Anisotropy Uncertainty on Flow Direction (degrees)	+0.98 (high), -1.10 (low), 2.08 (cumulative)		+3.99 (high), -3.92 (low), 7.91 (cumulative)	
Seepage Velocity for Estimated Flow Flag (ft/day)	0.64	0.64	0.54	0.56
Difference in Seepage Velocity Between Estimated and High 95% Confidence Interval Flow Flag (ft/day)	$+1.1 \times 10^{-2}$	$+5.0 \times 10^{-4}$	$+1.9 \times 10^{-3}$	$+1.2 \times 10^{-2}$
Difference in Seepage Velocity Between Estimated and Low 95% Confidence Interval Flow Flag (ft/day)	-1.1×10^{-2}	-5.0×10^{-4}	-1.2×10^{-3}	-1.1×10^{-2}
Cumulative Deviation from Estimated Seepage Velocity (ft/day)	2.2×10^{-2}	1.0×10^{-3}	3.1×10^{-3}	2.3×10^{-2}
Effects of Measurement Error and Anisotropy Uncertainty on Seepage Velocity (ft/day)	$+1.2 \times 10^{-2}$ (high), -1.2×10^{-2} (low), 2.4×10^{-2} (cumulative)		$+1.4 \times 10^{-2}$ (high), -1.2×10^{-2} (low), 2.6×10^{-2} (cumulative)	
Monitored Area (ft^2)	262,800		157,890	

4.5.4 Site B – Hydrograph

Figure 4.27 shows a hydrograph of the data used for the study at Site B (Flags A and B). The groundwater flow directions and seepage velocities remain relatively constant during the measurement error and anisotropy uncertainty simulations at Site B (Flags A and B). Although the head data in Figure 4.27 varies over time most variations are similar at each well. The similar variations at each well support the relatively constant groundwater flow directions and seepage velocities for the measurement error and anisotropy uncertainty simulations at Site B (Flags A and B). It should be noted that although the groundwater flow directions and seepage velocities remain relatively constant during the study at Site B, the 150-day study period may miss seasonal changes in head that could cause changes in groundwater flow directions and/or seepage velocities.

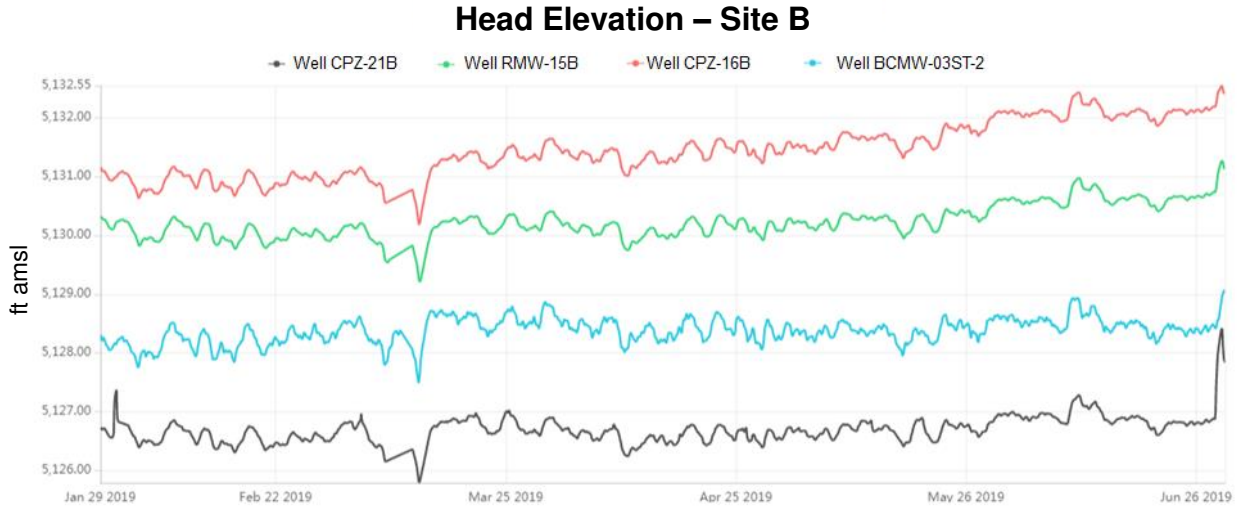

Figure 4.27: Hydrograph of head data used in the measurement error and anisotropy uncertainty simulations at Site B. This data has not been corrected for fluctuations in barometric pressure since the measurement error and anisotropy uncertainty models assume the effects of barometric pressure are common at all wells at each site, negating the need for barometric correction of head values.

4.6 Intersite Comparison of Measurement Error and Anisotropy Uncertainty

Sections 4.6.1-4.6.3 compare the effects of measurement error and anisotropy uncertainty on groundwater flow direction and seepage velocity between the ARDEC, ERC, Site A, Site B Flag A, and Site B Flag B sites. First, the effects of measurement error on groundwater flow direction and seepage velocity are compared between sites. Next, the effects of anisotropy uncertainty on groundwater flow direction and seepage velocity are compared between sites. Lastly the cumulative effects of measurement error and anisotropy uncertainty on groundwater flow direction and seepage velocity are compared between sites.

4.6.1 Intersite – Effect of Measurement Error on Variability in Groundwater Flow Direction and Seepage Velocity

The following table ranks the sites in this study from most to least affected, based on the effect of measurement error on the possible range of groundwater flow directions.

Table 4.10: Sites ranked from most affected to least affected based, on the effect of measurement error on possible range of groundwater flow directions.

	Site	Cumulative Deviation from Estimated Flow Direction (degrees)
Most affected ↓	Site A	20.54
	Site B Flag B	4.05
	ARDEC	1.80
	Site B Flag A	1.46
Least affected	ERC	0.29

The ERC site is the least affected by measurement error even though the site consists of the smallest monitored area (1,487 ft^2). This contradicts previous published work by Devlin and McElwee (2007) which states that with a smaller monitored area the effects of measurement error are expected to be greater. The reason for the discrepancy is thought to be due to vertical

groundwater flow violating one of the model assumptions (Section 3.4.1.1) and causing flawed results.

The deviation from the estimated groundwater flow path caused by measurement error is greater at Site A (20.54^{o}) than the ARDEC, ERC, Site B Flag A, and Site B Flag B sites combined (7.60^{o}). There are two reasons for this. First, the differences in well spacing and measurement error range used in the model influenced the results. Second, the gradient of the head surface at Site A is the least steep of all of the sites considered (Table 4.11).

Table 4.11: Sites ranked from least to most steep when considering the magnitude of the average hydraulic gradient (ft/ft) for each site during their periods of study (when not considering the effect of any sources of uncertainty).

	Site	Average Hydraulic Gradient (ft/ft)
Least steep hydraulic gradient ↓	Site A	3.4×10^{-3}
	Site B Flag B	4.7×10^{-3}
	Site B Flag A	5.5×10^{-3}
	ARDEC	5.8×10^{-3}
Most steep hydraulic gradient	ERC	0.31

At Site B the variability in direction of travel caused by measurement error is nearly three times smaller at Flag A than Flag B (1.37^{o} vs 4.05^{o}, respectively - cumulative deviations from estimated flow paths). The differences in the monitored areas between Flag A and B are: one monitoring location used to gain head values for each triangle and the triangle geometry of the monitored area for each flow flag. Numerically this difference results in a 40% larger monitored area for Flag A than Flag B and average difference of 4.75 feet of head between head values not shared between Flag A and B. The differences in results between Flag A and B are due to differences in monitored area, triangle geometry, and head values. Further explanation on the

effect that monitored area and triangle geometry have on uncertainty in hydraulic gradient estimates can be found in Devlin and McElwee (2007).

Table 4.12 ranks the sites in this study from most to least affected based on the effect of measurement error on the possible range of seepage velocities. In Table 4.12 deviation from the estimated seepage velocities are represented as percentages to make the deviation relative to the estimated seepage velocity comparable across sites.

Table 4.12: Sites ranked from most affected to least affected based on the effect of measurement error on the possible range of seepage velocities.

	Site	Deviation from Estimated Seepage Velocity (%)
Most affected	Site A	19.76
	Site B Flag A	3.44
	ARDEC	2.67
	ERC	1.41
Least affected	Site B Flag B	0.57

The deviation from the estimated seepage velocity caused by measurement error is greater at Site A (19.76%) than the ARDEC, ERC, Site B Flag A, and Site B Flag B sites combined (8.09%). This is also thought to be the result of differences in well spacing and measurement error between the sites, as well as the result of Site A having the least steep hydraulic gradient of all the sites. At Site B, the effects of measurement error on seepage velocity variability are greater by one order of magnitude for Flag A than Flag B (2.2×10^{-2} ft/day vs 3.1×10^{-3} ft/day - cumulative deviations from estimated seepage velocities). Again, this is attributed to the differences in the in monitored areas, triangle geometries, and head values between Flags A and B.

4.6.2 Intersite – Effect of Anisotropy Uncertainty on Variability in Groundwater Flow Direction and Seepage Velocity

The following table ranks the sites in this study from most to least affected, based on the effect of anisotropy uncertainty on the possible range of groundwater flow directions.

Table 4.13: Sites ranked from most affected to least affected based, on the effect of anisotropy uncertainty on the possible range of groundwater flow directions.

	Site	Cumulative Deviation from Estimated Flow Direction (degrees)
Most affected	Site B Flag B	3.86
	Site A	2.73
	ERC	0.97
	Site B Flag A	0.62
Least affected	ARDEC	0.62

The deviation from the estimated groundwater flow path caused by anisotropy uncertainty is the greatest at the Site B Flag B site and the least at the Site B Flag A and ARDEC sites. As previously mentioned, the differences in the monitored areas between the Site B Flags A and B are: one monitoring location used to gain head values for each triangle and the triangle geometry of the monitored area for each flow flag. The difference in deviation from the estimated groundwater flow path caused by anisotropy uncertainty between Site B Flags A and B provides evidence that the magnitude of the effect of anisotropy uncertainty on groundwater flow direction is affected by differences in monitored area, triangle geometry, and head values.

Table 4.14 ranks the sites in this study from most to least affected based on the effect of anisotropy uncertainty on the possible range of seepage velocities. In Table 4.14 deviation from the estimated seepage velocities are represented as percentages in Table 4.14 to make the deviation relative to the estimated seepage velocity comparable across sites.

Table 4.14: Sites ranked from most affected to least affected based, on the effect of anisotropy uncertainty on the possible range of seepage velocities.

	Site	Deviation from Estimated Seepage Velocity (%)
Most affected	ERC	15.38
↓	ARDEC	14.48
	Site B Flag B	4.11
	Site A	3.95
Least affected	Site B Flag A	0.16

The deviation from the estimated seepage velocity is the greatest at the ERC and ARDEC sites. As mentioned in Section 4.6.1 there is evidence that vertical groundwater flow has caused model breakdown at the ERC. The possibility of vertical flow at the ERC site should be kept in mind when considering the following results/discussion. At the ERC site the deviation from the estimated seepage velocity in ft/day is 4.0×10^{-2} ft/day which leads a 14.6-foot cumulative variation about the estimated groundwater flow path over the course of the year. At the ARDEC site the deviation from the estimated seepage velocity in ft/day is 1.16 ft/day which leads a 423-foot cumulative variation about the estimated groundwater flow path over the course of the year. Anisotropy uncertainty causes a greater effect on the deviation from the estimated seepage velocity if the direction of deposition (the direction in which the anisotropy factor and anisotropy uncertainty are applied) is in line with the primary direction of groundwater flow. Evidence for this is presented in Table 4.15.

Table 4.15: Sites ranked from most affected to least affected based, on the effect of anisotropy uncertainty on the possible range of seepage velocities. Direction of deposition (the direction in which the uncertainty in anisotropy was considered) and the primary direction of groundwater flow for the simulation are also shown.

	Site	Direction of Deposition	Primary Direction of Groundwater Flow
Most affected ↓	ERC	N/S	S
	ARDEC	E/W	E
	Site B Flag B	E/W	NW
	Site A	N/S	W/NW
Least affected	Site B Flag A	E/W	N

4.6.3 Intersite – Comparison of Measurement Error vs Anisotropy Uncertainty

Measurement error is seen to have a greater effect on the range of possible groundwater flow directions at the ARDEC, Site A, and Site B (both Flag A and B) sites. Anisotropy uncertainty is seen to have a greater effect on the range of possible groundwater flow directions at the ERC site. When considering the cumulative effects of both measurement error and anisotropy uncertainty on the range of possible groundwater flow directions, the ranking of sites from most affected to least affected are presented in the following table.

Table 4.16: Sites ranked from most affected to least affected based, on the cumulative effect of measurement error and anisotropy uncertainty on the possible range of groundwater flow directions.

	Site	Cumulative Deviation from Estimated Flow Direction (degrees)
Most affected ↓	Site A	23.27
	Site B Flag B	7.86
	ARDEC	2.42
	Site B Flag A	2.08
Least affected	ERC	1.26

Measurement error is seen to have a greater effect on the range of possible seepage velocities at the Site A and Site B (Flag A) sites. Anisotropy uncertainty is seen to have a greater effect on the range of possible groundwater flow directions at the ARDEC, ERC, and Site B (Flag B) sites. When considering the cumulative effects of both measurement error and anisotropy uncertainty

on the range of possible seepage velocities, the ranking of sites from most effected to least effected are presented in Table 4.17. In Table 4.17, deviations from the estimated seepage velocities are represented as percentages in Table 4.17 to make the deviation relative to the estimated seepage velocity comparable across sites.

Table 4.17: Sites ranked from most affected to least affected based, on the cumulative effect of measurement error and anisotropy uncertainty on the possible range of seepage velocities.

	Site	Deviation from Estimated Seepage Velocity (%)
Most affected ↓	Site A	23.53
	ARDEC	18.17
	ERC	17.50
	Site B Flag B	4.73
Least affected	Site B Flag A	3.59

4.7 Real-Time Groundwater Flow Dashboard

The current dashboard allows for head data to be transformed into vibrant graphics that display the movement of flow flags in real-time. Figure 4.28 provides a screen shot taken from the Ubidots dashboard for Site B. The cellular connected data acquisition systems (these systems designed by Dr. Jay Ham, CSU) provide real-time head data (as well as temperature and oxidation reduction potential (ORP) data) at four locations, allowing for two flow flags to be drawn. Data is displayed for a 150-day period where each flow flag was updated on an hourly basis.

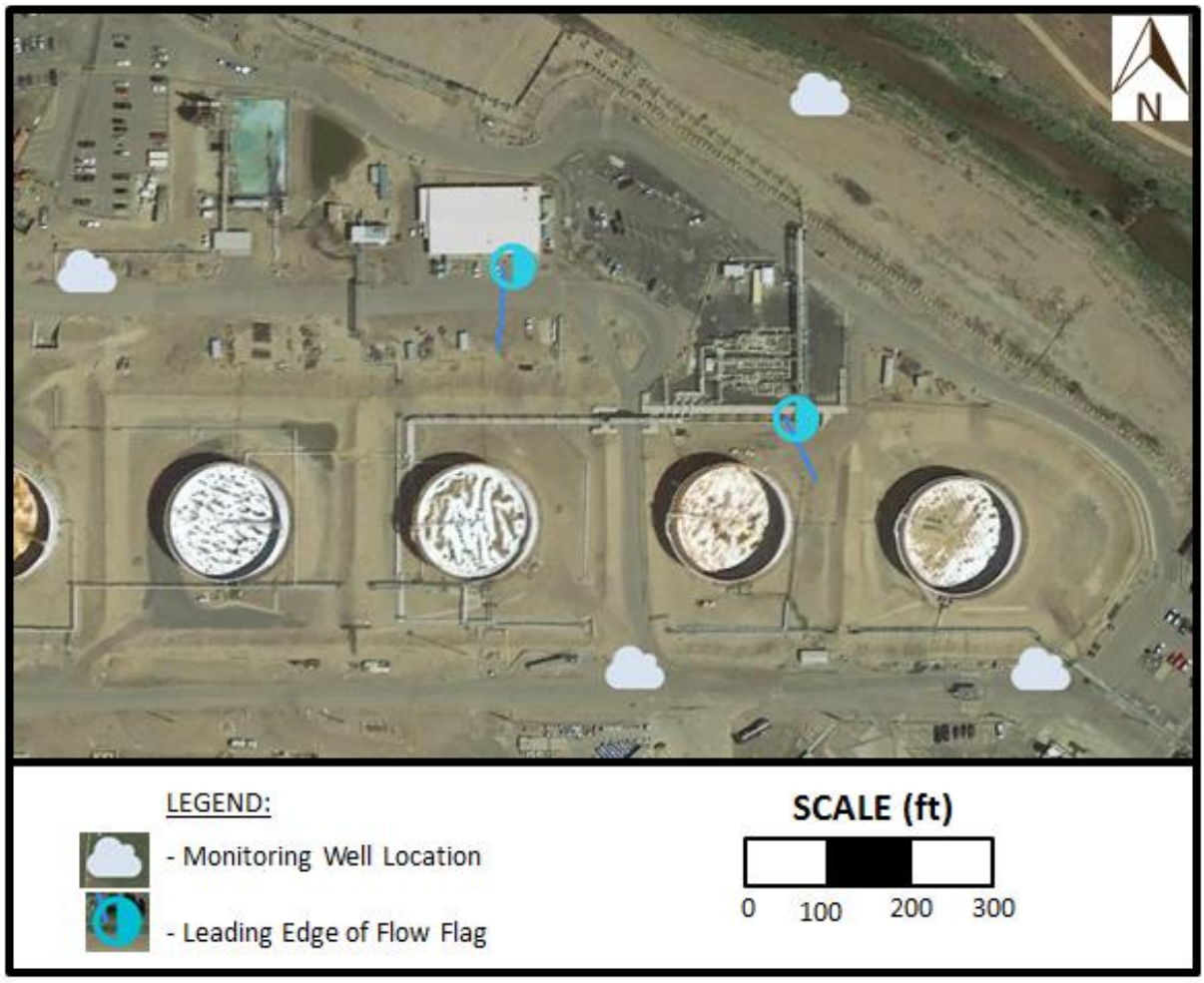

Figure 4.28: Flow flag dashboard visualization for Site B. The scale and legend have been added to after capturing the image from the dashboard.

CHAPTER 5 – SUMMARY AND CONCLUSIONS

With the aging of contaminated sites long-term monitoring is becoming the primary factor determining cost for managing historical releases to soil and groundwater. Differences in head values are a driving factor for the velocity and direction contaminants move in the subsurface, making them an important parameter to consistently measure for effective long-term monitoring. Furthermore, head data can complement other gathered parameters such as temperature and oxidation reduction potential (ORP) to paint a clearer picture of site conditions. This gives rise to the need for effective and affordable methods for gathering and analyzing head data for the purposes of long-term monitoring. With recent advancements in low-cost sensors and cloud-based data acquisition methods, gathering head data in real-time can be a cost effective method to gather and analyze large datasets for the purpose of real-time monitoring.

Furthermore, with additions such as real-time alerts site managers can be automatically notified of adverse conditions leading to quicker response times to potential site issues. This Thesis advances real-time visualization of advective groundwater flow and custom made, affordable hardware that can be used to gather and send head data to the cloud. Additionally, algorithms used to determine the effects of measurement error and anisotropy uncertainty on groundwater flow direction and seepage velocity are advanced, allowing for a clearer picture of possible groundwater flow paths.

5.1 Methods

5.1.1 Hardware

The hardware developed includes cellular connected data loggers and the modification of low-cost, vented pressure transducers into sealed pressure transducers (modified FYD-101s, Xi'an

Feng Yu). Excluding labor costs, the real-time data acquisition system for head measurements developed in this Thesis costs roughly $340.00 per well (Cellular Connected PT Logger V1.2). This includes the modified FYD-101 pressure transducer, cellular connected data logger, power management system, and weatherproof enclosure. When compared to a Campbell Scientific system of similar functionality the cost rises to roughly $3,200.00 per well. Since a minimum of three head measurements at three different wells are required for the flow flag algorithm this results in an initial cost savings of roughly $8,580.00 for the first flow flag and an added savings of $2,860.00 per each well/flow flag thereafter.

5.1.2 Software

All groundwater flow models utilize head and hydraulic conductivity. Measurements of head and hydraulic conductivity values are subject to error which will affect the model outcome. The effect of error in head and hydraulic conductivity estimates are not considered in modern numerical models such as MODFLOW or MODPATH and as a consequence these models paint an incomplete picture of the possible range of groundwater flow directions. In addition, the temporal and spatial discretization and prescribed boundary conditions of numerical models may be insufficient in accurately depicting the path of groundwater flow.

Using three wells equipped with pressure transducers, hydraulic head is measured on an hourly basis. Hydraulic head values are used to determine horizontal gradients of the head surface on an hourly basis. Using hydraulic head values and the seepage velocity equation, advective groundwater flow paths are advanced through time. The effects of measurement error are incorporated into the model by using synthetic dataset simulations to estimate the plausible effect of measurement error on groundwater flow paths at each site. Measurement error effected groundwater flow paths are drawn to visualize the 95% confidence interval of the possible

groundwater flow directions and seepage velocities, based on synthetic dataset simulations. The effects of anisotropy uncertainty are also estimated by way of a synthetic dataset simulation. Anisotropy uncertainty effected groundwater flow paths are drawn to visualize the 95% confidence interval of the possible groundwater flow directions and seepage velocities, based on the synthetic dataset simulation.

This research also generated a real-time dashboard for advective groundwater flow. Dashboards were constructed for all sites in this Thesis although only the Site B dashboard is shown to provide an example of online visualization. The automation of creating flow flags in real-time saves considerable time when compared to methods that require manual data collection and transforms. With the addition of alerts, the real-time dashboards promote timely reactions to adverse conditions unlike methods that require manual data collection and transforms.

5.2 Results

5.2.1 Effect of Pressure Transducer Drift on Variability in Groundwater Flow Directions and Seepage Velocities

Vented pressure transducer field testing revealed the FYD-101 pressure transducer to drift the least of the three low-cost pressure transducers tested. The FYD-101 drifted 0.018 feet of head over a 6.5 month study which is close to the quoted accuracy of ±0.012 feet of head. Overall the FYD-101 pressure transducer drifted very little over the study. Once modified into a sealed design, the FYD-101 pressure transducers experienced greater drift with maximum errors of 0.354-0.495 feet seen over a 5 month study, depending on the sensor. However, the increase in drift had little effect on model results, leading to an average difference in seepage velocity of $4.7x10^{-2}$ ft/day and average difference in direction of groundwater flow of 1.07^{o} when compared

to data gathered from more costly pressure transducers (Solinst, Levelogger) which drifted very little (0.016-0.061 feet, depending on the pressure transducer) over the course of the study. The reason the increased drift in FYD-101 readings had little effect on model results is that the sensors all experienced drift in a similar magnitude and direction leading to relative head values that still accurately represented the hydraulic gradient at the site.

5.2.2 Effect of Measurement Error on Groundwater Flow Directions and Seepage Velocities

Measurement error had a greater effect compared to anisotropy uncertainty on the range of possible groundwater flow directions at the ARDEC, Site A, and Site B (both Flag A and B) sites. This shows that in general, measurement error will affect the possible range of groundwater flow directions more than anisotropy uncertainty at a given site. Table 5.1 shows the effect of measurement error on cumulative deviation from the estimated direction of groundwater travel for all sites.

Table 5.1: Average estimated direction of travel (measured counterclockwise from the positive x-axis) and average deviation from the estimated direction of travel (deviation based on 95% confidence interval results for effect of measurement error) for each site.

Site	Estimated Direction of Travel (degrees)	Cumulative Deviation from Estimated Direction of Travel (degrees)
ARDEC	-84.87	1.80
ERC	7.72	0.29
Site A	153.34	20.54
Site B Flag A	86.42	1.46
Site B Flag B	117.54	4.05

Measurement error had a greater effect compared to anisotropy uncertainty on the range of possible seepage velocities at the Site A and Site B (Flag A) sites. Table 5.2 shows the effect of measurement error on cumulative deviation from the estimated seepage velocity for all sites.

Table 5.1: Average estimated seepage velocity and average deviation from the estimated seepage velocity (deviation based on 95% confidence interval results for effect of measurement error) for each site.

Site	Estimated Seepage Velocity (ft/day)	Cumulative Deviation from Estimated Seepage Velocity (ft/day)
ARDEC	6.74	0.18
ERC	0.22	3.1×10^{-3}
Site A	0.42	8.3×10^{-2}
Site B Flag A	0.64	2.2×10^{-2}
Site B Flag B	0.54	3.1×10^{-3}

5.2.3 Effect of Anisotropy Uncertainty on Groundwater Flow Directions and Seepage Velocities

Anisotropy uncertainty had a greater effect compared to measurement error on the range of possible groundwater flow directions at the ERC site. Table 5.3 shows the effect of anisotropy uncertainty on cumulative deviation from the estimated direction of groundwater travel for all sites.

Table 5.3: Average estimated direction of travel using the estimated anisotropy factor (measured counterclockwise from the positive x-axis) and average deviation from the estimated direction of travel (deviation based on 95% confidence interval results for effect of anisotropy uncertainty) for each site.

Site	Estimated Direction of Travel (degrees)	Cumulative Deviation from Estimated Direction of Travel (degrees)
ARDEC	-85.73	0.62
ERC	6.50	0.97
Site A	152.00	2.73
Site B Flag A	85.75	0.62
Site B Flag B	121.79	3.86

Anisotropy uncertainty had a greater effect compared to measurement error on the range of possible seepage velocities at the ARDEC, ERC, and Site B (Flag B) sites. This shows that in general, anisotropy uncertainty will affect the possible range of seepage velocities more than measurement error at a given site. Table 5.4 shows the effect of anisotropy uncertainty on cumulative deviation from the estimated seepage velocity for all sites.

Table 5.4: Average estimated seepage velocity using the estimated anisotropy factor and average deviation from the estimated seepage velocity (deviation based on 95% confidence interval results for effect of anisotropy uncertainty) for each site.

Site	Estimated Seepage Velocity (ft/day)	Cumulative Deviation from Estimated Seepage Velocity (ft/day)
ARDEC	8.01	1.16
ERC	0.26	4.0×10^{-2}
Site A	0.43	1.7×10^{-2}
Site B Flag A	0.64	1.0×10^{-3}
Site B Flag B	0.56	2.3×10^{-2}

5.2.4 Intersite Comparison

Intersite comparison revealed measurement error to have the greatest effect on the range of possible groundwater flow directions at the Site A site. The effect of measurement error on deviation from the estimated direction of travel was 20.54^{o} at Site A and 7.6^{o} for all other sites combined. Measurement error also had the greatest effect on the range of possible seepage velocities at the Site A. The effect of measurement error on deviation from the estimated seepage velocity was 19.76% (percent deviation from estimated seepage velocity) at Site A and 8.09% (percent deviation from estimated seepage velocity) for all other sites combined. Site A had the lowest hydraulic gradient which is thought to be the primary reason for the large range of groundwater flow directions and seepage velocities. This conclusion supports previous findings by Devlin and McElwee (2007) which states that hydraulic gradient estimates are more affected by measurement error at sites with shallow hydraulic gradients. Measurement error had the least effect on the range of possible groundwater flow directions at the ERC site (0.29^{o} deviation from the estimated direction of travel). The ERC site consists of the smallest monitored area (1,487 ft^2) which contradicts previous findings by Devlin and McElwee (2007) which states that generally estimations of hydraulic gradients in smaller monitored areas will be effected more by measurement error. The reason for these odd findings is thought to be due to vertical flow at the

ERC site violating the model assumption that flow in the vertical direction is negligible. Measurement error had the least effect on the range of possible seepage velocities at the Site B, Flag B site (0.57% deviation from estimated seepage velocity). This is thought to be due to a combination of factors including triangle geometry and hydraulic gradient.

Intersite comparison revealed anisotropy uncertainty to have the greatest effect on the range of possible groundwater flow directions at the Site B, Flag B site. The effect of anisotropy uncertainty on deviation from the estimated direction of travel was 3.86^{o} at Site B (Flag B) and 4.94^{o} for all other sites combined. Anisotropy uncertainty had the greatest effect on the range of possible seepage velocities at the ERC site. The effect of anisotropy uncertainty on deviation from the estimated seepage velocity was 15.38% at the ERC, 14.48% at ARDEC, and 8.22% (percent deviation from estimated seepage velocities) for all other sites combined. As previously noted vertical hydraulic gradients at the ERC site are possible which would violate the assumption that vertical hydraulic gradients are negligible, creating unreliable results. Anisotropy had the least effect on the range of possible groundwater flow directions at the ARDEC site (0.62^{o} deviation from the estimated direction of travel). Anisotropy uncertainty had the least effect on the range of possible seepage velocities at the Site B, Flag A site (0.16% deviation from estimated seepage velocity). This is thought to be due to a combination of factors including triangle geometry and hydraulic gradient. The sites whose range of seepage velocities were most affected by anisotropy uncertainty had their primary direction of groundwater flow in-line with the direction of deposition. This evidence has led to the conclusion that the effects of anisotropy uncertainty on the range of possible seepage velocities will be the greatest when the primary direction of groundwater flow is in-line with the direction of deposition.

5.3 Primary Conclusions

- Custom made data acquisition systems can be used to gather real-time data for an affordable price.
- Real-time dashboards can be used to provide simple and effective ways to visualize large data sets of groundwater head.
- Despite pressure transducer drift at the ARDEC site, the effects on the Flow Flag Model output were negligible since the direction and magnitude of drift was similar for all pressure transducers.
- The effects of anisotropy uncertainty and measurement error are site specific.
- Anisotropy uncertainty will have a greater effect on the possible range of seepage velocities if in-line with the primary direction of groundwater flow.
- Measurement error will have a greater effect on the possible range groundwater flow directions and seepage velocities at sites with flatter hydraulic gradients.

5.4 Limitations of the Flow Flag Algorithm

The Flow Flag Algorithm provides the ability to visualize groundwater flow paths in real-time as well as visualize the effect of measurement error and anisotropy uncertainty on causing deviation from the estimated groundwater flow path. Real-time visualization of groundwater flow paths has less benefit at sites where the hydraulic gradient is relatively constant (i.e. not dynamic) through time since data acquired from periodic manual measurements will provide similar model results. The benefit of examining the effect of anisotropy uncertainty on causing deviation from the estimated groundwater flow path is the greatest at sites where the direction of anisotropy is in-line with the primary direction of groundwater flow. At sites where the direction of anisotropy is perpendicular to the primary direction of groundwater flow, the effects of anisotropy

uncertainty will be less, resulting in less meaningful results from the anisotropy uncertainty simulation. Finally, the effects of measurement error are the greater at sites whose hydraulic gradients are flatter. As a result, at sites where the hydraulic gradient is relatively steep the measurement error simulation will provide less meaningful results.

5.5 Future Work

The current dashboards have the ability to display flow flags in real-time but do not show the error based flow flags or color the dashboard flow flag based on its seepage velocity. Advancements in dashboard display should be made to allow for the addition of error based flow flags and colored dashboard flow flags in real-time. Additionally, the current method to transform real-time head data into dashboard flow flags requires a physical computer to act as a server for real-time data transforms. Eventually algorithms should be coded to run in the cloud so that reliance on a physical computer is not required.

Continued advancement and testing of developed hardware should also be considered. Long-term field testing of the *Cellular Connected PT Loggers* should be conducted to ensure the functionality of these designs and modify the designs if necessary. Although the drift of the modified FYD-101 (Xi'an Feng Yu) sensors did not significantly affect the model results at ARDEC, their ability to give accurate absolute head was considerably lessened due to drift. In response to this, future work should include improving on the current pressure transducer by experimenting with different sealing methods or developing a custom made, affordable head measurement sensor. Additional field validation (particularly in more shallow hydraulic gradient sites) should be conducted to ensure that the model continues to give reasonable estimations of groundwater flow direction and seepage velocity when subject to pressure transducer drift. Tracer tests provide one option to compare model results with acquired field data.

Continued advancement of the flow flag algorithm should also be considered. This includes considering the effects of: 1) heterogeneity, 2) groundwater and contaminant flow in the z-direction, 3) varying chemical and microbial reactions and their effect on contaminant transport, and 4) preforming covariance tests to measure the joint variability between the measurement error and anisotropy uncertainty effected hydraulic gradients in the x and y-directions.

Algorithms have been developed which utilize subsurface temperature data to determine natural source zone depletion (NSZD) rates of released petroleum-based contaminants (e.g. Askarani et al., 2018; Askarani and Sale, 2019; Askarani and Sale, 2020). Using algorithms such as the NSZD algorithm, paired with the flow flag algorithm described in this Thesis provide opportunities for synergistically combining multiple data sets to paint a clearer picture of site conditions.

Finally, at Site B real-time data being gathered includes not only head but also subsurface temperature and ORP data (data acquisition system design by Dr. Jay Ham, CSU). The large datasets these systems acquire provide an opportunity to utilize emerging technologies such as Artificial Intelligence (AI) to identify relationships between groundwater, temperature, and ORP.

REFERENCES

Askarani, K.K.; Stockwell, E.B.; Piontek, K.R.; Sale, T.C. Dec. 2018. Thermal Monitoring of Natural Source Zone Depletion. *Groundwater Monitoring & Remediation*, vol. 38, no. 3, pp. 43–52.

Askarani, K.K. and Sale T.C. 2019. New Method for Transforming Temperature Data to Natural Source Zone Depletion Rates. In *AGU Fall Meeting 2019*. AGU.

Askarani, K.K. and Sale T.C. 2020. Thermal estimation of natural source zone depletion rates without background correction. *Water research* 169: 115245.

Beljin, M.; Ross, R.R.; Acree, S.D. 2014. 3PE: A Tool for Estimating Groundwater Flow Vectors. *United States Environmental Protection Agency*, EPA/600/R-14/273.

Bevington, P.R. and Robinson, D.K. 1992. Data Reduction and Error Analysis for the Physical Sciences. *McGraw-Hill*.

Bright, J.; Wang, F.; Close, M. 2002. Influence of the Amount of Available K Data on Uncertainty About Contaminant Transport Prediction. *Ground Water*, vol. 40, no. 5, pp. 529–534.

Burger, R.L. and Belitz, K. 1997. Measurement of Anisotropic Hydraulic Conductivity in Unconsolidated Sands: A Case Study from a Shoreface Deposit, Oyster, Virginia. *Water Resources Research*, vol. 33, no. 6, pp. 1515–1522.

Dagan, G. 1986. Statistical Theory of Groundwater Flow and Transport: Pore to Laboratory, Laboratory to Formation, and Formation to Regional Scale. *Water Resources Research*, vol. 22, no. 9S.

Devlin, J.F. 2003. A Spreadsheet Method of Estimating Best-Fit Hydraulic Gradients Using Head Data from Multiple Wells. *Ground Water*, vol. 41, no. 3, pp. 316–320.

Devlin, J.F. and McElwee, C.D. 2007. Effects of Measurement Error on Horizontal Hydraulic Gradient Estimates. *Ground Water*, vol. 45, no. 1, pp. 62–73.

Domenico, P.A. and Schwartz, F.W. 1997. Physical and Chemical Hydrogeology. *John Wiley Sons*.

United States Environmental Protection Agency. Jan. 2012. EPA On-Line Tools for Site Assessment Calculation – Hydraulic Gradient Magnitude and Direction. *EPA*, https://www3.epa.gov/ceampubl/learn2model/part-two/onsite/gradient4plus-ns.html.

Gao, Y. 2017. Particle Tracking Using Dynamic Water Level Data. *Masters Thesis. Colorado State University, Fort Collins, Colorado*.

Getzen, R.T. 1983. Soil Mechanics Related to Permeability Anisotropy of Costal Sand Deposits. *Coastal Zone '83: Proceedings of the Symposium on Coastal Ocean Management*, pp. 2413–2430.

Hantush, M.S. 1966. Analysis of Data from Pumping Tests in Anisotropic Aquifers. *Journal of Geophysical Research*, vol. 71, no. 2, pp. 421–426.

Jackson, C.R. 2002. Steady-State Particle Tracking in the Object-Oriented Regional Groundwater Model ZOOMQ3D. *British Geological Survey*. pp. 40, CR/02/210N.

Kelly, W.E. and Bogardi, I. 1989. Flow Directions With A Spreadsheet. *Ground Water*, vol. 27, no. 2, pp. 245–247.

Killey, R.W.D. and Moltyaner, G. L. 1988. Twin Lake Tracer Tests: Setting, Methodology, and Hydraulic Conductivity Distribution. *Water Resources Research*, vol. 24, no. 10, pp. 1585–1612.

Lu, N. 1994. A Semianalytical Method of Path Line Computation for Transient Finite-Difference Groundwater Flow Models. *Water Resources Research*, vol. 30, no. 8, pp. 2449–2459.

Subashini, M.M.; Das, S.; Heble S.; Raj, U.; Karthik, R. Jan. 2018. Internet of Things Based Wireless Plant Sensor for Smart Farming. *Indonesian Journal of Electrical Engineering and Computer Science*, vol. 10, no. 2, pp. 456–468.

Neuman, S.P.; Walter, G.R.; Bentley H.W.; Ward J.J.; Gonzalez, D.D. 1984. Determination of Horizontal Aquifer Anisotropy with Three Wells. *Ground Water*, vol. 22, no. 1, pp. 66–72.

Onset. 2019. HOBO U20 Water Level Logger (U20-001-0x and U20-001-0x-Ti) Manual.

Schwartz, F. W. and Zhang, H. 2002. Fundamentals of Ground Water. *Wiley.*

Shamsuddin, M.K.N.; Suratman, S.; Zakaria. M.P.; Aris, A.Z.; Sulaiman, W.N.A. Aug. 2014. Particle Tracking Analysis of River–Aquifer Interaction via Bank Infiltration Techniques. *Environmental Earth Sciences*, vol. 72, no. 8, pp. 3129–3142.

Silliman, S.E. and Mantz, G. 2000. The Effect of Measurement Error on Estimating the Hydraulic Gradient in Three Dimensions. *Ground Water*, vol. 38, no. 1, pp. 114–120.

Solinst. 2014. Levelogger 3001 User Guide.

Sorensen, James P.R. and Butcher, A.S. 2011. Water Level Monitoring Pressure Transducers-A Need for Industry-Wide Standards. *Ground Water Monitoring & Remediation*, vol. 31, no. 4, pp. 56–62.

TE Connectivity. 2016. Sealed-Vented-Absolute: How to Know Which Transducer to Specify.

Topcon. 2012. GR-5 GNSS Receiver Operator's Manual.

Way, S.C. and Mckee, C.R. 1982. In-Situ Determination of Three-Dimensional Aquifer Permeabilities. *Ground Water*, vol. 20, no. 5, pp. 594–603.

Xi'an Feng Yu Industry Co. 2019. FYD-1x Submersible Digital level transmitter datasheet.

Yidana, S.M. Jan. 2010. Groundwater Flow Modeling and Particle Tracking for Chemical Transport in the Southern Voltaian Aquifers. *Environmental Earth Sciences*, vol. 63, no. 4, pp. 709–721.

APPENDIX A – SUPPLEMENTARY INFORMATION FOR CHAPTER 3

Appendix A contains supplementary information in support of Chapter 3. This information includes an explanation of the mathematics behind the planar surface method for gaining slopes in the x and y directions using three head values, the results of the by-hand vs advective flow algorithm results for a synthetic dataset, and the data from the Analog to Digital Converter (ADC) test.

Explanation of Kramer's Rule which is used to calculate the results of a synthetic dataset by-hand to compare to the advective flow algorithm and confirm its proper working order.

$$a = \frac{\left|\begin{pmatrix} (z_2 - z_1) & (y_2 - y_1) \\ (z_3 - z_1) & (y_3 - y_1) \end{pmatrix}\right|}{\left|\begin{pmatrix} (x_2 - x_1) & (y_2 - y_1) \\ (x_3 - x_1) & (y_3 - y_1) \end{pmatrix}\right|}$$

$$b = \frac{\left|\begin{pmatrix} (x_2 - x_1) & (z_2 - z_1) \\ (x_3 - x_1) & (z_3 - z_1) \end{pmatrix}\right|}{\left|\begin{pmatrix} (x_2 - x_1) & (y_2 - y_1) \\ (x_3 - x_1) & (y_3 - y_1) \end{pmatrix}\right|}$$

(Devlin and McElwee, 2007)

where, x_1 , x_2 , and x_3 [L] represent the x coordinates of three wells, y_1 , y_2 , and y_3 [L] represent the y coordinates of the three wells, and z_1 , z_2 , and z_3 [L] represent the head measurements at the three wells. The values a and b [dimensionless] represent the gradient in the x and y directions, respectively when considering the equations for head at three well locations:

$$\begin{aligned} z_1 &= ax_1 + by_1 + c \\ z_2 &= ax_2 + by_2 + c \\ z_3 &= ax_3 + by_3 + c \end{aligned}$$

(Devlin and McElwee, 2007)

where, c [dimensionless] is a constant that results from the regression.

Results of the flow flag algorithm and by-hand calculations (using Kramer's Rule) used to test and confirm the working order of the flow flag algorithm for estimated and measurement effected flow paths.

	First Test		Second Test		Third Test	
	Simulation Result	By-Hand Result	Simulation Result	By-Hand Result	Simulation Result	By-Hand Result
X Location (Average)	3140125.6999	3140125.6999	3140125.7182	3140125.7182	3140125.7345	3140125.7345
Y Location (Average)	1481388.7899	1481388.7899	1481388.4891	1481388.4891	1481388.1880	1481388.1880
X Location (Low 95% confidence Interval)	3140125.7057	3140125.7057	3140125.7278	3140125.7278	3140125.7484	3140125.7484
Y Location (Low 95% confidence Interval)	1481388.7935	1481388.7935	1481388.4933	1481388.4933	1481388.1963	1481388.1963
X Location (High 95% confidence Interval)	3140125.6941	3140125.6941	3140125.7085	3140125.7085	3140125.7207	3140125.7207
Y Location (High 95% confidence Interval)	1481388.7862	1481388.7862	1481388.4849	1481388.4849	1481388.1797	1481388.1797

Raw data from the ADC test used to determine which of the two ADCs (MCP3424 and ADS1115) performed better for the intended application.

Difference in depth to water (DTW) when reading the same, two sealed pressure transducers between the two ADCs tested (MCP3424 and ADS1115).

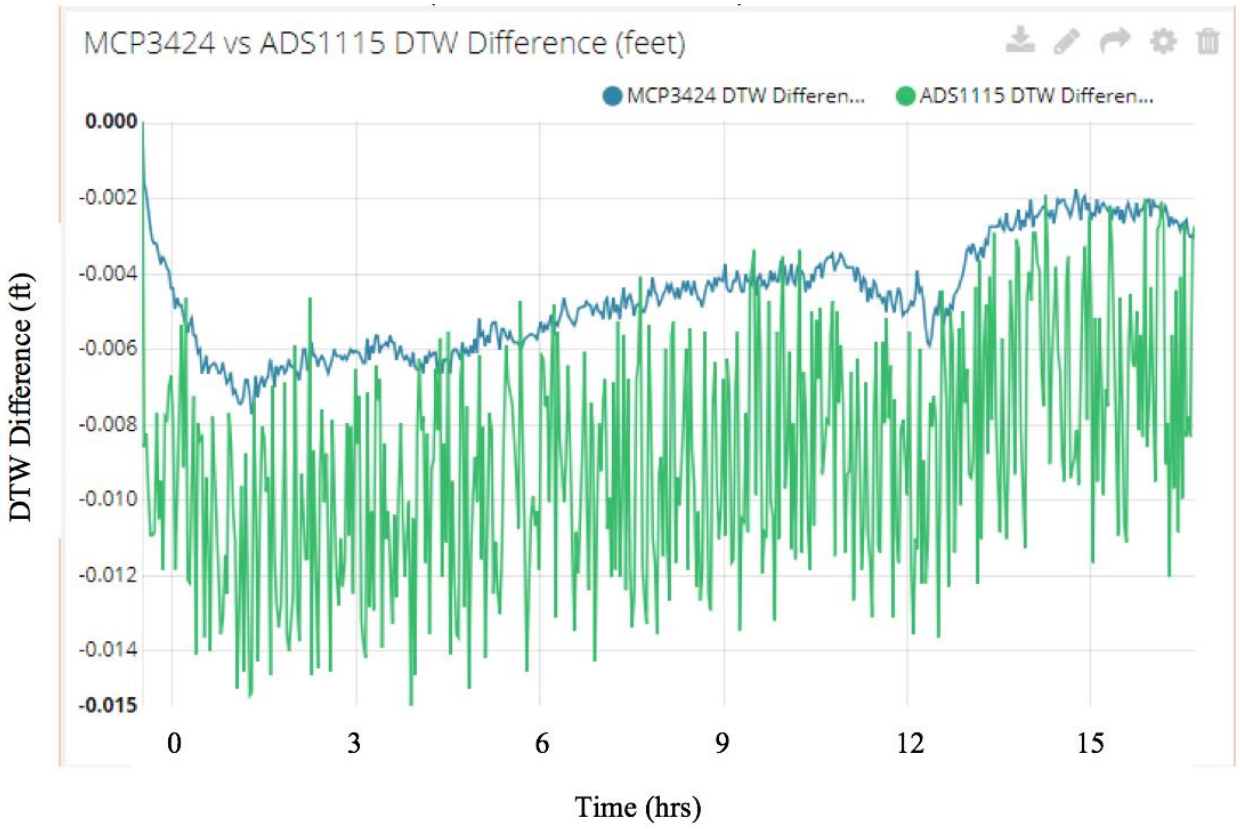

Code for creating .gif (video) files for dashboard display at ARDEC. The API key has been redacted for reasons of security.

```
plot_google_map('apiKey', 'INSERT_API_KEY_HERE') %if you have API KEY
hold on
lat = [40.65242078 40.65454819 40.65416964];
lon = [-104.9959206 -104.9957254 -104.9932989];
plot(lon, lat, '.w', 'MarkerSize', 40)
axis([-104.9972730571466 -104.9920898569569 40.65187558038719
40.65497702990462]);
plot_google_map('maptype','satellite')

%Track Starting Location
particle_x_start = (3139867.832 + 3139917.586 + 3140591.631) / 3;
particle_y_start = (1480916.879 + 1481692.233 + 1481558.16) / 3;

%Convert US survey feet coordinates to Lat and long degrees. code source =
https://www.mathworks.com/matlabcentral/fileexchange/26413-sp_proj
[startlong, startlat] = sp_proj('colorado north','inverse',particle_x_start,
particle_y_start,'sf');
plot(startlong, startlat, '*b', 'MarkerSize', 2);
gif('ARDEC_Flow_Path.gif');

particle1_US_x = particle_x_start;
particle1_US_y = particle_y_start;

%input initial values
ne = 0.25; %effective porosity (dimensionless)
K_iso = 12; %isotropic hydraulic conductivity (ft/hr)
t = 1; %time step (hr)

%IMPORT DATA - Be sure to "flip" data in Excel!
ARDEC_1Excel = xlsread('ARDEC_1_WT_forUpdate.xlsx'); %insert Excel file name
here
ARDEC_2Excel = xlsread('ARDEC_2_WL_NEW_forUpdate.xlsx');
ARDEC_3Excel = xlsread('ADREC_3_WL_forUpdate.xlsx');

%ARDEC Well Locations
Wellxy = [3139867.832 1480916.879; 3139917.586 1481692.233; 3140591.631
1481558.16]; %ARDEC_1, ARDEC_2, ARDEC_3

Ndata = %insert number of data points here
for i = 2:Ndata

%exract water table elevations
WL1 = ARDEC_1Excel(i,3);
WL2 = ARDEC_2Excel(i,3);
WL3 = ARDEC_3Excel(i,3);

WL_vector =  [WL1; WL2; WL3]; %create vector of water levels
```

```
Plane = [ones(3,1), Wellxy] \ WL_vector;
Slopex = Plane(2); %extract slope x
Slopey = Plane(3); %extract slope y

%change particle position based on new planar surface (Homogeneous,
Isotropic)
%particle 1
xpos1 = particle1_US_x - ((Slopex*K_iso*t)/ne);
ypos1 = particle1_US_y - ((Slopey*K_iso*t)/ne);

 %Convert US survey feet coordinates to Lat and long degress. code source =
https://www.mathworks.com/matlabcentral/fileexchange/26413-sp_proj
 [particle1_newlng,particle1_newlat] = sp_proj('colorado
north','inverse',xpos1,ypos1,'sf');
```

Software entered into Ubidots HTML *Widget* to display the ARDEC flow flag (video hosted on giphy.com) in the ARDEC dashboard. The address where the video is hosted has been redacted for reasons of security.

```
<div style="width:100%;height:0;padding-bottom:79%;position:relative;">
<iframe src="INSERT_VIDEO_WEBSITE_ADRESS_HERE"
width="100%" height="100%" style="position:absolute" frameBorder="0"
class="giphy-embed" allowFullScreen></iframe></div><p>
<a href=" INSERT_VIDEO_WEBSITE_ADRESS_HERE ">via GIPHY</a></p>
```

APPENDIX B – SUPPLEMENTARY INFORMATION FOR CHAPTER 4

Appendix B contains supplementary information for Chapter 4. This information includes results of the FYD-101 pressure transducer vs water level sounder readings for the ARDEC pressure transducer drift study and software used for the measurement error, anisotropy uncertainty, and real-time advective flow (flow flag) algorithms. This software was written using MATLAB R2018b software. It should be noted that sensitive and private information including API and TOKEN keys, device IDs, and variable IDs have been redacted from the code for reasons of security.

Comparison results for the FYD-101 pressure transducer vs water level sounder readings at ARDEC.

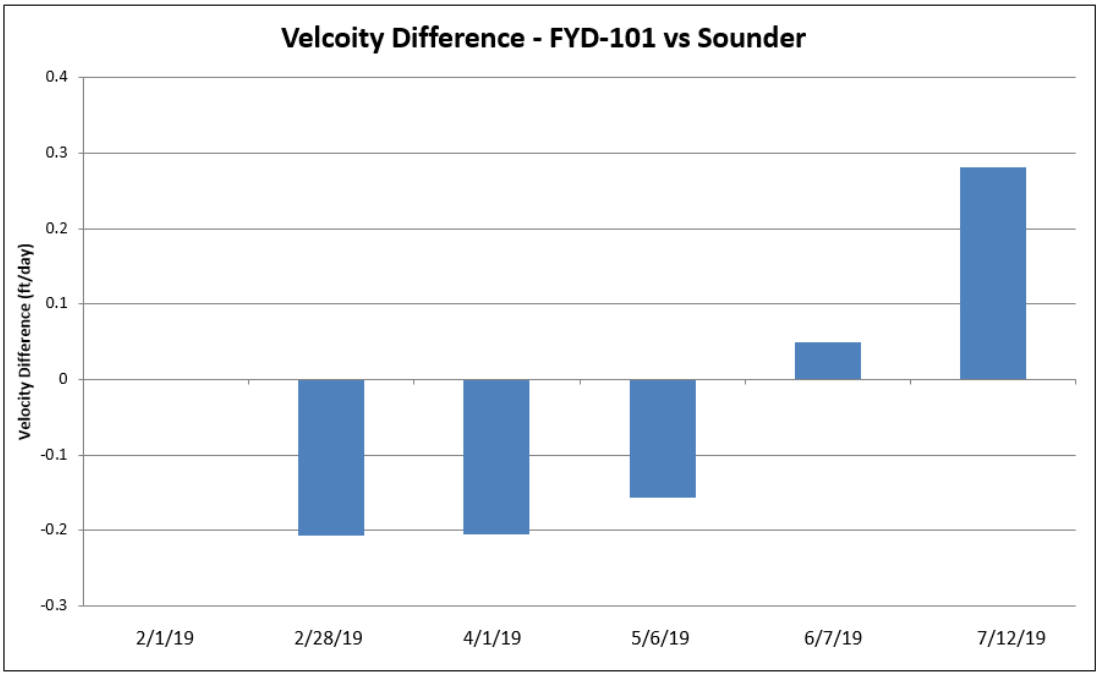

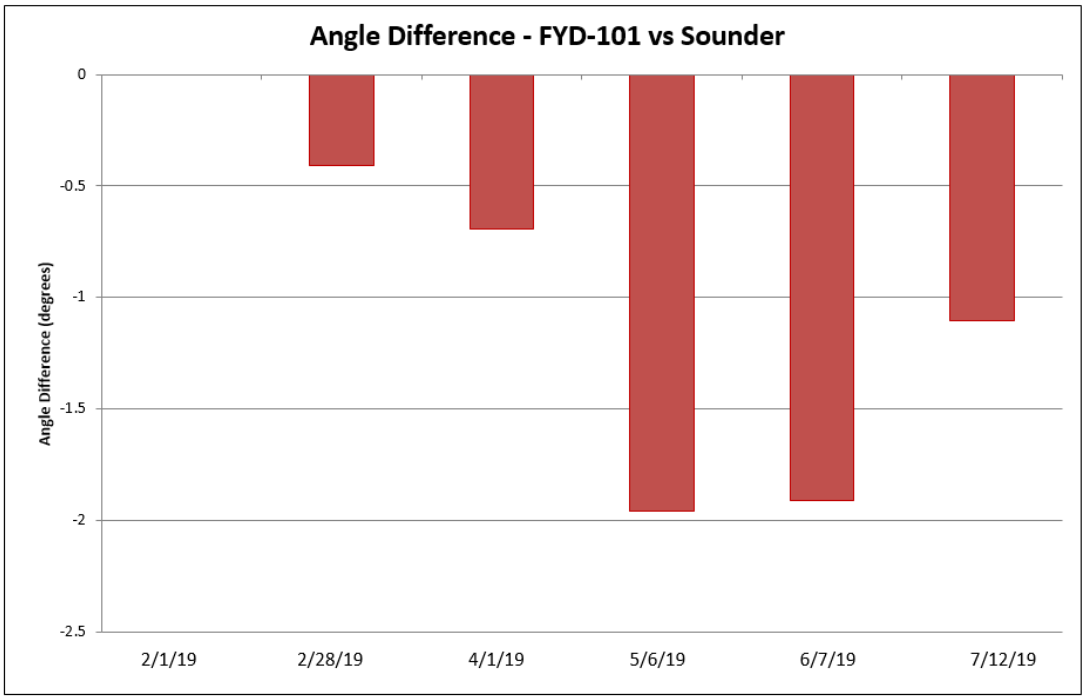

Code used to create anisotropy uncertainty synthetic data set.

```
p = 6; %smoothing factor
xmin=1; %constrain randomization (min)
xmax=1.38; %constrain randomization (max)
n=1000; %sample size
X = xmin + (xmax - xmin)*sum(rand(n,p),2)/p; %run Monte Carlo Simulation
histogram(X) %display histogram of data
```

Code for estimated and measurement uncertainty affected flow flag at ARDEC.

```
%For ARDEC
%Create a synthetic dataset to estimate measurement error's effect on
%groundwater flow to advance estimated and error based flow flags. Use
%colorbar to visualize the average speed of the estimated flow flag
%Zach Ferrie - CSU - September 2019

clear all
plot_google_map('apiKey', 'INSERT_API_KEY_HERE') %if you have API KEY
%follow this link to get API KEY:
https://developers.google.com/maps/documentation/javascript/get-api-
key?authuser=1#get-the-api-key
hold on
lat = [40.65242078 40.65454819 40.65416964];
lon = [-104.9959206 -104.9957254 -104.9932989];
plot(lon, lat, '.w', 'MarkerSize', 40)
plot(lon, lat, '--w', 'LineWidth', 2)
plot([-104.9959206 -104.9932989], [40.65242078 40.65416964], '--w',
'LineWidth', 2)
axis([-104.9972730571466 -104.9920898569569 40.65187558038719
40.65497702990462]);
plot_google_map('maptype','satellite')

%for colored velocity
%function source: https://www.mathworks.com/matlabcentral/fileexchange/30280-
stoplight
colormap stoplight
cb = colorbar();
set(cb, 'ylim', [0.1 10])
set(gca,'ColorScale','log')
caxis([0.1 10]);
cb.Ticks = [0.1 1 10];
cb.Ruler.Scale = 'log';
cb.Ruler.MinorTick = 'on';


%Flow flag Starting Location
particle_x_start = (3139867.832 + 3139917.586 + 3140591.631) / 3;
particle_y_start = (1480916.879 + 1481692.233 + 1481558.16) / 3;

%Convert US survey feet coordinates to Lat and long degrees.
%Function source =
https://www.mathworks.com/matlabcentral/fileexchange/26413-sp_proj
[startlong, startlat] = sp_proj('colorado north','inverse',particle_x_start,
particle_y_start,'sf');
plot(startlong, startlat, '*b', 'MarkerSize', 2);

xprev = particle_x_start;
yprev = particle_y_start;
particleLow_US_x = particle_x_start;
particleLow_US_y = particle_y_start;
particleHigh_US_x = particle_x_start;
particleHigh_US_y = particle_y_start;
```

```
%input initial values
ne = 0.25; %effective porosity (dimensionless)
K_iso = 12; %isotropic hydraulic conductivity (ft/hr)
t = 1; %time step (hr)
realizations = 1000; %number of realizations
%limitations of survey equipment = +/- 10mm+0.8ppm  -
https://www.topconpositioning.com/gnss/integrated-gnss-receivers/gr-5#panel-
product-specifications
%Actual Accuracy = sqrt(survey^2 + PT^2) = sqrt(0.0115^2 + 0.037^2) = 0.039ft
Accuracy = 39; %randomization only takes integer inputs (Accuracy = Actual
Accuracy (0.039ft) x 1000)

%IMPORT DATA - Be sure to "flip" data in Excel!
ARDEC_1Excel = xlsread('ARDEC_1_WT_forUpdate.xlsx'); %insert Excel file name
here
ARDEC_2Excel = xlsread('ARDEC_2_WL_NEW_forUpdate.xlsx');
ARDEC_3Excel = xlsread('ADREC_3_WL_forUpdate.xlsx');

%ARDEC Well Locations
Wellxy = [3139867.832 1480916.879; 3139917.586 1481692.233; 3140591.631
1481558.16]; %ARDEC_1, ARDEC_2, ARDEC_3

%Error Approximation
for j = 1:realizations %1000 realizations
%numbers must be entered into randi as integer values (hence divide by 1000
rand1 = randi([-Accuracy Accuracy])/1000;
rand2 = randi([-Accuracy Accuracy])/1000;
rand3 = randi([-Accuracy Accuracy])/1000;

well1_rand = rand1;
well2_rand = rand2;
well3_rand = rand3;

wellAll_rand = [well1_rand; well2_rand; well3_rand];

%randomization slopes
Plane = [ones(3,1), Wellxy] \ wellAll_rand;
Slopex_rand = Plane(2);
Slopey_rand = Plane(3);

x_array(j) = Slopex_rand;
y_array(j) = Slopey_rand;

end

    %x and y 95% confidence slopes
    X_95 = 2 * std(x_array)
    Y_95 = 2 * std(y_array)



Ndata = %insert number of data points here
Start = 2
```

```
for i = Start:Ndata

   %extract water table elevations
   WL1 = ARDEC_1Excel(i,3);
   WL2 = ARDEC_2Excel(i,3);
   WL3 = ARDEC_3Excel(i,3);

   WL_vector =  [WL1; WL2; WL3]; %create vector of water levels

   Plane = [ones(3,1), Wellxy] \ WL_vector;
   Slopex = Plane(2);
   Slopey = Plane(3);

   %for Low location
   xposLOW = particleLow_US_x - (((Slopex-X_95)*K_iso*t)/ne);
   yposLOW = particleLow_US_y - ((((Slopey-Y_95))*K_iso*t)/ne);
   m3 = (yposLOW-particleLow_US_y)/(xposLOW-particleLow_US_x);

   %for High location
   xposHIGH = particleHigh_US_x - (((Slopex+X_95)*K_iso*t)/ne);
   yposHIGH = particleHigh_US_y - ((((Slopey+Y_95))*K_iso*t)/ne);
   m2 = (yposHIGH-particleHigh_US_y)/(xposHIGH-particleHigh_US_x);

   %for estimated location
   xpos = xprev - ((Slopex*K_iso*t)/ne);
   ypos = yprev - ((Slopey*K_iso*t)/ne);
   m1 = (ypos-yprev)/(xpos-xprev);

   %store angles off of average path in array
   angle1_array(i) = atand((m1-m2)/(1+m1*m2));
   angle2_array(i) = atand((m1-m3)/(1+m1*m3));
   avgAngle_array(i) = atand(m1);


   % Convert US survey feet coordinates to Lat and long degrees.
   [particleAVG_newlng,particleAVG_newlat] = sp_proj('colorado
north','inverse',xpos,ypos,'sf');
   [particleLOW_newlng,particleLOW_newlat] = sp_proj('colorado
north','inverse',xposLOW,yposLOW,'sf');
   [particleHIGH_newlng,particleHIGH_newlat] = sp_proj('colorado
north','inverse',xposHIGH,yposHIGH,'sf');
   lat_array(i) = particleAVG_newlat;
   lng_array(i) = particleAVG_newlng;

   %plot 95% confidence locations
   hold on
   plot(particleLOW_newlng, particleLOW_newlat, '*b', 'MarkerSize', 5);
   plot(particleHIGH_newlng, particleHIGH_newlat, '*b', 'MarkerSize', 5);

   %for estimated velocity
   V_mag = sqrt(((Slopex*K_iso)/ne)^2 + ((Slopey*K_iso)/ne)^2)*24; %velocity
magnitude in ft/day
   V_array(i) = V_mag;
```

```
   %for low 95% confidence velocity
   V_mag_low = sqrt(((Slopex-X_95)*K_iso/ne)^2 + ((Slopey-
Y_95)*K_iso/ne)^2)*24; %velocity magnitude in ft/day
   V_array_low(i) = V_mag_low;

   %for high 95% confidence velocity
   V_mag_high = sqrt(((Slopex+X_95)*K_iso/ne)^2 +
((Slopey+Y_95)*K_iso/ne)^2)*24; %velocity magnitude in ft/day
   V_array_high(i) = V_mag_high;

   %store new location
   particleLow_US_x = xposLOW;
   particleLow_US_y = yposLOW;
   particleHigh_US_x = xposHIGH;
   particleHigh_US_y = yposHIGH;
   xprev = xpos;
   yprev = ypos;
end

%graph labels
xlabel('Longitude');
ylabel('Latitude');
ylabel(cb, 'ft/day', 'FontSize', 12);
title('INSERT_TITLE_HERE');

%average velocities and angels
V_avg = sum(V_array)/(Ndata-Start)
V_avg_ft_day_low = sum(V_array_low)/(Ndata-Start)
V_avg_ft_day_high = sum(V_array_high)/(Ndata-Start)
Angle_off_avg_1 = sum(angle1_array)/(Ndata-Start)
Angle_off_avg_2 = sum(angle2_array)/(Ndata-Start)
Avg_Angle = sum(avgAngle_array)/(Ndata-Start)

%plot estimated location
for i = Start:Ndata
    scatter(lng_array(i),lat_array(i), 5, V_array(i), 'filled');
end
```

Code for estimated and anisotropy uncertainty affected flow paths at ARDEC.

```
%For ARDEC
%Estimate anisotropy uncertainties effect on
%groundwater flow to advance estimated and error based flow flags. Use
%colorbar to visualize the average speed of the estimated flow flag
%Zach Ferrie - CSU - September 2019

clear all
plot_google_map('apiKey', 'INSERT_API_KEY_HERE') %if you have API KEY
%follow this link to get API KEY:
https://developers.google.com/maps/documentation/javascript/get-api-
key?authuser=1#get-the-api-key
hold on
lat = [40.65242078 40.65454819 40.65416964];
lon = [-104.9959206 -104.9957254 -104.9932989];
plot(lon, lat, '.w', 'MarkerSize', 50)
plot(lon, lat, '--w', 'LineWidth', 2)
plot([-104.9959206 -104.9932989], [40.65242078 40.65416964], '--w',
'LineWidth', 2)
axis([-104.9972730571466 -104.9920898569569 40.65187558038719
40.65497702990462]);
plot_google_map('maptype','satellite')

%for colored velocity
%function source: https://www.mathworks.com/matlabcentral/fileexchange/30280-
stoplight
colormap stoplight
cb = colorbar();
set(cb, 'ylim', [0.1 10])
set(gca,'ColorScale','log')
caxis([0.1 10]);
cb.Ticks = [0.1 1 10];
cb.Ruler.Scale = 'log';
cb.Ruler.MinorTick = 'on';

%Flow flag Starting Location
particle_x_start = (3139867.832 + 3139917.586 + 3140591.631) / 3;
particle_y_start = (1480916.879 + 1481692.233 + 1481558.16) / 3;

xprev = particle_x_start;
yprev = particle_y_start;
particleLow_US_x = particle_x_start;
particleLow_US_y = particle_y_start;
particleHigh_US_x = particle_x_start;
particleHigh_US_y = particle_y_start;

%input initial values
ne = 0.25; %effective porosity (dimensionless)
t = 1; %time step (hr)
V_add = 0;

%K1 is the K value NOT in the direction of deposition (always smaller than
K2)
K1 = 12; %hydraulic conductivity (ft/hr)
```

```
%IMPORT DATA - Be sure to "flip" data in Excel!
ARDEC_1Excel = xlsread('ARDEC_1_WT_forUpdate.xlsx'); %insert Excel file name
here
ARDEC_2Excel = xlsread('ARDEC_2_WL_NEW_forUpdate.xlsx');
ARDEC_3Excel = xlsread('ADREC_3_WL_forUpdate.xlsx');

%ARDEC Well Locations
Wellxy = [3139867.832 1480916.879; 3139917.586 1481692.233; 3140591.631
1481558.16]; %ARDEC_1, ARDEC_2, ARDEC_3

%anisotropy uncertainty values
K2_low = K1*1.10;
K2_high = K1*1.28;
K2_avg = K1*1.19;

Ndata =  %insert number of data points here
Start = 2

for i = Start:Ndata

   %extract water table elevations
   WL1 = ARDEC_1Excel(i,3);
   WL2 = ARDEC_2Excel(i,3);
   WL3 = ARDEC_3Excel(i,3);

   WL_vector =  [WL1; WL2; WL3]; %create vector of water levels

   Plane = [ones(3,1), Wellxy] \ WL_vector;
   Slopex = Plane(2);
   Slopey = Plane(3);

   %for low location
   xposLOW = particleLow_US_x - (Slopex*t*K1/ne);
   yposLOW = particleLow_US_y - (Slopey*t*K2_low/ne);
   m3 = (yposLOW-particleLow_US_y)/(xposLOW-particleLow_US_x);

   %for high location
   xposHIGH = particleHigh_US_x - (Slopex*t*K1/ne);
   yposHIGH = particleHigh_US_y - (Slopey*t*K2_high/ne);
   m2 = (yposHIGH-particleHigh_US_y)/(xposHIGH-particleHigh_US_x);

   %for estimated location
   xpos = xprev - (Slopex*t*K1/ne);
   ypos = yprev - (Slopey*t*K2_avg/ne);
   m1 = (ypos-yprev)/(xpos-xprev);

   %store angles off of average path in array
   angle1_array(i) = atand((m1-m2)/(1+m1*m2));
   angle2_array(i) = atand((m1-m3)/(1+m1*m3));
   avgAngle_array(i) = atand(m1);

   %Convert US survey feet coordinates to Lat and long degress.
```

```
   %Function source =
https://www.mathworks.com/matlabcentral/fileexchange/26413-sp_proj
   [particleAVG_newlng,particleAVG_newlat] = sp_proj('colorado
north','inverse',xpos,ypos,'sf');
   [particleLOW_newlng,particleLOW_newlat] = sp_proj('colorado
north','inverse',xposLOW,yposLOW,'sf');
   [particleHIGH_newlng,particleHIGH_newlat] = sp_proj('colorado
north','inverse',xposHIGH,yposHIGH,'sf');
   lat_array(i) = particleAVG_newlat;
   lng_array(i) = particleAVG_newlng;

   %plot 95% confidence locations
   hold on
   plot(particleLOW_newlng, particleLOW_newlat, '*b', 'MarkerSize', 5);
   plot(particleHIGH_newlng, particleHIGH_newlat, '*b', 'MarkerSize', 5);

   %average velocity
   V_mag = sqrt((Slopex*K1/ne)^2 + (Slopey*K2_avg/ne)^2)*24; %velocity
magnitude in ft/day
   V_array(i) = V_mag;

   %low 95% confidence velocity
   V_mag_low = sqrt((Slopex*K1/ne)^2 + (Slopey*K2_low/ne)^2)*24; %velocity
magnitude in ft/day
   V_array_low(i) = V_mag_low;

   %high 95% confidence velocity
   V_mag_high = sqrt((Slopex*K1/ne)^2 + (Slopey*K2_high/ne)^2)*24; %velocity
magnitude in ft/day
   V_array_high(i) = V_mag_high;

   %store new locations
   particleLow_US_x = xposLOW;
   particleLow_US_y = yposLOW;
   particleHigh_US_x = xposHIGH;
   particleHigh_US_y = yposHIGH;
   xprev = xpos;
   yprev = ypos;
end

%graph labels
xlabel('Longitude');
ylabel('Latitude');
ylabel(cb, 'ft/day', 'FontSize', 12);
title('INSERT_TITLE_HERE');

%average velocities and angels
V_avg = sum(V_array)/(Ndata-Start)
V_low = sum(V_array_low)/(Ndata-Start)
V_high = sum(V_array_high)/(Ndata-Start)
Angle_off_avg_1 = sum(angle1_array)/(Ndata-Start)
Angle_off_avg_2 = sum(angle2_array)/(Ndata-Start)
Avg_Angle = sum(avgAngle_array)/(Ndata-Start)
```

```
%plot estimated location
for i = Start:Ndata
    scatter(lng_array(i),lat_array(i), 3, V_array(i), 'filled');
end
```

Code for estimated and measurement uncertainty affected flow flag at the ERC.

```
%For ERC
%Create a synthetic dataset to estimate measurement error's effect on
%groundwater flow to advance estimated and error based flow flags. Use
%colorbar to visualize the average speed of the estimated flow flag
%Zach Ferrie - CSU - September 2019

clear all
plot_google_map('apiKey', 'INSERT_API_KEY_HERE') %if you have API KEY
%follow this link to get API KEY:
https://developers.google.com/maps/documentation/javascript/get-api-
key?authuser=1#get-the-api-key
hold on
lat = [40.58519294 40.58535872 40.58550011];
lon = [-105.1507323 -105.1509153 -105.1508941];
plot(lon, lat, '.w', 'MarkerSize', 50)
plot(lon, lat, '--w', 'LineWidth', 2)
plot([-105.1507323 -105.1508941], [40.58519294 40.58550011], '--w',
'LineWidth', 2)
axis([-105.1511 -105.1505 40.58515 40.58555]);
%axis([-105.15085 -105.150815 40.585339999999995 40.585364999999996])
plot_google_map('maptype','satellite')

%IMPORT DATA - Be sure to "flip" data in Excel!
ERC_1Excel = xlsread('ERC_well_1_Historic_WLs.xlsx'); %insert Excel file name
here
ERC_2Excel = xlsread('ERC_well_2_Historic_WLs.xlsx');
ERC_3Excel = xlsread('ERC_well_3_Historic_WLs.xlsx');

%for colored velocity
%function source: https://www.mathworks.com/matlabcentral/fileexchange/30280-
stoplight
colormap stoplight
cb = colorbar();
set(cb, 'ylim', [0.1 10])
set(gca,'ColorScale','log')
caxis([0.1 10]);
cb.Ticks = [0.1 1 10];
cb.Ruler.Scale = 'log';
cb.Ruler.MinorTick = 'on';

%input initial values
ne = 0.4; %effective porosity (dimensionless) - silt/loess
K_iso = 0.012; %isotropic hydraulic conductivity (ft/hr)- silt/loess
t = 1; %time step (hr)
realizations = 1000; %number of realizations
%limitations of survey equipment = +/- 10mm+0.8ppm  -
https://www.topconpositioning.com/gnss/integrated-gnss-receivers/gr-5#panel-
product-specifications
%Actual Accuracy = sqrt(survey^2 + PT^2) = sqrt(0.0115^2 + 0.037^2) = 0.039ft
Accuracy = 39; %randomization only takes integer inputs (Accuracy = Actual
Accuracy (0.039ft) x 1000)

%ERC Well Locations
```

```
Wellxy = [3097008.696 1456218.133; 3096957.61 1456278.328; 3096963.296
1456329.86]; %ERC_1, ERC_2, ERC_3

%Flow flag Starting Location
particle_x_start = (3097008.696 + 3096957.61 + 3096963.296) / 3;
particle_y_start = (1456218.133 + 1456278.328 + 1456329.86) / 3;
particle1_US_x = particle_x_start;
particle1_US_y = particle_y_start;

%Convert US survey feet coordinates to Lat and long degrees.
%Function source =
https://www.mathworks.com/matlabcentral/fileexchange/26413-sp_proj
[startlong, startlat] = sp_proj('colorado north','inverse',particle_x_start,
particle_y_start,'sf');
plot(startlong, startlat, '*b', 'MarkerSize', 2);

xprev = particle_x_start;
yprev = particle_y_start;
particleLow_US_x = particle_x_start;
particleLow_US_y = particle_y_start;
particleHigh_US_x = particle_x_start;
particleHigh_US_y = particle_y_start;

%Error Approximation
for j = 1:realizations %1000 realizations
%numbers must be entered into randi as integer values (hence divide by 1000)
rand1 = randi([-Accuracy Accuracy])/1000;
rand2 = randi([-Accuracy Accuracy])/1000;
rand3 = randi([-Accuracy Accuracy])/1000;

well1_rand = rand1;
well2_rand = rand2;
well3_rand = rand3;

wellAll_rand = [well1_rand; well2_rand; well3_rand];

%randomization slopes
Plane = [ones(3,1), Wellxy] \ wellAll_rand;
Slopex_rand = Plane(2);
Slopey_rand = Plane(3);

x_array(j) = Slopex_rand;
y_array(j) = Slopey_rand;

end

    %x and y 95% confidence slopes
    X_95 = 2 * std(x_array)
    Y_95 = 2 * std(y_array)

Ndata =  %insert number of data points here
Start = 2

for i = Start:Ndata
```

```
   %exract water table elevations
   WL1 = ERC_1Excel(i,3);
   WL2 = ERC_2Excel(i,3);
   WL3 = ERC_3Excel(i,3);

   WL_vector =  [WL1; WL2; WL3]; %create vector of water levels

   Plane = [ones(3,1), Wellxy] \ WL_vector;
   Slopex = Plane(2);
   Slopey = Plane(3);

   %for Low location
   xposLOW = particleLow_US_x - (((Slopex-X_95)*K_iso*t)/ne);
   yposLOW = particleLow_US_y - ((((Slopey-Y_95))*K_iso*t)/ne);
   m3 = (yposLOW-particleLow_US_y)/(xposLOW-particleLow_US_x);

   %for High location
   xposHIGH = particleHigh_US_x - (((Slopex+X_95)*K_iso*t)/ne);
   yposHIGH = particleHigh_US_y - ((((Slopey+Y_95))*K_iso*t)/ne);
   m2 = (yposHIGH-particleHigh_US_y)/(xposHIGH-particleHigh_US_x);

   %for estimated location
   xpos = xprev - ((Slopex*K_iso*t)/ne);
   ypos = yprev - ((Slopey*K_iso*t)/ne);
   m1 = (ypos-yprev)/(xpos-xprev);

   %store angles off of average path in array
   angle1_array(i) = atand((m1-m2)/(1+m1*m2));
   angle2_array(i) = atand((m1-m3)/(1+m1*m3));
    avgAngle = atan(m1);
    if avgAngle<0
       avgAngle_array(i) = (pi + avgAngle) * 180 / pi;
   else avgAngle_array(i) = avgAngle * 180 / pi;
   end


   %Convert US survey feet coordinates to Lat and long degrees.
   [particleAVG_newlng,particleAVG_newlat] = sp_proj('colorado
north','inverse',xpos,ypos,'sf');
   [particleLOW_newlng,particleLOW_newlat] = sp_proj('colorado
north','inverse',xposLOW_new,yposLOW_new,'sf');
   [particleHIGH_newlng,particleHIGH_newlat] = sp_proj('colorado
north','inverse',xposHIGH_new,yposHIGH_new,'sf');
   lat_array(i) = particleAVG_newlat;
   lng_array(i) = particleAVG_newlng;

   %for average velocity
   V_mag = sqrt((Slopex*K_iso/ne)^2 + (Slopey*K_iso/ne)^2)*24; %velocity
magnitude in ft/day
   V_array(i) = V_mag;

   %for low 95% confidence velocity
   V_mag_low = sqrt(((Slopex-X_95)*K_iso/ne)^2 + ((Slopey-
Y_95)*K_iso/ne)^2)*24; %velocity magnitude in ft/day
```

```
   V_array_low(i) = V_mag_low;

   %for high 95% confidence velocity
   V_mag_high = sqrt(((Slopex+X_95)*K_iso/ne)^2 +
((Slopey+Y_95)*K_iso/ne)^2)*24; %velocity magnitude in ft/day
   V_array_high(i) = V_mag_high;

   %plot 95% confidence locations
   hold on
   plot(particleLOW_newlng, particleLOW_newlat, '*b', 'MarkerSize', 3);
   plot(particleHIGH_newlng, particleHIGH_newlat, '*b', 'MarkerSize', 3);

   %store new locations
   particleLow_US_x = xposLOW;
   particleLow_US_y = yposLOW;
   particleHigh_US_x = xposHIGH;
   particleHigh_US_y = yposHIGH;
   xprev = xpos;
   yprev = ypos;
end

 %graph labels
xlabel('Longitude');
ylabel('Latitude');
ylabel(cb, 'ft/day', 'FontSize', 12);
title('INSERT_TITLE_HERE');

%average velocities and angels
V_avg = sum(V_array)/(Ndata-Start)
V_avg_ft_day_low = mean(V_array_low)
V_avg_ft_day_high = mean(V_array_high)
Angle_off_avg_1 = sum(angle1_array)/(Ndata-Start)
Angle_off_avg_2 = sum(angle2_array)/(Ndata-Start)
Avg_Angle = sum(avgAngle_array)/(Ndata-Start)

%plot estimated location
for i = Start:Ndata
    scatter(lng_array(i),lat_array(i), 3, V_array(i), 'filled');
end
```

Code for estimated and anisotropy uncertainty affected flow paths at the ERC.

```
%For ERC
%Estimate anisotropy uncertainties effect on
%groundwater flow to advance estimated and error based flow flags. Use
%colorbar to visualize the average speed of the estimated flow flag
%Zach Ferrie - CSU - September 2019

clear all
plot_google_map('apiKey', 'INSERT_API_KEY_HERE') %if you have API KEY
%follow this link to get API KEY:
https://developers.google.com/maps/documentation/javascript/get-api-
key?authuser=1#get-the-api-key
hold on
lat = [40.58519294 40.58535872 40.58550011];
lon = [-105.1507323 -105.1509153 -105.1508941];
plot(lon, lat, '.w', 'MarkerSize', 50)
plot(lon, lat, '--w', 'LineWidth', 2)
plot([-105.1507323 -105.1508941], [40.58519294 40.58550011], '--w',
'LineWidth', 2)
% axis([-105.1511 -105.1505 40.58515 40.58555]);
axis([-105.15085 -105.150815 40.585339999999995 40.585364999999996])
plot_google_map('maptype','satellite')

%IMPORT DATA - Be sure to "flip" data in Excel!
ERC_1Excel = xlsread('ERC_well_1_Historic_WLs.xlsx'); %insert Excel file name
here
ERC_2Excel = xlsread('ERC_well_2_Historic_WLs.xlsx');
ERC_3Excel = xlsread('ERC_well_3_Historic_WLs.xlsx');

%for colored velocity
%function source: https://www.mathworks.com/matlabcentral/fileexchange/30280-
stoplight
colormap stoplight
cb = colorbar();
set(cb, 'ylim', [0.1 10])
set(gca,'ColorScale','log')
caxis([0.1 10]);
cb.Ticks = [0.1 1 10];
cb.Ruler.Scale = 'log';
cb.Ruler.MinorTick = 'on';

%input initial values
ne = 0.4; %effective porosity (dimensionless) - silt/loess
K1 = 0.012; %isotropic hydraulic conductivity (ft/hr)- silt/loess
t = 1; %time step (hr)

%Anisotropy uncertainty values
K2_low = K1*1.10;
K2_high = K1*1.28;
K2_avg = K1*1.19;

%ERC Well Locations
Wellxy = [3097008.696 1456218.133; 3096957.61 1456278.328; 3096963.296
1456329.86]; %ERC_1, ERC_2, ERC_3
```

```
%Flow flag starting location
particle_x_start = (3097008.696 + 3096957.61 + 3096963.296) / 3;
particle_y_start = (1456218.133 + 1456278.328 + 1456329.86) / 3;
particle1_US_x = particle_x_start;
particle1_US_y = particle_y_start;

%Convert US survey feet coordinates to Lat and long degrees.
%function source =
https://www.mathworks.com/matlabcentral/fileexchange/26413-sp_proj
[startlong, startlat] = sp_proj('colorado north','inverse',particle_x_start,
particle_y_start,'sf');
plot(startlong, startlat, '*b', 'MarkerSize', 2);

xprev = particle_x_start;
yprev = particle_y_start;
particleLow_US_x = particle_x_start;
particleLow_US_y = particle_y_start;
particleHigh_US_x = particle_x_start;
particleHigh_US_y = particle_y_start;

Ndata =  %insert number of data points here
Start = 2

for i = Start:Ndata

   %extract water table elevations
   WL1 = ERC_1Excel(i,3);
   WL2 = ERC_2Excel(i,3);
   WL3 = ERC_3Excel(i,3);

   WL_vector =  [WL1; WL2; WL3]; %create vector of water levels


   Plane = [ones(3,1), Wellxy] \ WL_vector;
   Slopex = Plane(2);
   Slopey = Plane(3);

   %for Low location
   xposLOW = particleLow_US_x - (((Slopex*K2_low)/ne)*t);
   yposLOW = particleLow_US_y - (((Slopey*K1)/ne)*t);
   m3 = (yposLOW-particleLow_US_y)/(xposLOW-particleLow_US_x);

   %for High location
   xposHIGH = particleHigh_US_x - (((Slopex*K2_high)/ne)*t);
   yposHIGH = particleHigh_US_y - (((Slopey*K1)/ne)*t);
   m2 = (yposHIGH-particleHigh_US_y)/(xposHIGH-particleHigh_US_x);

   %for estimated location
   xpos = xprev - (((Slopex*K2_avg)/ne)*t);
   ypos = yprev - (((Slopey*K1)/ne)*t);
   m1 = (ypos-yprev)/(xpos-xprev);

   %store angles off of average path in array
```

```
   angle1_array(i) = atand((m1-m2)/(1+m1*m2));
   angle2_array(i) = atand((m1-m3)/(1+m1*m3));
    avgAngle = atan(m1);
    if avgAngle<0
       avgAngle_array(i) = (pi + avgAngle) * 180 / pi;
   else avgAngle_array(i) = avgAngle * 180 / pi;
    end

   %Convert US survey feet coordinates to Lat and long degrees.
   [particleAVG_newlng,particleAVG_newlat] = sp_proj('colorado
north','inverse',xpos,ypos,'sf');
   [particleLOW_newlng,particleLOW_newlat] = sp_proj('colorado
north','inverse',xposLOW,yposLOW,'sf');
   [particleHIGH_newlng,particleHIGH_newlat] = sp_proj('colorado
north','inverse',xposHIGH,yposHIGH,'sf');
   lat_array(i) = particleAVG_newlat;
   lng_array(i) = particleAVG_newlng;

    %average velocity
   V_mag = sqrt((Slopex*K2_avg/ne)^2 + (Slopey*K1/ne)^2)*24; %velocity
magnitude in ft/day
   V_array(i) = V_mag;

    %low 95% confidence velocity
   V_mag_low = sqrt((Slopex*K2_low/ne)^2 + (Slopey*K1/ne)^2)*24; %velocity
magnitude in ft/day
   V_array_low(i) = V_mag_low;

    %high 95% confidence velocity
   V_mag_high = sqrt((Slopex*K2_high/ne)^2 + (Slopey*K1/ne)^2)*24; %velocity
magnitude in ft/day
   V_array_high(i) = V_mag_high;

   %plot 95% confidence locations
   hold on
   plot(particleLOW_newlng, particleLOW_newlat, '*b', 'MarkerSize', 3);
   plot(particleHIGH_newlng, particleHIGH_newlat, '*b', 'MarkerSize', 3);

   %store new locations
   particleLow_US_x = xposLOW;
   particleLow_US_y = yposLOW;
   particleHigh_US_x = xposHIGH;
   particleHigh_US_y = yposHIGH;
   xprev = xpos;
   yprev = ypos;
end

%graph labels
xlabel('Longitude');
ylabel('Latitude');
ylabel(cb, 'ft/day', 'FontSize', 12);
title('INSERT_TITLE_HERE');

%average velocities and angels
V_avg = sum(V_array)/(Ndata-Start)
```

```
V_low = sum(V_array_low)/(Ndata-Start)
V_high = sum(V_array_high)/(Ndata-Start)
Angle_off_avg_1 = sum(angle1_array)/(Ndata-Start)
Angle_off_avg_2 = sum(angle2_array)/(Ndata-Start)
Avg_Angle = sum(avgAngle_array)/(Ndata-Start)

%plot estimated location
for i = Start:Ndata
    scatter(lng_array(i),lat_array(i), 3, V_array(i), 'filled');
end
```

Code for estimated and measurement uncertainty affected flow flag at Site A.

```
%For Site A
%Create a synthetic dataset to estimate measurement error's effect on
%groundwater flow to advance estimated and error based flow flags. Use
%colorbar to visualize the average speed of the estimated flow flag
%Zach Ferrie - CSU - December 2019

plot_google_map('apiKey', 'AIzaSyATfmc382_f6DpmDK3gfOAKsY-5mWkzaa0') %if you
have API KEY
%follow this link to get API KEY:
https://developers.google.com/maps/documentation/javascript/get-api-
key?authuser=1#get-the-api-key
hold on
lat = [39.6853764 39.6857705 39.685485];
lon = [-75.500472 -75.5004948 -75.5009252];
plot(lon, lat, '.w', 'MarkerSize', 50)
plot(lon, lat, '--w', 'LineWidth', 2)
plot([-75.500472 -75.5009252], [39.6853764 39.685485], '--w', 'LineWidth', 2)
axis([-75.501100000000008 -75.500200000000007 39.685300000000005
39.685800000000008]);
plot_google_map('maptype','satellite')

%for colored velocity
%function source: https://www.mathworks.com/matlabcentral/fileexchange/30280-
stoplight
colormap stoplight
cb = colorbar();
set(cb, 'ylim', [0.1 10])
set(gca,'ColorScale','log')
caxis([0.1 10]);
cb.Ticks = [0.1 1 10];
cb.Ruler.Scale = 'log';
cb.Ruler.MinorTick = 'on';

%Flow flag Starting Location
particle_x_start = (210573.0765 + 210568.2450 + 210445.9540) / 3
particle_y_start = (311886.5400 + 312030.1710 + 311927.5200) / 3

%Convert US survey feet coordinates to Lat and long degrees.
%Function source =
https://www.mathworks.com/matlabcentral/fileexchange/26413-sp_proj
[startlong, startlat] = sp_proj('new jersey','inverse',particle_x_start,
particle_y_start,'sf');
plot(startlong, startlat, '*b', 'MarkerSize', 2);

xprev = particle_x_start;
yprev = particle_y_start;
particleLow_US_x = particle_x_start;
particleLow_US_y = particle_y_start;
particleHigh_US_x = particle_x_start;
particleHigh_US_y = particle_y_start;

%input initial values
```

```
ne = 0.3; %effective porosity (dimensionless)
K_iso = 1.2; %isotropic hydraulic conductivity (ft/hr)
t = 1; %time step (hr)
realizations = 1000; %number of realizations
%limitations of survey equipment = +/- 10mm+0.8pppm  -
https://www.topconpositioning.com/gnss/integrated-gnss-receivers/gr-5#panel-
product-specifications
%Total Error = sqrt(survey^2 + PT^2)
%randomization only takes integer inputs (Accuracy = Actual Accuracy x 1000)
Accuracy_1 = 40; %for Wells I05-M01B, I05-M03B, SITE A_SC
Accuracy_2 = 38; %For Well I05-M02B

%IMPORT DATA - Be sure to "flip" data in Excel!
SITE A_1Excel = xlsread('SITE A_1.xlsx'); %insert Excel file name here
SITE A_2Excel = xlsread('SITE A_2.xlsx');
SITE A_3Excel = xlsread('SITE A_3.xlsx');

%SITE A Well Locations
Wellxy = [210573.0765 311886.5400; 210568.2450 312030.1710; 210445.9540
311927.5200]; %l05-M01B, 105-M02B, l05-M03B - coordinates in US survey feet
(State Plane New Jersey (ft NAD83) and NAVD88)

%Error Approximation
for j = 1:realizations %1000 realizations

rand1 = randi([-Accuracy_1 Accuracy_1])/1000;
rand2 = randi([-Accuracy_2 Accuracy_2])/1000;
rand3 = randi([-Accuracy_1 Accuracy_1])/1000;

well1_rand = rand1;
well2_rand = rand2;
well3_rand = rand3;

wellAll_rand = [well1_rand; well2_rand; well3_rand];

%randomization slopes
Plane = [ones(3,1), Wellxy] \ wellAll_rand;
Slopex_rand = Plane(2);
Slopey_rand = Plane(3);

x_array(j) = Slopex_rand;
y_array(j) = Slopey_rand;

end

    %x and y 95% confidence slopes
    X_95 = 2 * std(x_array)
    Y_95 = 2 * std(y_array)

Ndata = %insert number of data points here
Start = 2;

for i = Start:Ndata
```

```
%extract water table elevations
WL1 = SITE A_1Excel(i,3);
WL2 = SITE A_2Excel(i,3);
WL3 = SITE A_3Excel(i,3);


WL_vector =  [WL1; WL2; WL3]; %create vector of water levels

Plane = [ones(3,1), Wellxy] \ WL_vector;
Slopex = Plane(2);
Slopey = Plane(3);

   %for Low location
   xposLOW = particleLow_US_x - (((Slopex-X_95)*K_iso*t)/ne);
   yposLOW = particleLow_US_y - ((((Slopey-Y_95))*K_iso*t)/ne);
   m3 = (yposLOW-particleLow_US_y)/(xposLOW-particleLow_US_x);

   %for High location
   xposHIGH = particleHigh_US_x - (((Slopex+X_95)*K_iso*t)/ne);
   yposHIGH = particleHigh_US_y - ((((Slopey+Y_95))*K_iso*t)/ne);
   m2 = (yposHIGH-particleHigh_US_y)/(xposHIGH-particleHigh_US_x);

   %for estimated location
   xpos = xprev - ((Slopex*K_iso*t)/ne);
   ypos = yprev - ((Slopey*K_iso*t)/ne);
   m1 = (ypos-yprev)/(xpos-xprev);

   %store angles off of average path in array
   angle1_array(i) = atand((m1-m2)/(1+m1*m2));
   angle2_array(i) = atand((m1-m3)/(1+m1*m3));
    avgAngle = atan(m1);
    if avgAngle<0
       avgAngle_array(i) = (pi + avgAngle) * 180 / pi;
   else avgAngle_array(i) = avgAngle * 180 / pi;
   end

   %Convert US survey feet coordinates to Lat and long degrees.
   [particleAVG_newlng,particleAVG_newlat] = sp_proj('new
jersey','inverse',xpos,ypos,'sf');
   [particleLOW_newlng,particleLOW_newlat] = sp_proj('new
jersey','inverse',xposLOW,yposLOW,'sf');
   [particleHIGH_newlng,particleHIGH_newlat] = sp_proj('new
jersey','inverse',xposHIGH,yposHIGH,'sf');

    %for estimated velocity
    V_mag = sqrt((Slopex*K_iso/ne)^2 + (Slopey*K_iso/ne)^2)*24; %velocity
magnitude in ft/day
    V_array(i) = V_mag;

   %for low 95% confidence velocity
   V_mag_low = sqrt(((Slopex-X_95)*K_iso/ne)^2 + ((Slopey-
Y_95)*K_iso/ne)^2)*24; %velocity magnitude in ft/day
   V_array_low(i) = V_mag_low;

   %for high 95% confidence velocity
```

```
   V_mag_high = sqrt(((Slopex+X_95)*K_iso/ne)^2 +
((Slopey+Y_95)*K_iso/ne)^2)*24; %velocity magnitude in ft/day
   V_array_high(i) = V_mag_high;

    %plot
    hold on
    scatter(particleAVG_newlng, particleAVG_newlat, 3, V_mag, 'filled');
    plot(particleLOW_newlng, particleLOW_newlat, '*b', 'MarkerSize', 3);
    plot(particleHIGH_newlng, particleHIGH_newlat, '*b', 'MarkerSize', 3);

   %store new locations
   particleLow_US_x = xposLOW;
   particleLow_US_y = yposLOW;
   particleHigh_US_x = xposHIGH;
   particleHigh_US_y = yposHIGH;
   xprev = xpos;
   yprev = ypos;
end

%graph labels
xlabel('Longitude');
ylabel('Latitude');
ylabel(cb, 'ft/day', 'FontSize', 12);
title(' INSERT_TITLE_HERE');

%average velocities and angels
V_avg = sum(V_array)/(Ndata-Start)
V_avg_ft_day_low = mean(V_array_low)
V_avg_ft_day_high = mean(V_array_high)
Angle_off_avg_1 = sum(angle1_array)/(Ndata-Start)
Angle_off_avg_2 = sum(angle2_array)/(Ndata-Start)
Avg_Angle = sum(avgAngle_array)/(Ndata-Start)
```

Code for estimated and anisotropy uncertainty affected flow paths at Site A.

```
%For Site A
%Estimate anisotropy uncertainties effect on
%groundwater flow to advance estimated and error based flow flags. Use
%colorbar to visualize the average speed of the estimated flow flag
%Zach Ferrie - CSU - December 2019

plot_google_map('apiKey', 'INSERT_API_KEY_HERE') %if you have API KEY
%follow this link to get API KEY:
https://developers.google.com/maps/documentation/javascript/get-api-
key?authuser=1#get-the-api-key
hold on
lat = [39.6853764 39.6857705 39.685485];
lon = [-75.500472 -75.5004948 -75.5009252];
plot(lon, lat, '.w', 'MarkerSize', 50)
plot(lon, lat, '--w', 'LineWidth', 2)
plot([-75.500472 -75.5009252], [39.6853764 39.685485], '--w', 'LineWidth', 2)
axis([-75.501100000000008 -75.500200000000007 39.685300000000005
39.685800000000008]);
plot_google_map('maptype','satellite')

%for colored velocity
%function source: https://www.mathworks.com/matlabcentral/fileexchange/30280-
stoplight
colormap stoplight
cb = colorbar();
set(cb, 'ylim', [0.1 10])
set(gca,'ColorScale','log')
caxis([0.1 10]);
cb.Ticks = [0.1 1 10];
cb.Ruler.Scale = 'log';
cb.Ruler.MinorTick = 'on';

%Flow flag Starting Location
particle_x_start = (210573.0765 + 210568.2450 + 210445.9540) / 3
particle_y_start = (311886.5400 + 312030.1710 + 311927.5200) / 3

%Convert US survey feet coordinates to Lat and long degrees.
%Fuction source = https://www.mathworks.com/matlabcentral/fileexchange/26413-
sp_proj
[startlong, startlat] = sp_proj('new jersey','inverse',particle_x_start,
particle_y_start,'sf');
plot(startlong, startlat, '*b', 'MarkerSize', 2);

xprev = particle_x_start;
yprev = particle_y_start;
particleLow_US_x = particle_x_start;
particleLow_US_y = particle_y_start;
particleHigh_US_x = particle_x_start;
particleHigh_US_y = particle_y_start;

%input initial values
ne = 0.3; %effective porosity (dimensionless)
K1 = 1.2; %isotropic hydraulic conductivity (ft/hr)
```

```
t = 1; %time step (hr)

%anisotropy uncertainty values
K2_low = K1*1.10;
K2_high = K1*1.28;
K2_avg = K1*1.19;

%IMPORT DATA - Be sure to "flip" data in Excel!
SITE A_1Excel = xlsread('SITE A_1.xlsx'); %insert Excel file name here
SITE A_2Excel = xlsread('SITE A_2.xlsx');
SITE A_3Excel = xlsread('SITE A_3.xlsx');

%SITE A Well Locations
Wellxy = [210573.0765 311886.5400; 210568.2450 312030.1710; 210445.9540
311927.5200]; %l05-M01B, 105-M02B, l05-M03B - coordinates in US survey feet
(State Plane New Jersey (ft NAD83) and NAVD88)

Ndata = %insert number of data points here
Start = 2;

for i = Start:Ndata

   %exract water table elevations
   WL1 = SITE A_1Excel(i,3);
   WL2 = SITE A_2Excel(i,3);
   WL3 = SITE A_3Excel(i,3);

   WL_vector =  [WL1; WL2; WL3]; %create vector of water levels

   Plane = [ones(3,1), Wellxy] \ WL_vector;
   Slopex = Plane(2);
   Slopey = Plane(3);

   %for Low location
   xposLOW = particleLow_US_x - (((Slopex*K1)/ne)*t);
   yposLOW = particleLow_US_y - (((Slopey*K2_low)/ne)*t);
   m3 = (yposLOW-particleLow_US_y)/(xposLOW-particleLow_US_x);

   %for High location
   xposHIGH = particleHigh_US_x - (((Slopex*K1)/ne)*t);
   yposHIGH = particleHigh_US_y - (((Slopey*K2_high)/ne)*t);
   m2 = (yposHIGH-particleHigh_US_y)/(xposHIGH-particleHigh_US_x);

   %for estimated location
   xpos = xprev - (((Slopex*K1)/ne)*t);
   ypos = yprev - (((Slopey*K2_avg)/ne)*t);
   m1 = (ypos-yprev)/(xpos-xprev);

   %store angles off of average path in array
   angle1_array(i) = atand((m1-m2)/(1+m1*m2));
   angle2_array(i) = atand((m1-m3)/(1+m1*m3));
    avgAngle = atan(m1);
    if avgAngle<0
       avgAngle_array(i) = (pi + avgAngle) * 180 / pi;
```

```
   else avgAngle_array(i) = avgAngle * 180 / pi;
    end

   %Convert US survey feet coordinates to Lat and long degrees.
   [particleAVG_newlng,particleAVG_newlat] = sp_proj('new
jersey','inverse',xpos,ypos,'sf');
   [particleLOW_newlng,particleLOW_newlat] = sp_proj('new
jersey','inverse',xposLOW,yposLOW,'sf');
   [particleHIGH_newlng,particleHIGH_newlat] = sp_proj('new
jersey','inverse',xposHIGH,yposHIGH,'sf');
   lat_array(i) = particleAVG_newlat;
   lng_array(i) = particleAVG_newlng;

     %average velocity
   V_mag = sqrt((Slopex*K1/ne)^2 + (Slopey*K2_avg/ne)^2)*24; %velocity
magnitude in ft/day
   V_array(i) = V_mag;

    %low 95% confidence velocity
   V_mag_low = sqrt((Slopex*K1/ne)^2 + (Slopey*K2_low/ne)^2)*24; %velocity
magnitude in ft/day
   V_array_low(i) = V_mag_low;

    %high 95% confidence velocity
   V_mag_high = sqrt((Slopex*K1/ne)^2 + (Slopey*K2_high/ne)^2)*24; %velocity
magnitude in ft/day
   V_array_high(i) = V_mag_high;

   %plot
   hold on
   plot(particleLOW_newlng, particleLOW_newlat, '*b', 'MarkerSize', 3);
   plot(particleHIGH_newlng, particleHIGH_newlat, '*b', 'MarkerSize', 3);

   %store new locations
   particleLow_US_x = xposLOW;
   particleLow_US_y = yposLOW;
   particleHigh_US_x = xposHIGH;
   particleHigh_US_y = yposHIGH;
   xprev = xpos;
   yprev = ypos;
end

%graph labels
xlabel('Longitude');
ylabel('Latitude');
ylabel(cb, 'ft/day', 'FontSize', 12);
title('INSERT_TITLE_HERE');

%average velocities and angels
V_avg = sum(V_array)/(Ndata-Start)
V_avg_ft_day_low = mean(V_array_low)
V_avg_ft_day_high = mean(V_array_high)
Angle_off_avg_1 = sum(angle1_array)/(Ndata-Start)
Angle_off_avg_2 = sum(angle2_array)/(Ndata-Start)
Avg_Angle = sum(avgAngle_array)/(Ndata-Start)
```

```
%plot estimated location
for i = Start:Ndata
    scatter(lng_array(i),lat_array(i), 3, V_array(i), 'filled');
end
```

Code for estimated and measurement uncertainty affected flow flag at Site B.

```
%For SITE B
%Create a synthetic dataset to estimate measurement error's effect on
%groundwater flow to advance estimated and error based flow flags. Use
%colorbar to visualize the average speed of the estimated flow flag
%Zach Ferrie - CSU - October 2019

clear all
plot_google_map('apiKey', 'INSERT_API_KEY_HERE') %if you have API KEY
hold on
lat = [39.8073977 39.8068358 39.8055664 39.8055678];
lon = [-104.9451542 -104.9481973 -104.9442387 -104.9459236];
plot(lon, lat, '.w', 'MarkerSize', 40)
plot([-104.9451542 -104.9481973], [39.8073977 39.8068358], '--w',
'LineWidth', 2)
plot([-104.9442387 -104.9459236], [39.8055664 39.8055678], '--w',
'LineWidth', 2)
plot([-104.9451542 -104.9459236], [39.8073977 39.8055678], '--w',
'LineWidth', 2)
plot([-104.9451542 -104.9442387], [39.8073977 39.8055664], '--w',
'LineWidth', 2)
plot([-104.9459236 -104.9481973], [39.8055678 39.8068358], '--w',
'LineWidth', 2)
axis([-104.9485 -104.944 39.8055 39.8075]);
plot_google_map('maptype','satellite')

%for colored velocity
%function source: https://www.mathworks.com/matlabcentral/fileexchange/30280-
stoplight
colormap stoplight
cb = colorbar();
set(cb, 'ylim', [0.1 10])
set(gca,'ColorScale','log')
caxis([0.1 10]);
cb.Ticks = [0.1 1 10];
cb.Ruler.Scale = 'log';
cb.Ruler.MinorTick = 'on';

%staring flow flag locations
particle1_y_start = (1719242.07 + 1719452.252 + 1718784.09) / 3;
particle1_x_start = (3155030.31 + 3155883.52 + 3155671.92) / 3;
particle2_y_start = (1719452.252 + 1718786.48 + 1718784.09) / 3;
particle2_x_start = (3155883.52 + 3156145.3 + 3155671.92) / 3;

%Convert US survey feet coordinates to Lat and long degrees.
%Function source =
https://www.mathworks.com/matlabcentral/fileexchange/26413-sp_proj
[startlong1, startlat1] = sp_proj('colorado
north','inverse',particle1_x_start, particle1_y_start,'sf');
plot(startlong1, startlat1, '*b', 'MarkerSize', 2);
[startlong2, startlat2] = sp_proj('colorado
north','inverse',particle2_x_start, particle2_y_start,'sf');
plot(startlong2, startlat2, '*b', 'MarkerSize', 2);
```

```
particle1_US_x = particle1_x_start;
particle1_US_y = particle1_y_start;
particle1_US_x_LOW = particle1_x_start;
particle1_US_y_LOW = particle1_y_start;
particle1_US_x_HIGH = particle1_x_start;
particle1_US_y_HIGH = particle1_y_start;

particle2_US_x = particle2_x_start;
particle2_US_y = particle2_y_start;
particle2_US_x_LOW = particle2_x_start;
particle2_US_y_LOW = particle2_y_start;
particle2_US_x_HIGH = particle2_x_start;
particle2_US_y_HIGH = particle2_y_start;

%input initial values
ne = 0.25; %effective porosity (dimensionless)
K_iso = 1.2; %isotropic hydraulic conductivity (ft/hr)
t = 1; %time step (hr)
realizations = 1000; %number realizations for error approximation
%limitations of survey equipment = +/- 10mm+0.8ppm  -
https://www.topconpositioning.com/gnss/integrated-gnss-receivers/gr-5#panel-
product-specifications
%Actual Accuracy = sqrt(survey^2 + PT^2) = sqrt(0.0115^2 + 0.037^2) = 0.039ft
Accuracy = 39; %randomization only takes integer inputs (Accuracy = Actual
Accuracy (0.039ft) x 1000)

%IMPORT DATA - Be sure to "flip" data from Ubidots in Excel!
SITE B_1Excel = xlsread('Site B_1-wt-elev.xlsx'); %insert Excel file name
here
SITE B_3Excel = xlsread('Site B_3-wt-elev.xlsx');
SITE B_4Excel = xlsread('Site B_4-wt-elev.xlsx');
SITE B_6Excel = xlsread('Site B_6-wt-elev.xlsx');

%SITE B Well Locations
%CPZ-16 (SITE B_3),     CPZ-21 (SITE B_4),    CPZ-27 (SITE B_5),    RMW-15
(SITE B_6),     BCMW-03ST-2 (SITE B_1),   WPB-05T-2(SITE B_2)
%Wellxy = [3155030.31 1719242.07; 3156145.3 1718786.48; 3155498.37
1719245.31; 3155671.92 1718784.09; 3155883.52 1719452.252; 3154384.896
1719923.63]; %CPZ-16, CPZ-21, CPZ-27, RMW-15, BCMW-03ST-2, WPB-05T-2 -
coordinates in US survey feet (State Plane Colorado Central (ft NAD83) and
NAVD88)
Particle1_Wellxy =  [3155030.31 1719242.07; 3155883.52 1719452.252;
3155671.92 1718784.09];
Particle2_Wellxy =  [3155883.52 1719452.252; 3156145.3 1718786.48; 3155671.92
1718784.09];

%Error Approximation (flow flag 1)
for j = 1:realizations %1000 realizations
%numbers must be entered into randi as integer values (hence divide by
%1000 (e.g. [-12 12] = [-0.012 0.012]) )
rand1 = randi([-Accuracy Accuracy])/1000;
rand2 = randi([-Accuracy Accuracy])/1000;
rand3 = randi([-Accuracy Accuracy])/1000;
```

```
well1_rand = rand1;
well2_rand = rand2;
well3_rand = rand3;

wellAll_rand = [well1_rand; well2_rand; well3_rand];

%randomization slopes
Plane = [ones(3,1), Particle1_Wellxy] \ wellAll_rand;
Slopex_rand = Plane(2);
Slopey_rand = Plane(3);

x_array1(j) = Slopex_rand;
y_array1(j) = Slopey_rand;

end

%x and y 95% confidence
    X_95_1 = 2 * std(x_array1)
    Y_95_1 = 2 * std(y_array1)


%Error Approximation (flow flag 2)
for j = 1:realizations %1000 realizations
%numbers must be entered into randi as integer values (hence divide by
%1000 (e.g. [-12 12] = [-0.012 0.012]) )
rand1 = randi([-Accuracy Accuracy])/1000;
rand2 = randi([-Accuracy Accuracy])/1000;
rand3 = randi([-Accuracy Accuracy])/1000;

well1_rand = rand1;
well2_rand = rand2;
well3_rand = rand3;

wellAll_rand = [well1_rand; well2_rand; well3_rand];

%randomization slopes
Plane = [ones(3,1), Particle2_Wellxy] \ wellAll_rand;
Slopex_rand = Plane(2);
Slopey_rand = Plane(3);

x_array2(j) = Slopex_rand;
y_array2(j) = Slopey_rand;

end

    %x and y 95% confidence
    X_95_2 = 2 * std(x_array2)
    Y_95_2 = 2 * std(y_array2)


Ndata = %insert number of data points here

for i = 2:Ndata
```

```
%extract water table elevations
WL1 = SITE B_1Excel(i,3);
WL3 = SITE B_3Excel(i,3);
WL4 = SITE B_4Excel(i,3);
WL6 = SITE B_6Excel(i,3);

%create vector of water levels
Particle1_vector =  [WL1; WL3; WL6];
Particle2_vector =  [WL1; WL4; WL6];

%%%%%%%%%%%%%%%%%%     flow flag 1        %%%%%%%%%%%%%%%%%%%%%%%%%%%%%%%%
Plane = [ones(3,1), Particle1_Wellxy] \ Particle1_vector;
Slopex1 = Plane(2); %extract slope x
Slopey1 = Plane(3); %extract slope y

%for estimated location
xpos1 = particle1_US_x - ((Slopex1*K_iso*t)/ne);
ypos1 = particle1_US_y - ((Slopey1*K_iso*t)/ne);
m1_1 = (ypos1-particle1_US_y)/(xpos1-particle1_US_x);

   %for Low location
   xposLOW1 = particle1_US_x_LOW - (((Slopex1-X_95_1)*K_iso*t)/ne);
   yposLOW1 = particle1_US_y_LOW - ((((Slopey1-Y_95_1))*K_iso*t)/ne);
   m3_1 = (yposLOW1-particle1_US_y_LOW)/(xposLOW1-particle1_US_x_LOW);

   %for High location
   xposHIGH1 = particle1_US_x_HIGH - (((Slopex1+X_95_1)*K_iso*t)/ne);
   yposHIGH1 = particle1_US_y_HIGH - ((((Slopey1+Y_95_1))*K_iso*t)/ne);
   m2_1 = (yposHIGH1-particle1_US_y_HIGH)/(xposHIGH1-particle1_US_x_HIGH);

   %store angles off of average path in array
   angle1_array_1(i) = atand((m1_1-m2_1)/(1+m1_1*m2_1));
   angle2_array_1(i) = atand((m1_1-m3_1)/(1+m1_1*m3_1));
   avgAngle_1 = atan(m1_1);
    if avgAngle_1<0
       avgAngle_array_1(i) = (pi + avgAngle_1) * 180 / pi;
   else avgAngle_array_1(i) = avgAngle_1 * 180 / pi;
    end

%%%%%%%%%%%%%%%%%%%%%     flow flag 2      %%%%%%%%%%%%%%%%%%%%%%%%%%%%%%%%
Plane = [ones(3,1), Particle2_Wellxy] \ Particle2_vector;
Slopex2 = Plane(2); %extract slope x
Slopey2 = Plane(3); %extract slope y

%for estimated location
xpos2 = particle2_US_x - ((Slopex2*K_iso*t)/ne);
ypos2 = particle2_US_y - ((Slopey2*K_iso*t)/ne);
m1_2 = (ypos2-particle2_US_y)/(xpos2-particle2_US_x);

   %for Low location
   xposLOW2 = particle2_US_x_LOW - (((Slopex2-X_95_2)*K_iso*t)/ne);
   yposLOW2 = particle2_US_y_LOW - ((((Slopey2-Y_95_2))*K_iso*t)/ne);
   m3_2 = (yposLOW2-particle2_US_y_LOW)/(xposLOW2-particle2_US_x_LOW);
```

```
   %for High location
   xposHIGH2 = particle2_US_x_HIGH - (((Slopex2+X_95_2)*K_iso*t)/ne);
   yposHIGH2 = particle2_US_y_HIGH - ((((Slopey2+Y_95_2))*K_iso*t)/ne);
   m2_2 = (yposHIGH2-particle2_US_y_HIGH)/(xposHIGH2-particle2_US_x_HIGH);

   %store angles off of average path in array
   angle1_array_2(i) = atand((m1_2-m2_2)/(1+m1_2*m2_2));
   angle2_array_2(i) = atand((m1_2-m3_2)/(1+m1_2*m3_2));
   avgAngle_2 = atan(m1_2);
   if avgAngle_2<0
       avgAngle_array_2(i) = (pi + avgAngle_2) * 180 / pi;
   else avgAngle_array_2(i) = avgAngle_2 * 180 / pi;
   end


   %Convert US survey feet coordinates to Lat and long degrees.
 [particle1_newlng,particle1_newlat] = sp_proj('colorado
central','inverse',xpos1,ypos1,'sf');
 [particle2_newlng,particle2_newlat] = sp_proj('colorado
central','inverse',xpos2,ypos2,'sf');
 [particleLOW_newlng1,particleLOW_newlat1] = sp_proj('colorado
central','inverse',xposLOW1,yposLOW1,'sf');
 [particleHIGH_newlng1,particleHIGH_newlat1] = sp_proj('colorado
central','inverse',xposHIGH1,yposHIGH1,'sf');
 [particleLOW_newlng2,particleLOW_newlat2] = sp_proj('colorado
central','inverse',xposLOW2,yposLOW2,'sf');
 [particleHIGH_newlng2,particleHIGH_newlat2] = sp_proj('colorado
central','inverse',xposHIGH2,yposHIGH2,'sf');

 array_lng1(i) = particle1_newlng;
 array_lat1(i) = particle1_newlat;

 array_lng2(i) = particle2_newlng;
 array_lat2(i) = particle2_newlat;

   %plot 95% confidence locations
  hold on
 plot(particleLOW_newlng1, particleLOW_newlat1, '*b', 'MarkerSize', 5);
 plot(particleHIGH_newlng1, particleHIGH_newlat1, '*b', 'MarkerSize', 5);
 plot(particleLOW_newlng2, particleLOW_newlat2, '*b', 'MarkerSize', 5);
 plot(particleHIGH_newlng2, particleHIGH_newlat2, '*b', 'MarkerSize', 5);

%for average velocities
V_mag1 = sqrt(((Slopex1*K_iso)/ne)^2 + ((Slopey1*K_iso)/ne)^2)*24; %velocity
magnitude in ft/day
V_mag_array1(i) = V_mag1;
V_mag2 = sqrt(((Slopex2*K_iso)/ne)^2 + ((Slopey2*K_iso)/ne)^2)*24; %velocity
magnitude in ft/day
V_mag_array2(i) = V_mag2;

%for low 95% confidence velocities
V_mag1_low = sqrt((((Slopex1-X_95_1)*K_iso)/ne)^2 + (((Slopey1-
Y_95_1)*K_iso)/ne)^2)*24; %velocity magnitude in ft/day
V_mag_array1_low(i) = V_mag1_low;
```

```
V_mag2_low = sqrt((((Slopex2-X_95_2)*K_iso)/ne)^2 + (((Slopey2-
Y_95_2)*K_iso)/ne)^2)*24; %velocity magnitude in ft/day
V_mag_array2_low(i) = V_mag2_low;

%for high 95% confidence velocities
V_mag1_high = sqrt((((Slopex1+X_95_1)*K_iso)/ne)^2 +
(((Slopey1+Y_95_1)*K_iso)/ne)^2)*24; %velocity magnitude in ft/day
V_mag_array1_high(i) = V_mag1_high;
V_mag2_high = sqrt((((Slopex2+X_95_2)*K_iso)/ne)^2 +
(((Slopey2+Y_95_2)*K_iso)/ne)^2)*24; %velocity magnitude in ft/day
V_mag_array2_high(i) = V_mag2_high;


  %store new locations
  particle1_US_x = xpos1;
  particle1_US_y = ypos1;
  particle1_US_x_LOW = xposLOW1;
  particle1_US_y_LOW = yposLOW1;
  particle1_US_x_HIGH = xposHIGH1;
  particle1_US_y_HIGH = yposHIGH1;

  particle2_US_x = xpos2;
  particle2_US_y = ypos2;
  particle2_US_x_LOW = xposLOW2;
  particle2_US_y_LOW = yposLOW2;
  particle2_US_x_HIGH = xposHIGH2;
  particle2_US_y_HIGH = yposHIGH2;

end

%graph labels
xlabel('Longitude');
ylabel('Latitude');
ylabel(cb, 'ft/day', 'FontSize', 12);
title('INSERT_TITLE_HERE');

%velocity and angle calculations (flow flag 1)
V_avg_ft_day1 = mean(V_mag_array1)
V_avg_ft_day1_low = mean(V_mag_array1_low)
V_avg_ft_day1_high = mean(V_mag_array1_high)
Angle_off_avg_1_1 = mean(angle1_array_1)
Angle_off_avg_2_1 = mean(angle2_array_1)
Avg_Angle_1 = mean(avgAngle_array_1)

%velocity and angle calculations (flow flag 2)
V_avg_ft_day2 = mean(V_mag_array2)
V_avg_ft_day2_low = mean(V_mag_array2_low)
V_avg_ft_day2_high = mean(V_mag_array2_high)
Angle_off_avg_1_2 = mean(angle1_array_2)
Angle_off_avg_2_2 = mean(angle2_array_2)
Avg_Angle_2 = mean(avgAngle_array_2)
```

```
%plot colored, estimated flow flags
for i = 2:Ndata
 scatter(array_lng1(i),array_lat1(i), 5, V_mag_array1(i), 'filled')
 scatter(array_lng2(i),array_lat2(i), 5, V_mag_array2(i), 'filled')
end
```

Code for estimated and anisotropy uncertainty affected flow paths at Site B.

```
%For SITE B
%Estimate anisotropy uncertainties effect on
%groundwater flow to advance estimated and error based flow flags. Use
%colorbar to visualize the average speed of the estimated flow flag
%Zach Ferrie - CSU - October 2019

clear all
plot_google_map('apiKey', 'INSERT_API_KEY_HERE') %if you have API KEY
%follow this link to get API KEY:
https://developers.google.com/maps/documentation/javascript/get-api-
key?authuser=1#get-the-api-key
hold on
lat = [39.8073977 39.8068358 39.8055664 39.8055678];
lon = [-104.9451542 -104.9481973 -104.9442387 -104.9459236];
plot(lon, lat, '.w', 'MarkerSize', 40)
plot([-104.9451542 -104.9481973], [39.8073977 39.8068358], '--w',
'LineWidth', 2)
plot([-104.9442387 -104.9459236], [39.8055664 39.8055678], '--w',
'LineWidth', 2)
plot([-104.9451542 -104.9459236], [39.8073977 39.8055678], '--w',
'LineWidth', 2)
plot([-104.9451542 -104.9442387], [39.8073977 39.8055664], '--w',
'LineWidth', 2)
plot([-104.9459236 -104.9481973], [39.8055678 39.8068358], '--w',
'LineWidth', 2)
axis([-104.9485 -104.944 39.8055 39.8075]);
plot_google_map('maptype','satellite')

% %for colored velocity
%function source: https://www.mathworks.com/matlabcentral/fileexchange/30280-
stoplight
colormap stoplight
cb = colorbar();
set(cb, 'ylim', [0.1 10])
set(gca,'ColorScale','log')
caxis([0.1 10]);
cb.Ticks = [0.1 1 10];
cb.Ruler.Scale = 'log';
cb.Ruler.MinorTick = 'on';

%staring flow flag locations
particle1_y_start = (1719242.07 + 1719452.252 + 1718784.09) / 3;
particle1_x_start = (3155030.31 + 3155883.52 + 3155671.92) / 3;
particle2_y_start = (1719452.252 + 1718786.48 + 1718784.09) / 3;
particle2_x_start = (3155883.52 + 3156145.3 + 3155671.92) / 3;

%Convert US survey feet coordinates to Lat and long degrees.
%Function source =
https://www.mathworks.com/matlabcentral/fileexchange/26413-sp_proj
[startlong1, startlat1] = sp_proj('colorado
north','inverse',particle1_x_start, particle1_y_start,'sf');
plot(startlong1, startlat1, '*b', 'MarkerSize', 2);
```

```
[startlong2, startlat2] = sp_proj('colorado
north','inverse',particle2_x_start, particle2_y_start,'sf');
plot(startlong2, startlat2, '*b', 'MarkerSize', 2);

particle1_US_x = particle1_x_start;
particle1_US_y = particle1_y_start;
particle1_US_x_LOW = particle1_x_start;
particle1_US_y_LOW = particle1_y_start;
particle1_US_x_HIGH = particle1_x_start;
particle1_US_y_HIGH = particle1_y_start;

particle2_US_x = particle2_x_start;
particle2_US_y = particle2_y_start;
particle2_US_x_LOW = particle2_x_start;
particle2_US_y_LOW = particle2_y_start;
particle2_US_x_HIGH = particle2_x_start;
particle2_US_y_HIGH = particle2_y_start;

%input initial values
ne = 0.25; %effective porosity (dimensionless)
K1 = 1.2; %isotropic hydraulic conductivity (ft/hr)
t = 1; %time step (hr)

%IMPORT DATA - Be sure to "flip" data in Excel!
SITE B_1Excel = xlsread('Site B_1-wt-elev.xlsx'); %insert Excel file name
here
SITE B_3Excel = xlsread('Site B_3-wt-elev.xlsx');
SITE B_4Excel = xlsread('Site B_4-wt-elev.xlsx');
SITE B_6Excel = xlsread('Site B_6-wt-elev.xlsx');

%SITE B Well Locations
% CPZ-16 (SITE B_3),     CPZ-21 (SITE B_4),    CPZ-27 (SITE B_5),    RMW-15
(SITE B_6),     BCMW-03ST-2 (SITE B_1),   WPB-05T-2(SITE B_2)
%Wellxy = [3155030.31 1719242.07; 3156145.3 1718786.48; 3155498.37
1719245.31; 3155671.92 1718784.09; 3155883.52 1719452.252; 3154384.896
1719923.63]; %CPZ-16, CPZ-21, CPZ-27, RMW-15, BCMW-03ST-2, WPB-05T-2 -
coordinates in US survey feet (State Plane Colorado Central (ft NAD83) and
NAVD88)
Particle1_Wellxy =  [3155030.31 1719242.07; 3155883.52 1719452.252;
3155671.92 1718784.09];
Particle2_Wellxy =  [3155883.52 1719452.252; 3156145.3 1718786.48; 3155671.92
1718784.09];

%anisotropy uncertainty factors
K2_low = K1*1.10;
K2_high = K1*1.28;
K2_avg = K1*1.19;


Ndata = %insert number of data points here

for i = 2:Ndata

%extract water table elevations
WL1 = SITE B_1Excel(i,3);
```

```
WL3 = SITE B_3Excel(i,3);
WL4 = SITE B_4Excel(i,3);
WL6 = SITE B_6Excel(i,3);

%create vector of water levels
Particle1_vector =  [WL1; WL3; WL6];
Particle2_vector =  [WL1; WL4; WL6];

%%%%%%%%%%%%%%%%%%%     flow flag 1        %%%%%%%%%%%%%%%%%%%%%%%%%%%%%%%%
Plane = [ones(3,1), Particle1_Wellxy] \ Particle1_vector;
Slopex1 = Plane(2); %extract slope x
Slopey1 = Plane(3); %extract slope y

%for estimated location
xpos1 = particle1_US_x - ((Slopex1*K2_avg)/ne)*t;
ypos1 = particle1_US_y - ((Slopey1*K1)/ne)*t;
m1_1 = (ypos1-particle1_US_y)/(xpos1-particle1_US_x);

   %for low location
   xposLOW1 = particle1_US_x_LOW - ((Slopex1*K2_low)/ne)*t;
   yposLOW1 = particle1_US_y_LOW - ((Slopey1*K1)/ne)*t;
   m3_1 = (yposLOW1-particle1_US_y_LOW)/(xposLOW1-particle1_US_x_LOW);

   %for high location
   xposHIGH1 = particle1_US_x_HIGH - ((Slopex1*K2_high)/ne)*t;
   yposHIGH1 = particle1_US_y_HIGH - ((Slopey1*K1)/ne)*t;
   m2_1 = (yposHIGH1-particle1_US_y_HIGH)/(xposHIGH1-particle1_US_x_HIGH);

   %store angles off of average path in array
   angle1_array_1(i) = atand((m1_1-m2_1)/(1+m1_1*m2_1));
   angle2_array_1(i) = atand((m1_1-m3_1)/(1+m1_1*m3_1));
   avgAngle_1 = atan(m1_1);
    if avgAngle_1<0
       avgAngle_array_1(i) = (pi + avgAngle_1) * 180 / pi;
   else avgAngle_array_1(i) = avgAngle_1 * 180 / pi;
   end



%%%%%%%%%%%%%%%%%%%%%     flow flag 2      %%%%%%%%%%%%%%%%%%%%%%%%%%%%%%%%
Plane = [ones(3,1), Particle2_Wellxy] \ Particle2_vector;
Slopex2 = Plane(2); %extract slope x
Slopey2 = Plane(3); %extract slope y

%Estimated location
xpos2 = particle2_US_x - ((Slopex2*K2_avg)/ne)*t;
ypos2 = particle2_US_y - ((Slopey2*K1)/ne)*t;
m1_2 = (ypos2-particle2_US_y)/(xpos2-particle2_US_x);

   %for low location
   xposLOW2 = particle2_US_x_LOW - ((Slopex2*K2_low)/ne)*t;
   yposLOW2 = particle2_US_y_LOW - ((Slopey2*K1)/ne)*t;
   m3_2 = (yposLOW2-particle2_US_y_LOW)/(xposLOW2-particle2_US_x_LOW);
```

```
   %for high location
   xposHIGH2 = particle2_US_x_HIGH - ((Slopex2*K2_high)/ne)*t;
   yposHIGH2 = particle2_US_y_HIGH - ((Slopey2*K1)/ne)*t;
   m2_2 = (yposHIGH2-particle2_US_y_HIGH)/(xposHIGH2-particle2_US_x_HIGH);

   %store angles off of average path in array
   angle1_array_2(i) = atand((m1_2-m2_2)/(1+m1_2*m2_2));
   angle2_array_2(i) = atand((m1_2-m3_2)/(1+m1_2*m3_2));
   avgAngle_2 = atan(m1_2);
   if avgAngle_2<0
       avgAngle_array_2(i) = (pi + avgAngle_2) * 180 / pi;
   else avgAngle_array_2(i) = avgAngle_2 * 180 / pi;
   end


   %Convert US survey feet coordinates to Lat and long degrees.
 [particle1_newlng,particle1_newlat] = sp_proj('colorado
central','inverse',xpos1,ypos1,'sf');
 [particle2_newlng,particle2_newlat] = sp_proj('colorado
central','inverse',xpos2,ypos2,'sf');
 [particleLOW_newlng1,particleLOW_newlat1] = sp_proj('colorado
central','inverse',xposLOW1,yposLOW1,'sf');
 [particleHIGH_newlng1,particleHIGH_newlat1] = sp_proj('colorado
central','inverse',xposHIGH1,yposHIGH1,'sf');
 [particleLOW_newlng2,particleLOW_newlat2] = sp_proj('colorado
central','inverse',xposLOW2,yposLOW2,'sf');
 [particleHIGH_newlng2,particleHIGH_newlat2] = sp_proj('colorado
central','inverse',xposHIGH2,yposHIGH2,'sf');

 array_lng1(i) = particle1_newlng;
 array_lat1(i) = particle1_newlat;

 array_lng2(i) = particle2_newlng;
 array_lat2(i) = particle2_newlat;

 %plot 95% confidence locations
  hold on
 plot(particleLOW_newlng1, particleLOW_newlat1, '*b', 'MarkerSize', 5);
 plot(particleHIGH_newlng1, particleHIGH_newlat1, '*b', 'MarkerSize', 5);
 plot(particleLOW_newlng2, particleLOW_newlat2, '*b', 'MarkerSize', 5);
 plot(particleHIGH_newlng2, particleHIGH_newlat2, '*b', 'MarkerSize', 5);

 %for average velocities
V_mag1 = sqrt(((Slopex1*K2_avg)/ne)^2 + ((Slopey1*K1)/ne)^2)*24; %velocity
magnitude in ft/day
V_mag_array1(i) = V_mag1;
V_mag2 = sqrt(((Slopex2*K2_avg)/ne)^2 + ((Slopey2*K1)/ne)^2)*24; %velocity
magnitude in ft/day
V_mag_array2(i) = V_mag2;

%for low 95% confidence velocities
V_mag1_low = sqrt(((Slopex1*K2_low)/ne)^2 + ((Slopey1*K1)/ne)^2)*24;
%velocity magnitude in ft/day
V_mag_array1_low(i) = V_mag1_low;
```

```
V_mag2_low = sqrt(((Slopex2*K2_low)/ne)^2 + ((Slopey2*K1)/ne)^2)*24;
%velocity magnitude in ft/day
V_mag_array2_low(i) = V_mag2_low;

%for high 95% confidence velocities
V_mag1_high = sqrt(((Slopex1*K2_high)/ne)^2 + ((Slopey1*K1)/ne)^2)*24;
%velocity magnitude in ft/day
V_mag_array1_high(i) = V_mag1_high;
V_mag2_high = sqrt(((Slopex2*K2_high)/ne)^2 + ((Slopey2*K1)/ne)^2)*24;
%velocity magnitude in ft/day
V_mag_array2_high(i) = V_mag2_high;

  %store new locations
  particle1_US_x = xpos1;
  particle1_US_y = ypos1;
  particle1_US_x_LOW = xposLOW1;
  particle1_US_y_LOW = yposLOW1;
  particle1_US_x_HIGH = xposHIGH1;
  particle1_US_y_HIGH = yposHIGH1;

  particle2_US_x = xpos2;
  particle2_US_y = ypos2;
  particle2_US_x_LOW = xposLOW2;
  particle2_US_y_LOW = yposLOW2;
  particle2_US_x_HIGH = xposHIGH2;
  particle2_US_y_HIGH = yposHIGH2;

end

%graph labels
xlabel('Longitude');
ylabel('Latitude');
ylabel(cb, 'ft/day', 'FontSize', 12);
title('INSERT_TITLE_HERE');

%velocity and angle calculations (flow flag 1)
V_avg_ft_day1 = mean(V_mag_array1)
V_avg_ft_day1_low = mean(V_mag_array1_low)
V_avg_ft_day1_high = mean(V_mag_array1_high)
Angle_off_avg_1_1 = mean(angle1_array_1)
Angle_off_avg_2_1 = mean(angle2_array_1)
Avg_Angle_1 = mean(avgAngle_array_1)

%velocity and angle calculations (flow flag 2)
V_avg_ft_day2 = mean(V_mag_array2)
V_avg_ft_day2_low = mean(V_mag_array2_low)
V_avg_ft_day2_high = mean(V_mag_array2_high)
Angle_off_avg_1_2 = mean(angle1_array_2)
Angle_off_avg_2_2 = mean(angle2_array_2)
Avg_Angle_2 = mean(avgAngle_array_2)
```

```
%plot colored, estimated flow flags
for i = 2:Ndata
 scatter(array_lng1(i),array_lat1(i), 3, V_mag_array1(i), 'filled')
 scatter(array_lng2(i),array_lat2(i), 3, V_mag_array2(i), 'filled')
end
```

Real-time flow flag code for Site B dashboard (Ubidots). Note that to run this software in real-time a computer must be set up to run the code at a specified time interval. This can be done using software such as Windows Task Scheduler.

```
%Run flow flag model in real-time using Ubdiots
%For SITE B
%Zach Ferrie - CSU - 2019

%The below code is run once to provide the starting point of the advective
%flow path. Comment this code out afterwards.
%%%%%%%%%%%%%%%%%%%%%%%%%SET_INTIAL_LOCATION%%%%%%%%%%%%%%%%%%%%%%%%%%%%%

%staring Particle locations
particle1_y_start = (1719242.07 + 1719452.252 + 1718784.09) / 3;
particle1_x_start = (3155030.31 + 3155883.52 + 3155671.92) / 3;
particle2_y_start = (1719452.252 + 1718786.48 + 1718784.09) / 3;
particle2_x_start = (3155883.52 + 3156145.3 + 3155671.92) / 3;

%Convert US survey feet coordinates to Lat and long degress. code source =
https://www.mathworks.com/matlabcentral/fileexchange/26413-sp_proj
[particle1_newlng,particle1_newlat] = sp_proj('colorado
north','inverse',particle1_x_start, particle1_y_start,'sf');
[particle2_newlng,particle2_newlat] = sp_proj('colorado
north','inverse',particle2_x_start, particle2_y_start,'sf');
new_cntr1 = 0;
new_cntr2 = 0;

% Send JSON payloads (lat and long) to Ubidots

% particle 1
ubidotsURL = 'http://industrial.api.ubidots.com/api/v1.6/devices/Site
B_particletrack_1/gps/values?token=INSERT_TOKEN_HERE';
%for more insight as to reasons for choosing 10 as the number of significant
digits see -  https://gis.stackexchange.com/questions/8650/measuring-
accuracy-of-latitude-and-longitude/8674#8674
latstr1 = num2str(particle1_newlat, 10); %convert number to string, max
number of significant digits = 10 (1.1 mm accuracy - 8 decimal places)
lngstr1 = num2str(particle1_newlng, 10); %convert number to string, max
number of significant digits = 10 (1.1 mm accuracy - 8 decimal places)
new_cntr1_str = num2str(new_cntr1, 100); %convert counter to string
data1 = ['{"value":',new_cntr1_str, ', "context": {"lat":', latstr1, ',
"lng":', lngstr1, '}}']; %create JSON formatted string
options = weboptions('MediaType','application/json', 'Timeout', 120);
%specify JSON formatted content and set timeout to 2 min
response = webwrite(ubidotsURL, data1, options); %send JSON payload to
Ubidots

% particle 2
ubidotsURL = 'http://industrial.api.ubidots.com/api/v1.6/devices/Site
B_particletrack_2/gps/values?token=INSERT_TOKEN_HERE';
```

```
%for more insight as to reasons for choosing 10 as the number of significant
digits see -  https://gis.stackexchange.com/questions/8650/measuring-
accuracy-of-latitude-and-longitude/8674#8674
latstr2 = num2str(particle2_newlat, 10); %convert number to string, max
number of significant digits = 10 (1.1 mm accuracy - 8 decimal places)
lngstr2 = num2str(particle2_newlng, 10); %convert number to string, max
number of significant digits = 10 (1.1 mm accuracy - 8 decimal places)
new_cntr2_str = num2str(new_cntr2, 100); %convert counter to string
data2 = ['{"value":',new_cntr2_str, ', "context": {"lat":', latstr2, ',
"lng":', lngstr2, '}}']; %create JSON formatted string
options = weboptions('MediaType','application/json', 'Timeout', 120);
%specify JSON formatted content and set timeout to 2 min
response = webwrite(ubidotsURL, data2, options); %send JSON payload to
Ubidots

%%%%%%%%%%%%%%%%%%%%%%%%%%%%%%%%%%%%%%%%%%%%%%%%%%%%%%%%%%%%%%%%%%%%%%%%%%%%%%%


%input initial values
ne = 0.25; %effective porosity (dimensionless)
K_iso = 1.2; %isotropic hydraulic conductivity (ft/hr)
t = 1; %time step (hr)

%SITE B Well Locations
%          CPZ-16 (SITE B_3),     CPZ-21 (SITE B_4),    CPZ-27 (SITE B_5),
RMW-15 (SITE B_6),     BCMW-03ST-2 (SITE B_1),   WPB-05T-2(SITE B_2)
%Wellxy = [3155030.31 1719242.07; 3156145.3 1718786.48; 3155498.37
1719245.31; 3155671.92 1718784.09; 3155883.52 1719452.252; 3154384.896
1719923.63]; %CPZ-16, CPZ-21, CPZ-27, RMW-15, BCMW-03ST-2, WPB-05T-2 -
coordinates in US survey feet (State Plane Colorado Central (ft NAD83) and
NAVD88)
Particle1_Wellxy =  [3155030.31 1719242.07; 3155883.52 1719452.252;
3155671.92 1718784.09];
Particle2_Wellxy =  [3155883.52 1719452.252; 3156145.3 1718786.48; 3155671.92
1718784.09];

%Get current water level data and particle positions
track1 = webread('http://industrial.api.ubidots.com/api/v1.6/devices/Site
B_particletrack_1/gps/values?token=INSERT_TOKEN_HERE'); %particle track 1
track2 = webread('http://industrial.api.ubidots.com/api/v1.6/devices/Site
B_particletrack_2/gps/values?token=INSERT_TOKEN_HERE'); %particle track 2
SITE B_1 =
webread('http://industrial.api.ubidots.com/api/v1.6/variables/INSERT_VARAIBLE
_ID_HERE/values?token=INSERT_TOKEN_HERE'); %water table elevation - SITE B_1
SITE B_3 =
webread('http://industrial.api.ubidots.com/api/v1.6/variables/INSERT_VARAIBLE
_ID_HERE/values?token=INSERT_TOKEN_HERE'); %water table elevation - SITE B_3
SITE B_4 =
webread('http://industrial.api.ubidots.com/api/v1.6/variables/INSERT_VARAIBLE
_ID_HERE/values?token=INSERT_TOKEN_HERE'); %water table elevation - SITE B_4
SITE B_6 =
webread('http://industrial.api.ubidots.com/api/v1.6/variables/INSERT_VARAIBLE
_ID_HERE/values?token=INSERT_TOKEN_HERE'); %water table elevation - SITE B_6

%extract water level values from SITE B 1-6
WL1 = SITE B_1.results.value;
```

```
WL3 = SITE B_3.results.value;
WL4 = SITE B_4.results.value;
WL6 = SITE B_6.results.value;

%extract particle locations
particleOld_1 = track1.results.context;
particleOld_2 = track2.results.context;

%extract update counter variable
cntr1 = track1.results.value;
cntr2 = track2.results.value;

%update counter variable
new_cntr1 = cntr1 + 1;
new_cntr2 = cntr2 + 1;

%create vector of water levels
Particle1_vector =  [WL1; WL3; WL6];
Particle2_vector =  [WL1; WL4; WL6];


%load particle locations into matrices
particleOld_1_cell = struct2cell(particleOld_1);
particleOld_1_mat = cell2mat(particleOld_1_cell);
particleOld_2_cell = struct2cell(particleOld_2);
particleOld_2_mat = cell2mat(particleOld_2_cell);

%extract particle lat/long from matrices
particleOld_1_lat = particleOld_1_mat(1, 1);
particleOld_1_long = particleOld_1_mat(2, 1);
particleOld_2_lat = particleOld_2_mat(1, 1);
particleOld_2_long = particleOld_2_mat(2, 1);

%Convert Lat/Long to US survey feet. code source =
https://www.mathworks.com/matlabcentral/fileexchange/26413-sp_proj
[particle1_US_x, particle1_US_y] = sp_proj('colorado central', 'forward',
particleOld_1_long, particleOld_1_lat, 'sf');
[particle2_US_x, particle2_US_y] = sp_proj('colorado central', 'forward',
particleOld_2_long, particleOld_2_lat, 'sf');


%%%%%%%%%%%%%%%%%%%     particle 1        %%%%%%%%%%%%%%%%%%%%%%%%%%%%%%%%
Plane = [ones(3,1), Particle1_Wellxy] \ Particle1_vector;
Slopex1 = Plane(2); %extract slope x
Slopey1 = Plane(3); %extract slope y

xpos1 = particle1_US_x - ((Slopex1*K_iso*t)/ne);
ypos1 = particle1_US_y - ((Slopey1*K_iso*t)/ne);


%%%%%%%%%%%%%%%%%%%%%     particle 2      %%%%%%%%%%%%%%%%%%%%%%%%%%%%%%%%
Plane = [ones(3,1), Particle2_Wellxy] \ Particle2_vector;
Slopex2 = Plane(2); %extract slope x
Slopey2 = Plane(3); %extract slope y
```

```
xpos2 = particle2_US_x - ((Slopex2*K_iso*t)/ne);
ypos2 = particle2_US_y - ((Slopey2*K_iso*t)/ne);



   %Convert US survey feet coordinates to Lat and long degress. code source =
https://www.mathworks.com/matlabcentral/fileexchange/26413-sp_proj
 [particle1_newlng,particle1_newlat] = sp_proj('colorado
central','inverse',xpos1,ypos1,'sf');
 [particle2_newlng,particle2_newlat] = sp_proj('colorado
central','inverse',xpos2,ypos2,'sf');

 % Send JSON payloads (lat and long) to Ubidots

% particle 1
ubidotsURL = 'http://industrial.api.ubidots.com/api/v1.6/devices/Site
B_particletrack_1/gps/values?token=INSERT_TOKEN_HERE';
%for more insight as to reasons for choosing 10 as the number of significant
digits see -  https://gis.stackexchange.com/questions/8650/measuring-
accuracy-of-latitude-and-longitude/8674#8674
latstr1 = num2str(particle1_newlat, 10); %convert number to string, max
number of significant digits = 10 (1.1 mm accuracy - 8 decimal places)
lngstr1 = num2str(particle1_newlng, 11); %convert number to string, max
number of significant digits = 10 (1.1 mm accuracy - 8 decimal places)
new_cntr1_str = num2str(new_cntr1, 100); %convert counter to string
data1 = ['{"timestamp":', timestampstr, ', "value":',new_cntr1_str, ',
"context": {"lat":', latstr1, ', "lng":', lngstr1, '}}']; %create JSON
formatted string
options = weboptions('MediaType','application/json', 'Timeout', 120);
%specify JSON formatted content and set timeout to 2 min
response = webwrite(ubidotsURL, data1, options); %send JSON payload to
Ubidots

% particle 2
ubidotsURL = 'http://industrial.api.ubidots.com/api/v1.6/devices/Site
B_particletrack_2/gps/values?token=INSERT_TOKEN_HERE';
%for more insight as to reasons for choosing 10 as the number of significant
digits see -  https://gis.stackexchange.com/questions/8650/measuring-
accuracy-of-latitude-and-longitude/8674#8674
latstr2 = num2str(particle2_newlat, 10); %convert number to string, max
number of significant digits = 10 (1.1 mm accuracy - 8 decimal places)
lngstr2 = num2str(particle2_newlng, 11); %convert number to string, max
number of significant digits = 10 (1.1 mm accuracy - 8 decimal places)
new_cntr2_str = num2str(new_cntr2, 100); %convert counter to string
data2 = ['{"timestamp":', timestampstr, ', "value":',new_cntr2_str, ',
"context": {"lat":', latstr2, ', "lng":', lngstr2, '}}']; %create JSON
formatted string
options = weboptions('MediaType','application/json', 'Timeout', 120);
%specify JSON formatted content and set timeout to 2 min
response = webwrite(ubidotsURL, data2, options); %send JSON payload to
Ubidots
```